Technische Universität München
Lehrstuhl für Technische Chemie II

Sorption and transport of aromatic over MFI zeolites

Rino Rakhmata Mukti

Vollständiger Abdruck der von der Fakultät für Chemie der Technischen Universität München zur Erlangung des akademischen Grades eines

Doktor der Naturwissenschaften (Dr.rer.nat.)

genehmigten Dissertation.

Vorsitzender: Univ.-Prof. Dr. Klaus Köhler

Prüfer der Dissertation:

1. Univ.-Prof. Dr. Johannes A. Lercher
2. Univ.-Prof. Dr. Ulrich K. Heiz

Die Dissertation wurde am 21.06.2007 bei der Technischen Universität München eingereicht und durch die Fakultät für Chemie am 18.07.2007 angenommen.

Along with the soul of my beloved Mother.
To Papah, Bunda, Ayah,
Vinda, Naqisya and Kayn.

Acknowledgments

Praise to God, the Most Gracious and Most Merciful, Who has created the mankind with knowledge, wisdom, and power. Being the best creation of God, one still has to depend on others for many aspects directly or indirectly.

My first gratitude goes to Johannes (Prof. Johannes A. Lercher) for giving me an opportunity, a primary financial support and scientific knowledge during PhD life at Technische Universität München. Additionally, I have learned on how to follow the rhythm of such a big group.

On the same level, I thank Andy (PD. Dr. Andreas Jentys) after his guidance and inspiration throughout this research. You have taught me well and criticised all aspects for the better future. Eventually, I have shaped myself and will think before act.

I would like also to acknowledge Hendrik Dathe and Carsten Sievers for introducing me the IR and TG-DSC setup along with its technical discussion. Appreciation has to be given to Stephan Reitmeier as the project successor and our knowledge exchange that we had in the past one year.

It has been the greatest moment in my life to be here in Munich with all relatives. For the TC2 member, your shared time and feeling can not be forgotten. I have classified 3 generations that I met personally below:
First generation: Philipp, Christian, Florencia, Iker, Oriol, Alex, Xuebing, Shourong, Toshi, Ayumu, Peter Haider, Peter Schärringer, Felix, Maria, Krishna, Renate, Adam, Jan Kornatowski, Gabriela, Stefan Gaab, Qing, Chintan, Rahul, Prashant, Chirag and Hitri.
Second generation: Manuel, Lay-Hwa, Aon, Yongzhong, Praveen, Anirban Ghosh, Herui, Benjamin, Virginia, Elvira, Wolfgang, Suppan, Sabine, Tobias, Matteo, Prado,

Cristoph, Manuela, Dechao, Luca Maselli, Olga, Sandra, Ana, Richard, Frederik, Vanessa, Mahdi, Neeraj, Oliver, Florian and Jürgen.
Having all time generations: Xaver Hect, Martin Neukamm, Andreas Marx, Roberta Olindo, Thomas Müller, Heike Schüler, Helen Lemmermöhle and Steffi Maier.

To Indonesian (Syukri, Maulana, Sofian, Sugeng, Rangga, Bambang Arianto, Bambang Darwanto, Adit, Jeffry, Panji, Rika, Dody, Deddy, Dani, Emil, Ahya, Eriza, Aulia, Ilyas, Salafudin, Firdaus, Elka, Ika, Tiwi, Sian Spohn, Justina, Susan, Prio, Nano, Ridwan, Tresna, etc), Badminton (Kossy, Angka, Dian, Eduard, Matiin, Ivan, etc), Freisinger (Abdulwasey, Anggoro, Ricco, Indah, Erna, Rian, Danang, Joko, etc), Olympiadorfer (Isa, Edo, Masria, Ikhwan, Wani, Deski, Chris and Wiwit) and TUM-Department Chemie (Akef, Ahmed, Susan, Monika, Angela, Filipe, Manoj, Khiran and Alejandro) community, your lovely help and kindness particularly involving my family are truly noble.

Finally, I would like to express sincere appreciation to my brothers (Rhenda R. Mukti and Radhi Viandarno) and sister (Rhiren R. Mukti) who have been supporting me to wherever I am going.

Sincerely yours,
Rino

Table of Contents

Chapter 1 Introduction

1.1. Application of zeolites as adsorbent and catalyst 2
1.2. Structure and reactivity of ZSM-5 5
1.3. Surface phenomena of aromatic molecules in MFI zeolites 8
1.3.1. Molecular sorption processes 8
1.3.2. Molecular diffusion processes 13
1.3.3. Sticking probability in zeolites 17
1.4. Objective, structure and scope of thesis 19
References 20

Chapter 2 Experimental

2.1. Introduction 27
2.2. Sorption measurement 28
2.2.1. Thermogravimetry-Differential Scanning Calorimetry 28
2.2.1.1. Adsorption isotherms 28
2.2.1.2. Heat of adsorption 32
2.2.2. IR spectroscopy 34
2.3. Transport measurement 37
2.3.1. Fast time-resolved (rapid scan) IR spectroscopy 37
2.3.1.1. Apparatus setup 38
2.3.1.2. Spectral recording principle 39
2.3.1.3. Data analysis 41
2.3.2. Frequency response 42
2.3.2.1. Diffusion in infinite plane sheet 44
2.3.2.2. Other diffusion models 46
References 47

Chapter 3 Energetic and entropic contributions controlling the sorption of benzene in zeolites

3.1. Abstract 50
3.2. Introduction 50
3.3. Experimental 54
3.3.1. Materials 54
3.3.2. Thermogravimetry 54
3.3.3. IR spectroscopy 54
3.4. Results 55
3.5. Discussion 64
3.6. Conclusions 71
3.7. Acknowledgments 72
References 72

Chapter 4 Orientations of alkyl-substituted aromatic molecules during sorption in the pores of zeolite HZSM-5

4.1. Abstract 77
4.2. Introduction 77
4.3. Experimental 81
4.3.1. Materials 81
4.3.2. Thermogravimetry 81
4.3.3. IR spectroscopy 82
4.4. Results 82
4.5. Discussion 91
4.6. Conclusion 98
4.7. Acknowledgments 99
References 99

Chapter 5 Surface transport processes and sticking probability of aromatic in HZSM-5

5.1. Abstract 104
5.2. Introduction 104
5.3. Experimental 107
5.3.1. Materials 107
5.3.2. Fast time-resolved (rapid scan) IR spectroscopy 107
5.3.3. Diffusion coefficients 108
5.4. Results 109
5.4.1. Kinetics of surface transport processes of aromatic in HZSM-5 109
5.4.2. Sticking probability of aromatic molecules on HZSM-5 and Aerosil 114
5.4.3. Transport diffusivity of aromatic in HZSM-5 115
5.5. Discussion 118
5.6. Conclusions 122
5.7. Acknowledgment 123
References 123

Chapter 6 Summary

6.1. Summary 126
6.2. Zusammenfassung 131

Curriculum vitae 136
List of publications 137
List of presentations 138

Chapter 1

Introduction

1. INTRODUCTION

1.1. Application of zeolites as adsorbent and catalyst

It has been more than 60 years since zeolites were introduced and extensively used as adsorbent, catalyst as well as ion exchanger in various applications of science and technology [1-6]. The fundamental investigations on zeolites synthesis in the level of industry were initiated in 1940s by Linde Division of Union Carbide Corporation aiming at new approaches for separation and purification of air [7]. The various types of synthetic zeolites (A, X and Y) were rapidly recognized as potential catalysts for many industrial applications as they combine the key properties of being shape selective and strongly acidic. Zeolite Y was introduced in 1959 as catalyst for the production of high octane gasoline in petrochemical industry via fluidized catalytic cracking (FCC) from heavy petroleum distillates [8, 9]. The development of zeolites as cracking catalyst was even marked by the presence of rare-earth containing zeolite X, which replaced the amorphous silica-alumina catalysts in the FCC plants to increasing the yield of gasoline [5, 10]. The use of zeolites as catalyst has certainly established reduced cost of petroleum refining by at least 10 billion US dollars throughout the year [11].

The control of the pore network topology and nature of the active sites allows to tailor the sorption capabilities and the reactivity of the materials, thus enabling the rational design of catalysts and sorbents in the fields of separation, refining and catalytic production of fine chemicals [12]. The development of ZSM-5 (i.e. Zeolite Socony Mobil-5) by Mobil Oil in 1972 [13] introduced a new class of “shape selective catalyst” within pentasil family of zeolites. ZSM-5 was originally designed for the production of synthetic gasoline (conversion of methane to a mixture of aliphatic and aromatic hydrocarbons) but nowadays it

has been industrially well-known for reactions with aromatic molecules such as benzene alkylation, xylene isomerization, toluene disproportionation and transalkylation [14-21]. In the separation of xylene isomers, ZSM-5 is highly selective for p-xylene [22], which is utilized in the Parex™ process. This process was developed by UOP [23, 24] and the worldwide production of p-xylene has reached 18 million tons per year from 88 Parex™ units [25]. However, the global demand for p-xylene in 2006 is still around 32 million tons, hence further development of processes for the production of p-xylene will be necessary [26, 27].

Generally, aromatic compounds have a wide variety of applications in the petrochemical and chemical industries. For example, benzene, toluene and p-xylene (BTX) are basic commodities and valuable intermediates for production of fine chemicals which are typically used as monomers for polyesters, engineering plastics, detergents and pharmaceuticals. Benzene itself is a building block for over 250 products including ethyl benzene (for styrene), cumene (for phenol) and cyclohexane, while toluene has become increasingly valuable for the production of xylenes through the toluene dispropotionation and transalkylation with C_9/C_{10} aromatic compounds [28, 29]. Along with four different xylene C_8 isomers (para, ortho, meta and ethylbenzene), p-xylene is the broadest commercial product which is used for the production of polyester fibers, resins and films. o-Xylene and m-xylene are currently used for the production of phtalic anhydride and iso-phtalic acid which are typically utilized as plasticizers and PET resin blends, respectively [30].

Haag and Olson were the first who demonstrated the high para selectivity of HZSM-5 (acidic ZSM-5) in the toluene disproportionation reaction [31, 32], which had a significant improvement compared to the various other catalysts (e.g. nickel, platinum, palladium, boria deposited on alumina) used for this reaction [33, 34]. The concept of shape selectivity was developed, which distinguishes three cases depending on whether pore size limits the

entrance/exit of the sorbing/reacting molecules or the formation of a product via the geometry of the transition state: (1) reactant selectivity (involving the reactant size to diffuse inside the pores), (2) product selectivity (involving the capability of converted products to diffuse out of the pore) and (3) restricted transition-state selectivity (state of transition mechanism in the pores where only limits to certain possible reactions) [22, 35].

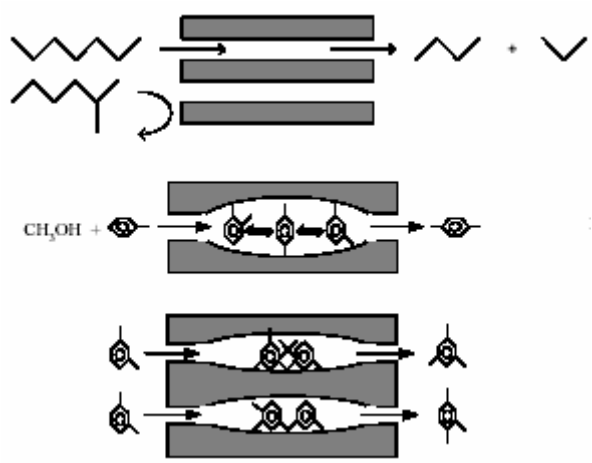

Figure 1.1. Concept of shape selectivity describing (a) reactant, (b) product and (c) restricted transition-state selectivity [36].

A number of different modification techniques were found to improve the para selectivity. The basic principle of improving the para selectivity includes the reduction of diffusivity by blocking or narrowing of the pore-mouth or the inactivation of sites at the pore mouth, which are not shape selective. This method can inhibit secondary isomerization and retain the p-xylene selectivity as product diffusing out from the zeolite pores. For the post synthetic modification, pre-coking or silica deposition (including chemical vapor deposition, CVD or chemical liquid deposition, CLD method) are most frequently applied in combination with a selection of the crystal size, Si/Al ratio and morphology of the parent zeolite. Other techniques of blocking the surface

sites can include impregnation methods using rare-earth, boron, and large amine molecules [37-41].

ZSM-5 was also applied in the alkylation of benzene with ethylene replacing the homogeneous Friedel-Crafts catalysts, which could reduce the amount of solid and liquid waste to 7 and 33 %, respectively, in the production of ethylbenzene with volume of 390,000 tones per year [42, 43]. This process named Mobil-Badger reaction has worldwide demand for ethylbenzene, a raw material for styrene production reaching to 22×10^6 tons/year [44].

Zeolites can be found in nature and have been known for almost 250 years as aluminosilicate minerals [11]. However, their naturally occurring forms are of limited value to be applied in catalysis which is reasonably due to (1) undesired impurity phases, (2) excess variety of chemical compositions and (3) inability of nature to optimize their properties for specified catalytic applications.

1.2. Structure and reactivity of ZSM-5

ZSM-5 has two 10-membered ring channels. The straight along the [010] axis has a diameter of 5.3×5.6 Å and sinusoidal channel along the [100] axis has a diameter of 5.1×5.5 Å. The two channels are perpendicular to each other and generate an intersection with diameter of 8.9 Å. The unit cell of ZSM-5 consists of 196 T atoms and the material can be synthesized with Si/Al ratios between 10 and ∞. The purely siliceous material (i.e. Si/Al = ∞) is called Silicalite-1. The IZA structure code for ZSM-5 and Silicalite-1 is MFI [13, 45-47]. The schematic structure of the building block, the secondary building unit and the framework of MFI zeolite is illustrated in Figure 1.2, the two channels with intersection as well as the crystal morphology is depicted in Figure 1.3.

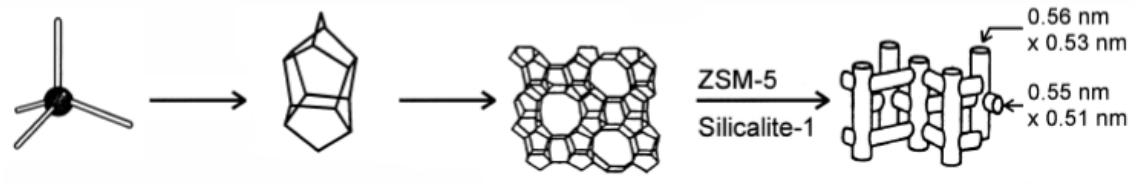

Figure 1.2. Structure of MFI zeolite including the micropore systems and dimensions [11].

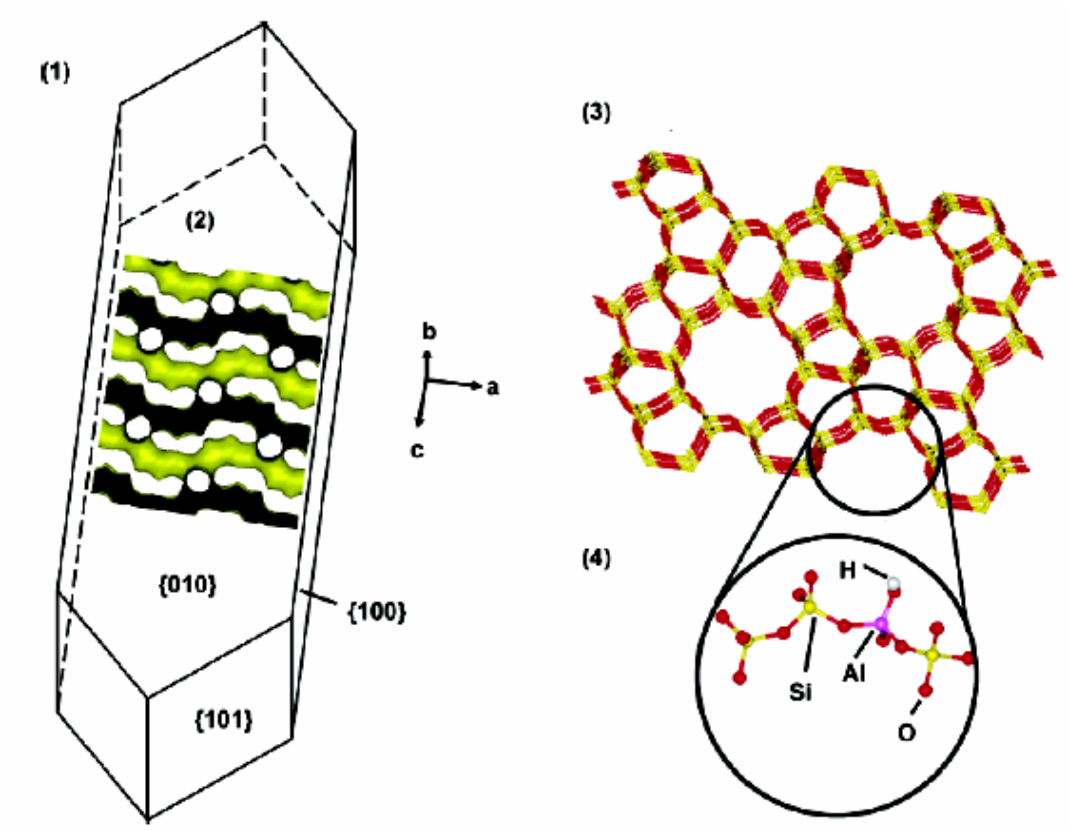

Figure 1.3. Key features of MFI zeolite: (1) crystal morphology, (2) straight and sinusoidal channels with intersection, (3) crystal framework and (4) detail of atomic structure [48].

The presence of Al in the framework introduces negative formal charge which is compensated by a proton forming a Brønsted acid site (i.e. SiOHAl or bridging hydroxyl groups) or a monovalent cation. The hydroxyl groups can be studied by infrared (IR) spectroscopy in the range between of 4000 to 3200 cm^{-1}. For SiOHAl groups in HZSM-5 (protonic form of ZSM-5) the band is observed at 3610 cm^{-1}. Additionally the bands at 3745, 3725 3660 and ~3500 cm^{-1} can be assigned to SiOH groups at terminal sites, to free hydroxyl groups at defect sites, to hydroxyl groups on nanoparticle Al-oxide species (clustered EFAL-oxide species) and to hydrogen bonded hydroxyl groups at defect sites. Most of these groups were observed in acidic zeolites (e.g. HZSM-5, Hβ, HY, etc) and amorphous aluminosilicates. The structural model for acidic hydroxyl groups has been proposed [49], which are depicted in Figure 1.4. The acidity of SiOHAl groups is described due to the presence of fully bridged oxygen between the Al and Si atoms with a weakly bonded proton as being the negative charge compensation.

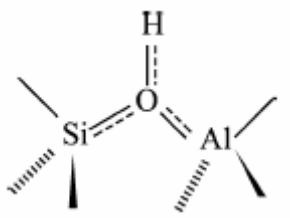

Figure 1.4. Structural model of reactive bridging hydroxyl groups in zeolites [12].

It is known that the total number of Brønsted acid sites is in principle directly related to the total number of Al^{3+} present. However, not all high Al content samples are considered to have strong acidity (acid strength). This phenomenon is related to the number of Al atoms in the next nearest neighbor position (NNN) to the other Al atoms. A completely isolated Al tetrahedron will

have zero NNN and forms the strongest Brønsted acid site [50, 51]. Barthomeuf [52, 53] extended this idea using topological density theory and predicted the acid strength by changing the framework Si/Al ratio, either by synthesis or postchemical synthesis. Consequently not only the total number of Brønsted acid sites, but also their acid strength is a function of the Si/Al ratio. Thus, when catalytic reactions demand low acidity it requires zeolite with lower Si/Al ratio (high Al content). In contrast, when strong acidity is required, zeolites with isolated framework Al atoms (low Al content) will be chosen. The acid strength of the Brønsted acid sites can also be tuned through isomorphous substitution of Si with other trivalent atoms, for example Ga-substituted zeolites gave stronger acid sites than boron and weaker sites than Al-substituted zeolites [54].

1.3. Surface phenomena of aromatic molecules in MFI zeolites

The interaction of aromatic compounds such as benzene, toluene and xylene isomers with MFI zeolites has been intensively studied due to the promising applications on industrial scale. The surface phenomena describing on how these molecules adsorb, orient and diffuse into the pores of zeolite are explored together with the probability of molecules to be initially sticked on the surface of pre-adsorbed state (sticking probability). The introduction presented below will try to correlate the experimental and theoretical (simulation) findings.

1.3.1. Molecular sorption processes

Sorption (i.e. sorption of gaseous molecules on solid surface) includes the process of sorbate-pore interaction as the result of greater pore curvature and with better fit in size between pore and sorbate molecule. Sorption is strongly influenced by the entropy (i.e. ability to fit in a confined space),

therefore the issue focuses not only on how much the molecule can adsorb but also on where and how it is oriented. The sorption of aromatic compounds such as benzene, toluene and xylene isomers has often been of interest since these compounds are valuable raw materials for the chemical industry. The channels (straight and sinusoidal) in MFI zeolites are sufficiently wide to allow diffusion of single aromatic molecule which has kinetic diameter of maximum 6.3 Å as in the case of p-xylene.

The sorption can generally be investigated by macroscopic and microscopic techniques. The macroscopic techniques typically describe sorption based on the measure of the adsorption isotherms either by gravimetric, volumetric methods which thermodynamically interprets as the enthalpic and entropic parameters describing the uptake. The microscopic approach provides a detailed description of the local interaction between the molecules and the functional groups of the zeolite on an atomistic level using spectroscopic techniques such as NMR, neutron diffraction, Raman and IR spectroscopy.

Benzene has been one of the most frequent probe molecules being applied for the evaluation of the acid/base properties of zeolites and in particular for the strength of the acid sites [55-57]. The sorption of benzene was experimentally studied over wide range of characterization techniques. From the adsorption isotherm data [58, 59] supported by Raman spectroscopy, neutron and X-ray diffraction studies [60, 61], it was proposed that the benzene molecules can be transported in the pores of MFI zeolites into three different locations of sites (straight, sinusoidal and intersection) depending on the loadings and applied temperatures. All MFI zeolites (i.e. HZSM-5 and Silicalite-1) can be loaded up to 8 benzene molecules per unit cell [62-64] where three ranges of loading refer to the three stages of molecules to reside. In the low loading range (1-4 molecules per unit cell) benzene is populated at intersections while in the intermediate loading range (5-6 molecules per unit cell) the four molecules of benzene tend to move into the sinusoidal channel.

Eventually in the high loading range (7-8 molecules per unit cell), strong sorbate-sorbate interactions are believed to occur and the benzene molecules were said to be located in the midsection of the straight channels.

From the theoretical approach, calculations on DFT level [65, 66] predicted that the aromatic molecules interact *via* the π-electrons with the protons of the zeolite. This agrees to some experimental clarification for the interaction of aromatic with SiOH and SiOHAl groups of HZSM-5 using vibrational spectroscopy [67-70]. According to the Guttman's rule of EPA-EPD interaction, the hydrogen bonding between the electron donor function of the aromatic molecules and the hydroxyl groups of the zeolite leads to the bond length variations. This is associated with charge density shift and polarization of the bonds meaning that the increase of bond length relates to the increase in strength of interaction which parallels to the increase of ionicity in the bond for charge transfer from a more electropositive atom to a more electronegative atom. Since acid strength is counted as the strength of interaction, the frequency shift of the hydroxyl groups stretching vibration to lower wavenumber in IR spectrum reflects the strength of the EPA-EPD interaction as well as the local geometry of the molecules at the sorption sites. The evaluation of this acid strength can then be followed from the wavenumber difference ($\Delta\nu_{OH}$) between the perturbed and the unperturbed hydroxyl groups vibration frequencies and this technique has been frequently described as probe for the acid strength describing the effects of steric constraints on the hydroxyl groups perturbation [71-74].

In principle, the strength of the EPA-EPD interaction is directly proportional to perturbation of the hydroxyl groups and, therefore, the correlation of $\Delta\nu_{SiOH}$ (of amorphous silica) versus $\Delta\nu_{SiOHAl}$ (of a zeolite) for a series of molecules should lead to a linear relation, the so-called Bellamy-Hallam-Williams (BHW) plot (Figure 1.5) [75]. The slope of this graph is a measure for the acid strength of the zeolite, if steric constraints for the sorbates are absent (e.g. alkanes, N_2, CO). For larger molecules such as benzene, a deviation to

smaller shifts for $\Delta\nu_{SiOHAl}$ was reported using several type of zeolites [76] and this indicates a sterically constrained geometry of molecules during sorption in the pore of the zeolites. Frequently, more than one band of perturbed hydroxyl groups was seen after sorption of benzene, toluene and p-xylene which can be assigned to different geometric locations/orientations of the molecules within the pores of the zeolite or to the presence of hydroxyl groups with non-uniform acid strength [70, 77, 78]. However, a detailed study still needs to be carried out clarifying the acid strengths from the interpretation of several perturbed hydroxyl groups.

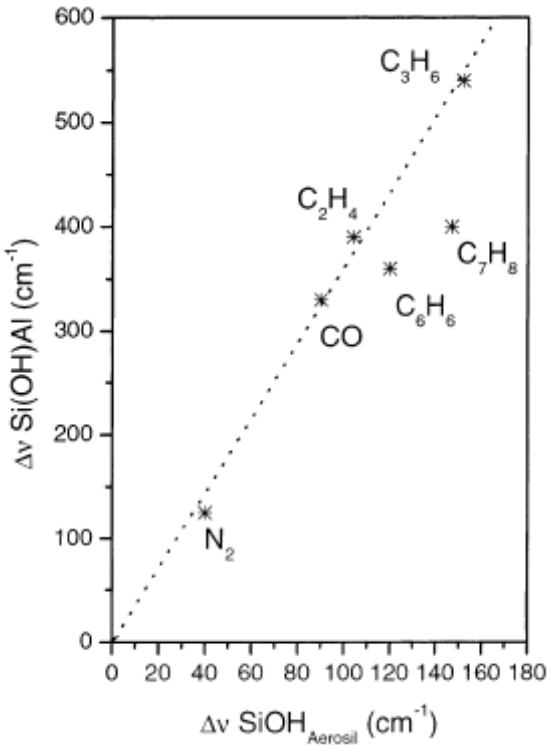

Figure 1.5. Bellamy-Hallam-Williams plot displaying the interaction strength of several molecules in zeolite ZSM-5 [76].

In order to explore the sorption energy and molecular orientation that controls the aromatic sorption within the loading up to 8 molecules per unit cell,

the study was extended by means of calorimetry method. Thamm [79] reported the results of the heat of adsorption (differential molar enthalpy) particularly for the interaction of benzene, toluene and p-xylene in Silicalite-1. For loading below 4 molecules per unit cell, the heat of adsorption of benzene is approximately reached 55-60 kJ/mol while at higher loading the high heat of adsorption is present due to the intermolecular interactions. For the sorption of toluene and p-xylene, the heat of adsorption was reported to be higher than benzene due to the additional interaction from the methyl groups on which attached to the aromatic ring. The discussion on whether the acidity influences the sorption of aromatic becomes topic of interest for investigation. Pope [80, 81] reported the heat, entropy and Gibbs free energy of sorption using set of isochores (isosteric) data obtained from the adsorption isotherm comparing the sorption of benzene, toluene, p-xylene in HZSM-5 and Silicalite-1. Although the reported heat of adsorption below 4 molecules per unit cell as for the sorption in HZSM-5 is not totally constant, however they concluded that the Al contents do vary the interaction properties in a systematic and regular way where in particular a slight higher heat of adsorption was found for the acidic MFI zeolite.

The entropy issue of aromatic sorption in zeolite has been the least found in the literature discussion. Pope discussed that the entropy becomes more unfavorable at high sorption loadings whereas the heat of adsorption grows more exothermic with the loadings. This result was then used as initial explanation for the step after loading of 4 molecules per unit cell in the adsorption isotherm of p-xylene as reported by Olson et al. [59] in a so called unusual adsorption isotherm. The step of transforming the adsorption isotherm from type I to type IV was also proposed as the phase transition phenomenon to the crystal morphology of MFI zeolites. Snurr et al. [82] simulated the transition of the $P2_1/n$-Pnma (monoclinic/ORTHO) to the Pnma-$P2_12_12_1$ (orthorhombic/PARA) symmetry in the polymorphic framework of MFI structural model. However, the signature of the phase transition was denied by Floquet et al. [83] who concluded that the shape only correlates to the different

sorption stages (intersection, sinusoidal and straight) during the loadings as demonstrated by benzene using detailed in situ neutron diffraction.

1.3.2. Molecular diffusion processes

Most of the active sites are located in the cavities of porous materials and the ability to accumulate molecules in their interior to much larger concentrations than in the surrounding atmosphere has become the key properties to be applied as promising catalyst for practical application [84]. In order to create a reaction, reactant molecules have to diffuse into the channels which are prior to the adsorption process. The mass transport of reactant molecules becomes an important issue when the kinetic diameter of reactant and/or product molecules is comparable to the size of pore opening. If the mass transport is a slow process compared to the reaction process, the overall reaction is controlled by the mass transport. This phenomenon is used to be recognized as diffusion limitation and prevention of this occurrence is necessary when designing such a catalytic reaction system. In fact, experiments show that the equilibration of molecules onto the surface is significantly slower than expectation based on the applied partial pressures, heat of adsorption characteristic and mobility under pore access condition. This hindrance has concluded that the direct transport (directed fluxes) of molecules is improbable, thus a term namely surface barriers is used [85]. Eventually, it is rather being accomplished by the stochastic thermal motion of the individual molecules, a process which is referred to as Brownian motion or simply diffusion. Therefore, understanding the characteristic of diffusion or mass transport process in the porous materials is an important subject particularly in the area of catalysis, gas-solid reactions, adsorptive and membrane separations along with the improvement towards the intrinsic reaction rate involving the active sites.

The diffusion mechanism is different in various regions of pores. In micropores ($0.5 \leq x \leq 1$ nm), diffusion is dominated by interaction between molecule and the pore walls. This is known as configurational or intracrystalline diffusion. In mesopores ($1 \leq x \leq 50$ nm), the mean free path of molecules is known greater than the pore size but diffusion still occurs which is interrupted by momentary sorption on the walls (i.e. Knudsen diffusion). In macropores ($\geq$ 50 nm), diffusion occurs generally by a bulk mechanism. The diffusion of aromatic in MFI zeolites is categorized as configurational diffusion since the kinetic diameter is in the same dimension as the pore size of MFI zeolites. The relationship of diffusivity with the pore diameter for small gaseous sorbates is depicted in Figure 1.6.

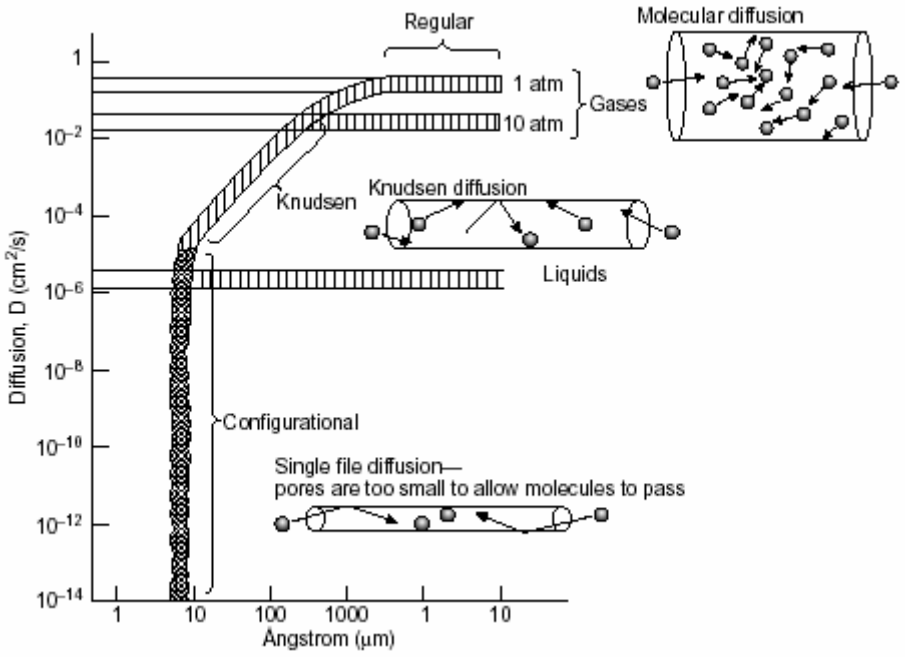

Figure 1.6. Diffusion regime and the influence of pore size on diffusivity of small gaseous sorbates [86].

A large variety of techniques has been applied to measure diffusivity of various molecules in the porous materials (e.g. zeolites). The techniques are basically based on continuum models and classified into equilibrium and

nonequilibrium conditions (Figure 1.7). The mass transfer process from the gas phase to site inside the pores under equilibrium is described by the self-diffusivity while the mobility of the molecules inside the pores under nonequilibrium is described by the transport diffusivity. Due to the different physical situation during the measurement, the coefficient of self and transport diffusion cannot be expected to be identical. The measurements based on equilibrium include pulsed-field gradient (PFG) NMR [87, 88], quasielastic neutron scattering (QENS) [89], zero-length column (ZLC) [90, 91] and tracer exchange [92]. The measurement based on nonequilibrium are sorption uptake rates measurement using ring deformation vibration of IR spectroscopy [93] and frequency response (FR) method [62, 63, 94]. The latter has been often implemented since it has several advantages of distinguishing multi-kinetic processes which may be present in FR spectra. Other benefits from this technique can be considered such as ease of use, good accuracy and multi applications as it is applicable for investigating the binary diffusion of compound mixtures.

The properties of zeolite may influence the diffusivity of aromatic in the pores of MFI zeolites. The transport of toluene in the pore system of ZSM-5 strongly depends upon degree of crystal intergrowth. Lercher and co-workers [95] measured the diffusion coefficient using time-resolved FTIR microscopy which shows the value with single crystal resulting three orders of magnitude higher than the measured with polycrystalline sample. Using FR method, Rees and co-workers [63] distinguish the transport of benzene in sphere (twinned) and cube-shape Silicalite-1 where the diffusion coefficients differ in the range from one to three orders of magnitude at the same loading and temperature. The acidity of zeolite was observed to affect the diffusion of aromatic molecules in the pores. Several reports claimed that the diffusion of benzene in HZSM-5 is slower than in Silicalite-1 [96-101].

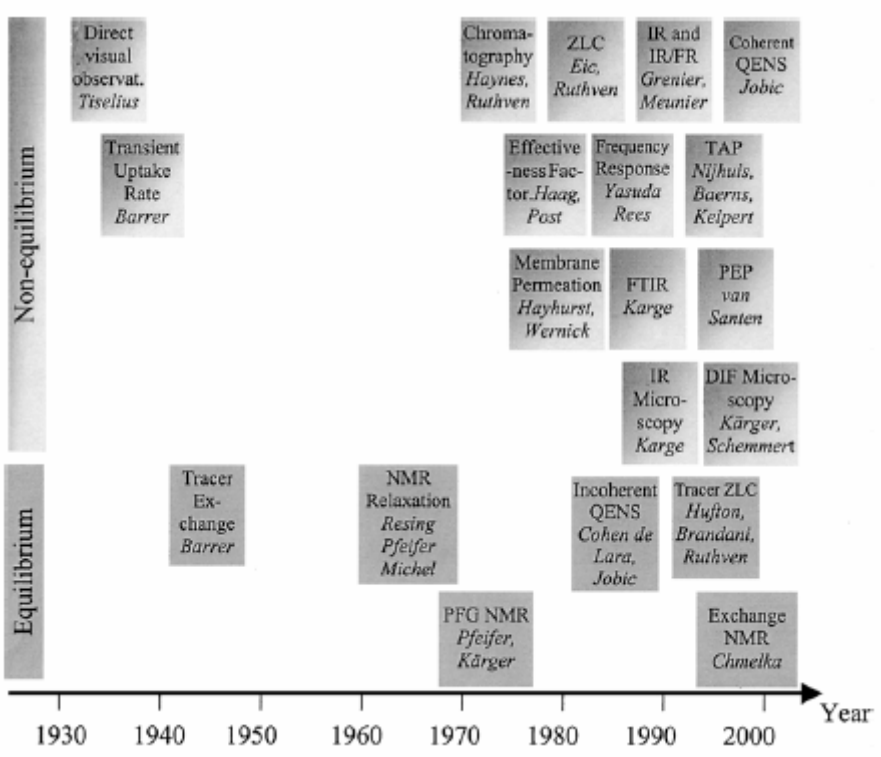

Figure 1.7. Pioneers on inventing and developing the diffusion measurement techniques throughout the years [102].

The FR spectra shows bimodal behavior for diffusion of benzene in Silicalite-1 at loading above 4 molecules per unit cell while at low loading only single process was resulted. Similar to benzene, diffusion of toluene and p-xylene in Silicalite-1 shows two processes at high loading and single process at low loading. The single diffusion process was assigned as the mass transfer of aromatic molecule being transported along the straight channel as confirmed by molecular dynamics (MD) simulation. The second diffusion process with new peak appearing at a frequency much higher than that observed at low loading however may not be ascribed as subsequent process which may be described as the diffusion to the sinusoidal channel since the solid docking simulation, thermodesorption and NMR measurement suggest that the bimodal behavior is independent diffusion processes taking place in

the system. The solid docking results simulate that some of the sorbed molecules are clustered at high loading leading to different states of the sorbed aromatic molecules existing in the framework, i.e. clustered and unclustered state. The bimodal behavior is also known to be dependent on crystal structure where larger crystal of Silicalite-1 with the sphere-shape can only show single process of aromatic diffusion. For the diffusion in HZSM-5, two processes for the transport of benzene [103], toluene [104, 105] and p-xylene [103] were always resulted even at low loading below 4 molecules per unit cell. The diffusivity was reported to decrease in the order of p-xylene>toluene>benzene with the diffusion coefficient of p-xylene being about one order of magnitude higher than the others [103].

Diffusivity in zeolites varies widely with molecular structure configurations. The increase of number of C atoms or chains brings to the drop of diffusivity in the case with ZSM-5 (Figure 1.8). The diffusion rate of p-xylene is at least 1000 times faster than that of the other isomers. Therefore, p-xylene could rapidly diffuse out from the zeolite pores.

1.3.3. Sticking probability in zeolites

The sticking probability, i.e. the probability for a molecule to stay on the surface after a collision, is one of the key properties when describing the sorption. In addition to mass transfer resistances in the intra- and interparticle spaces, it notably counts on how fast the molecules encountering the outer surface of the particle before penetrating into the pore interior. According to its classical definition, the sticking coefficient represents the probability that on encountering the surface, captured molecules will preferably enter the intraparticle space rather than being rejected to continue its trajectory in the space between particles, thus such value gives the feeling of how many collisions are needed for a successful sorption process (i.e. the capability of

molecules sticking on sorption sites, either on the external surface or in the pores) [106].

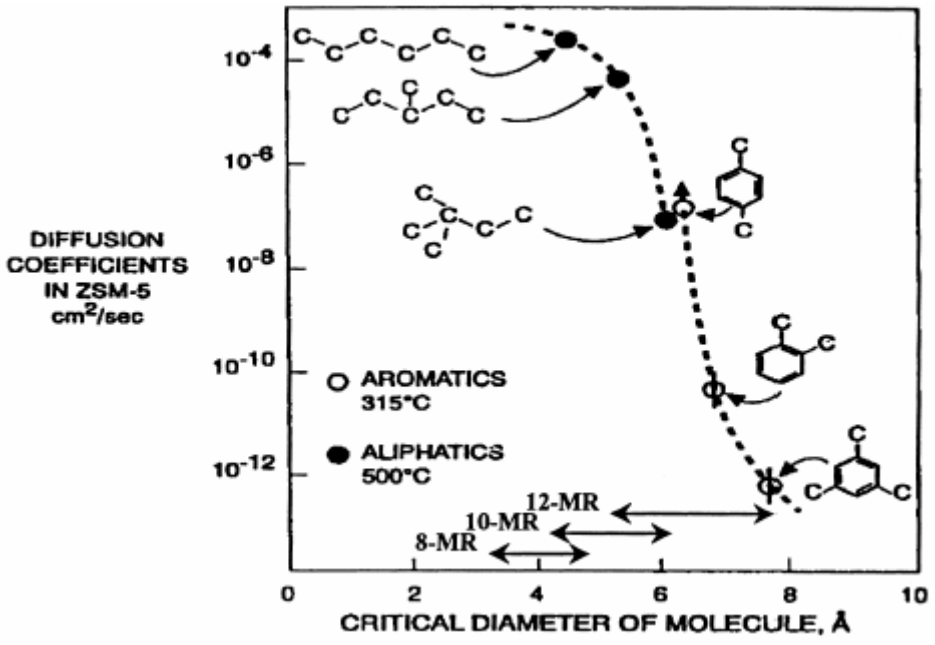

Figure 1.8. Diffusion rate of various aliphatic and aromatic molecules over zeolite ZSM-5. The arrows showing capability of zeolites with pore openings of 8, 10 and 12 membered-rings to allow the access of molecules with corresponding size [107].

The molecular transport into the intracrystalline space of porous material primarily involves the sorption on outer surface. In essence, the sticking probability represents a fundamental quantity of molecular dynamics on interfaces which can be defined as the ratio of the overall rate of initial sorption to the collision rate of the sorbed molecule [108]. Experimental studies have been conducted and reported since 1964 but only recently the sticking probability of aromatic in Aerosil (amorphous silica) was reported [109, 110]. Based on newly developed fast time-resolved (rapid scan) IR spectroscopy, Jentys et al. [109] carried out a direct spectroscopic measurement from which

the rate of sorption either on SiOHAl or SiOH groups are feasible to be estimated. The sorption on SiOH groups was concluded to give an effect onto the subsequent sorption at the intracrystalline and proposed to be the initial transport process for the sorption of aromatic molecules in HZSM-5. Thus, the rate of aromatic on SiOH groups was used to calculate the sticking probability and resulting values that is in the order of 10^{-6} to 10^{-7}. These numbers were considerably low since the previous estimation on sticking coefficient was typically between 0.1 and 1 [111].

1.4. Objective, structure and scope of thesis

Sorption and transport of aromatic consisting of benzene, toluene and p-xylene in acidic and non acidic MFI zeolites (HZSM-5 and Silicalite-1) were studied using gravimetry, calorimetry, IR spectroscopy and frequency response method. The aim of this thesis is to describe the complex interactions of the bulky aromatic molecules in a tight-fit situation inside the pores of zeolite in relation to the local steric constraints.

In Chapter 2, the detailed descriptions on the experimental setup, measurement principle as well as data analysis of the sorption and transport of aromatic in MFI zeolites are presented. One of the techniques used include fast time-resolved (rapid scan) IR spectroscopy for investigating the kinetic sorption rate of molecular transport within timescale of milliseconds.

Chapter 3 describes the enthalpic and entropic contribution controlling the sorption of benzene. The influence of acidity in MFI is understood from the overall sorption processes. The localized and unspecific energetic and entropic contributions for the sorption on the SiOHAl groups were described using a Langmuir isotherm model.

The study of tight-fit sorptive properties of aromatic is extended in Chapter 4 describing the sorption of alkyl-substituted benzene molecules, i.e.

toluene and p-xylene. The local interactions with SiOHAl groups were used to discuss the orientations at intersection between the straight and sinusoidal channel of MFI.

The study in Chapter 5 is conducted to the atomistic level of elementary steps. The transport of aromatic to the sites inside the pores is described and the sticking probability of the molecules in a weakly adsorbed state is calculated. The information of sticking probability deepens the understanding of the overall complex molecular sorption and transport of aromatic in MFI zeolites postulating the pre-adsorbed state as non-direct precursor preceding the sorption into the pores.

Finally, Chapter 6 summarizes the steps of the molecular sorption and transport explaining the overall role of steric constraint environment of aromatic in shape selective MFI zeolites.

References

1. Breck, D. W., *Zeolite Molecular Sieves*; Wiley: London, **1974**.
2. Breck, D. W., Eversole, W. G., Milton, R. M., *J. Am. Chem. Soc.*, **1956**, **78**, 2338.
3. Breck, D. W., Eversole, W. G., Milton, R. M., Reed, T. B., Thomas, T. L., *J. Am. Chem. Soc.*, **1956**, 78, 5963.
4. Breck, J. W., *J. Chem. Educ.*, **1964**, 48, 678.
5. Weisz, P. B., Frilette, V. J., *J. Phys. Chem.*, **1960**, 64, 382.
6. Bhatia, S., *Zeolite catalysis*; CRC Pr.: Boca Raton Fla., **1990**.
7. Davis, B. H., Singh, K. S. W., *Handbook of Porous Solids*; Schüth, F., Singh, K. S. W., Weitkamp, J. (eds); Wiley-VCH: Weinheim, **2002**, Vol. 1.
8. Al-Amer, A., Al-Khattaf, S., *Xylenes transformation over ZSM-5 zeolite in a fluidized-bed reactor*. In *Molecular Sieves: From Basic Research To Industrial Applications*, **2005**, 1613.

9. Al-Khattaf, S., Tukur, N. M., Al-Amer, A., *Ind. Eng. Chem. Res.*, **2005**, 44, 7957.
10. Venuto, P. B., Habib, E. T., *Fluid Catalytic Cracking with Zeolite Catalysts*; Dekker: New York, **1979**.
11. Weitkamp, J., *Solid State Ionics*, **2000**, 131, 175.
12. Corma, A., *J. Catal.*, **2003**, 216, 298.
13. Argauer, R. J., Kensington, M., Landolt, G. R., U.S. Patent 3 702 886, **1972**.
14. Chen, N. Y., Garwood, W. E., *Catal. Rev. Sci. Eng.*, **1986**, 28, 185.
15. Chen, N. Y., Garwoord, W. E., *J. Catal.*, **1978**, 52, 453.
16. Young, L. B., Butter, S. A., Kaeding, W. W., *J. Catal*., **1982**, 76, 418.
17. Tabak, S. A., Krambeck, F. J., Garwood, W. E., *AiChe J.*, **1986**, 32, 1526.
18. Chen, N. Y., *J. Catal*., **1988**, 114, 17.
19. Palomares, A. E., Eder-Mirth, G., Lercher, J. A., *J. Catal*., **1997**, 168, 442.
20. Sharanappa, N., Pai, S., Bokade, V. V., *J. Mol. Catal. A*, **2004**, 217, 185.
21. Llopis, F. J., Sastre, G., Corma, A., *J. Catal*., **2004**, 227, 227.
22. Csicsery, S. M., *Pure Appl. Chem.*, **1986**, 58, 841.
23. Broughton, D. B., *Abstr. Pap. Am. Chem. Soc*., **1983**, 186, 43.
24. Vener, K., Velker, Y., Zaidel, G., *Petrol. Chem*., **1971**, 11, 50.
25. Gomes, P. S., Minceva, M., Rodrigues, A. E., *Adsorption*, **2006**, 12, 375.
26. Tsai, T. C., Liu, S. B., Wang, I., *Appl. Catal. A*, **1999**, 181*,* 355.
27. Minceva, M., Rodrigues, A. E., *AiChe J*., **2007**, 53, 138.
28. Sato, M., Sonoda, T., Kinoshita, Y., Mizushima, T., Kashiwagi, M., *U.S. Patent* 3 413 374, **1968**.
29. Planchard Jr., J. A., *U.S. Patent* 3 126 422, **1964**.
30. Armor, J. N., *Appl. Catal.*, **1991**, 78, 141.
31. Haag, W. O., Olson, D. H., *U.S. Patent* 4 117 026, **1978**.
32. Haag, W.O., Olson, D. H., *U.S. Patent* 4 097 053, **1978**.
33. Kovach, S.M.*. U.S. Patent*, 3 598 878, **1968**.
34. Kovach, S. M., Kmecak, R. A., *U.S. Patent* 3 607 961, **1971**.

35. Weisz, P.B., *Pure Appl. Chem*., **1980**, 52, 2091.
36. Csicsery, S. M., *Zeolites*, **1984**, 4, 202.
37. Kaeding, W. W., Young, L. B., Weinstein, B., Butter, S. B., *J. Catal*., **1981**, 67, 159.
38. Kaeding, W. W., Chu, C., Young, L. B., Butter, S. B., *J. Catal*., **1981**, 69, 392.
39. Kaeding, W. W., Young, L. B. Chu, C., *J. Catal*., **1984**, 89, 267.
40. Young, L. B., Butter, S. B., Kaeding, W. W., *J. Catal*., **1982**, 76, 418.
41. Wang, I., Ay, C. L, Lee, B. J., Chen, M. H., *Appl. Catal.*, **1989**, 54 , 257.
42. Guisnet, M., Gnep, N. S., Morin, S., *Microp. Mesop. Mater*., **2000**, 35, 47.
43. Meriaudeau, P., Naccache, C., *Catal. Rev. Sci. Eng*., **1997**, 39, 5.
44. Hartmann, M., *Angew. Chem. Intl. Ed*., **2004**, 43, 5880.
45. Flanigen, E. M., Bennet, J. M., Grose, R. W., Cohen, J. P., Patton, R. L., Kirchner, R. M., Smith, J. V., *Nature*, **1978**, 271, 512.
46. Meier, W. M., Olson, D. H., *Atlas of zeolite structure types*; Intl. Zeolite Assoc.; 3rd ed.; Butterworth-Heinemann: Boston, MA, **1992**.
47. Kokotailo, G. T., Lawton, S. L., Olson, D. H., Meier, W. M., *Nature*, **1978**, 272, 437.
48. Cundy, C. S., Cox, P. A., *Chem. Rev*., **2003**, 103, 663.
49. Mortier, W. J., Sauer, J., Lercher, J. A., Noller, H., *J. Phys. Chem.*, **1984**, 88, 905.
50. Hunger, B., Heuchel, M., Clark, L. A., Snurr, R. Q., *J. Phys. Chem. B*, **2002**, 106, 3882.
51. Janssens, G. O. A., Toufar, H., Baekelandt, B. G., Mortier, W. J., Schoonheydt, R. A., *J. Phys. Chem*., **1996**, 100, 14443.
52. Barthomeuf, D., *Mater. Chem. Phys*., **1987**, 17, 49.
53. Barthomeuf, D., *J. Phys. Chem*., **1993**, 97, 10092.
54. Fricke, R., Kosslick, H., Lischke, G., Richter, M., *Chem. Rev*., **2000**, 100, 2303.

55. Muller, G., Bodis, E., Kornatowski, J., Lercher, J. A., *Phys. Chem. Chem. Phys.*, **1999**, 1, 571.
56. Sun, X. D., Wang, Q. X., Xu, L. Y., Liu, S. L., *Catal. Lett*., **2004**, 94, 75.
57. Datka, J., Boczar, M., *React. Kinet. Catal. Lett*., **1993**, 51, 161.
58. Talu, O., Guo, C. J., Hayhurst, D. T., *J. Phys. Chem*., **1989**, 93, 7294.
59. Olson, D. H., Kokotailo, G. T., Lawton, S. L., Meier, W. M., *J. Phys. Chem*., **1981**, 85, 2238.
60. Huang, Y. N., Havenga, E. A., *J. Phys. Chem. B*, **2000**, 104, 5084.
61. Goyal, R., Fitch, A. N., Jobic, H., *J. Phys. Chem.* B, **2000**, 104, 2878.
62. Song, L. J., Sun, Z. L., Ban, H. Y., Dai, M., Rees, L. V. C., *Adsorption*, **2005**, 11, 325.
63. Song, L. J., Sun, Z. L., Ban, H. Y., Dai, M., Rees, L. V. C., *Phys. Chem. Chem. Phys*., **2004**, 6, 4722.
64. Ban, H. Y., Gui, J. Z., Duan, L. H., Zhang, X. T. , Song, L. J., Sun, J. L., *Fluid Phase Equil.*, **2005**, 232, 149.
65. Ryder, J. A., Chakraborty, A. K., Bell, A. T., *J. Phys. Chem. B*, **2000**, 104, 6998.
66. Nicholas, J. B., *Top. Catal*., **1997**, 4, 157.
67. Jentys, A., Warecka, G., Lercher, J. A., *J. Mol. Catal*., **1989**, 51, 309.
68. Armaroli, T.,Bevilacqua, M., Trombetta, M, Alejandre, A. G., Ramirez, J., Busca, G., *Appl. Catal. A*, **2001**, 220, 181.
69. Armaroli, T., Trombetta, M., Alejandre, A. G., Solis, J. R., Busca, G., *Phys. Chem. Chem. Phys.*, **2000**, 2, 3341.
70. Trombetta, M., Alejandre, A. G., Solis, J. R., Busca, G., *Appl. Catal. A*, **2000**, 198, 81.
71. Jacobs, P. A., Martens, J. A., Weitkamp, J., *Faraday Discuss*., **1981**, 72, 353.
72. Horill, P., Noller, H., *Z. Phys. Chem.*, **1976**, 100, 155.
73. Eder, F., Lercher, J. A., *J. Phys. Chem. B*, **1997**, 101, 1273.

74. Eder, F., Stockenhuber, M., Lercher, J. A., *J. Phys. Chem. B*, **1997**, 101, 5414.
75. Bellamy, L. J., Hallam, H. E., Williams, R. L., *J. Chem. Soc. Faraday Trans.*, **1958**, **54,** 1120.
76. Onida, B., Bonelli, B., Borello, L., Fiorilli, S., Geobaldo, F., Garrone, E., *J. Phys. Chem. B*, **2002**, 106, 10518.
77. Jentys, A., Lercher, J. A., *Stud. Surf. Sci. Catal*., **1989**, 46, 585.
78. Trombetta, M., Armaroli, T., Alejandre, A. G., Gonzalez, H., Solis, J. R. Busca, G., *Catal. Today*, **2001**, 65, 285.
79. Thamm, H., *J. Phys. Chem*., **1987**, 91, 8.
80. Pope, C. G., *J. Phys. Chem*., **1984**, 88, 6312.
81. Pope, C. G., *J. Phys. Chem*., **1986**, 90, 835.
82. Snurr, R. Q., Bell, A. T., Theodorou, D. N., *J. Phys. Chem*., **1993**, 97, 13742.
83. Floquet, N., Coulomb, J. P., Weber, G., Bertrand, O., Bellat, J. P., *J. Phys. Chem. B*, **2003**, 107, 685.
84. Kärger, J., Ruthven, D. M., *Handbook of Porous Solids*; Schüth, F., Singh, K. S. W., Weitkamp, J. (eds.); Wiley-VCH: Weinheim, **2002**, Vol. 4, 2089.
85. Kärger, J., Caro, J., *J. Chem. Soc. Faraday Trans*., **1977**, 73, 1363.
86. Bhatia, S. K., *Adsorption Sci. Tech*., **2006**, 24, 101.
87. Kärger, J., Pfeifer, H., *J. Chem. Soc. Faraday Trans*., **1991**, 87, 1989.
88. Kärger, J., Jobic, H., *Coll. Surf.*, **1991**, 58, 203.
89. Jobic, H., Bee, H., Caro, J., Bullow, M., Kärger, J., Pfeifer, H., *Stud. Surf. Sci. Catal*., **1991**, 65, 445.
90. Brandani, S., Jama, M., Ruthven, D. M., *Ind. Eng. Chem. Res*., **2000**, 39, 821.
91. Brandani, S., Jama, M., Ruthven, D. M., *Microp. Mesop. Mater*., **2000**, 35, 283.
92. Joly, G. Tessa, N., *Bull. Soc. Chim. France*, **1993**, 130, 223.

93. Karge, H. G., *C. R. Chimie*, **2005**, 8, 303.
94. Yasuda, Y., *Heterog. Chem. Rev.*, **1994**, 1, 103.
95. Muller, G., Narbeshuber, T., Mirth, G., Lercher, J. A., *J. Phys. Chem*., **1994**, 98, 7436.
96. Choudhary, V. R., Srinivasan, K. R., *J. Catal*., **1986**, 102, 316.
97. Choudhary, V. R., Srinivasan, K. R., *J. Catal*., **1986**, 102, 329.
98. Masuda, T., Fujikata, Y., Nishida, T., Hashimoto, K., *Microp. Mesop. Mater*., **1998**, 23, 157.
99. Shen, D. M., Rees, L. V. C., *Zeolites*, **1991**, 11, 666.
100. Zikanova, A., Bullow, M., Schlodder, H., *Zeolites*, **1987**, 7, 115.
101. Qureshi, W. R., Wei, J., *J. Catal*., **1990**, 126, 147.
102. Kärger, J., *Adsorption*, **2003**, 9, 29.
103. Song, L. J., Rees, L. V. C., *Microp. Mesop. Mater*., **2000**, 35, 301-314.
104. Zheng, S., Tanaka, H., Jentys, A., Lercher, J. A., *J. Phys. Chem. B*, **2004**, 108, 1337.
105. Zheng, S., Heydenrych, H, Roger, H. P., Jentys, A., Lercher, J. A., *Top. Catal*., **2003**, 22, 101.
106. Ashmore, P. G., *Catalysis and inhibition of chemical reactions*; Butterworth: London, **1963**.
107. Chen, N. Y., *Stud. Surf. Sci. Catal*., **1988**, 38, 153.
108. *Compendium of Chemical Terminology IUPAC*; Research Triangle Park NC, **1997**.
109. Jentys, A., Tanaka, H., Lercher, J. A., *J. Phys. Chem. B*, **2005**, 109, 2254.
110. Tanaka, H., Jentys, A., Lercher, J. A., *Stud. Surf. Sci. Catal*., **2002**, 1619.
111. Trapnell, B. M. W., *Chemisorption*; Butterworth: London, **1964**.

Chapter 2

Experimental

2. EXPERIMENTAL

2.1. Introduction

The sorption of aromatic molecules (benzene, toluene and p-xylene) on MFI zeolites was experimentally studied from the measurement of gravimetric adsorption isotherms, characteristic heats of adsorption and infrared (IR) spectra. IR spectroscopy was used to study localized adsorption isotherms on specific sites and the thermodynamical interpretation led to an intense discussion on structural interactions between sorbate and sorbent. The transport of aromatic molecules to the sites of MFI zeolites, the rate of transport and diffusion coefficients were followed by kinetic studies using fast time-resolved (rapid scan) IR spectroscopy and frequency response technique, respectively.

The gravimetric adsorption isotherms and the characteristic heats of adsorption of aromatic molecules were measured using a modified Thermogravimetry-Differential Scanning Calorimetry (TG-DSC) SETARAM 111 instrument. The IR spectra were measured using an IR spectrometer from Bruker (IFS 66 v/S). Both instruments were connected to high vacuum environments to perform *in situ* studies. Fast time-resolved (rapid scan) IR spectroscopy allowed the direct investigation of the surface transport. A detailed description regarding the instrument setup, measurement principle and data analysis is presented in this chapter.

2.2. Sorption measurement

2.2.1. Thermogravimetry-Differential Scanning Calorimetry

Gravimetry is a method in which the sample is precisely weighed on a microbalance during the sorption experiment. The measurements of adsorption isotherms by gravimetry and determination of the heat of adsorption by calorimetry were simultaneously performed in a TG-DSC instrument. For gravimetry, the instrument contains a microbalance device with a sensitivity of 10^{-7} g. The sample has to be used in the form of pellets to avoid that powder is being sucked into the vacuum system. The pressure inside the system can be as low as 10^{-7} mbar and the temperature can be adjusted from 25 to 750°C. The weight of samples used in the TG-DSC experiment was between 13 to 22 mg, which is sufficient to obtain a sufficient signal-to-noise ratio in the DSC signal to calculate the heat of adsorption. Before the measurements, the samples were activated at 823 K for 1 h with heating rate of 10 $K.min^{-1}$ under vacuum. Aromatic molecules were adsorbed using stepwise pressure increases with steps of 0.01 to 0.02 mbar. The increase of weight was related to the heat flux to calculate the heat of adsorption.

2.2.1.1. Adsorption isotherms

The gas and the sorbate (i.e. the adsorbed gas) are in a dynamic equilibrium, in which the coverage of the surface depends on the pressure of the sorbing gas and the temperature. The dependence of the coverage on the pressure at a given temperature can be described with a adsorption isotherm. Several models for adsorption isotherms exist including the Langmuir, Freundlich and Temkin isotherms. The assumptions for a Langmuir isotherm are as follows [1]:

i. Sorption cannot proceed beyond monolayer coverage.
ii. All sites are equivalent and the surface is uniform
iii. The ability of a molecule to adsorb at a given site is independent of the occupation of neighboring sites.

From these assumptions, Langmuir equation is derived based on dynamic equilibrium with rate constants, k_{ad} for adsorption and k_{de} for desorption. The rate of coverage change due to adsorption is proportional to the partial pressure and number of vacant sites $N(1-\theta)$. The rate of coverage change due to desorption is proportional to the number of adsorbed species $N\theta$. The equations are presented as follows:

$$\frac{d\theta}{dt} = k_{ad} N(1-\theta) \tag{2.1}$$

$$\frac{d\theta}{dt} = -k_{de} N\theta \tag{2.2}$$

where θ is the fractional coverage and N the total number sites. At equilibrium the rate of adsorption is equal to the rate of desorption the fractional coverage can be expressed as:

$$\theta = \frac{K \cdot p}{1 + K \cdot p} \tag{2.3}$$

with

$$K = \frac{k_{ad}}{k_{de}} \tag{2.4}$$

and

$$\theta = \frac{q}{q_{sat}} \tag{2.5}$$

where *p* is the partial pressure of the sorbate, K is the equilibrium constant, q is the experimental coverage and q_{sat} is the saturation coverage (monolayer coverage). The typical shape of Langmuir isotherms are depicted in Figure 2.1.

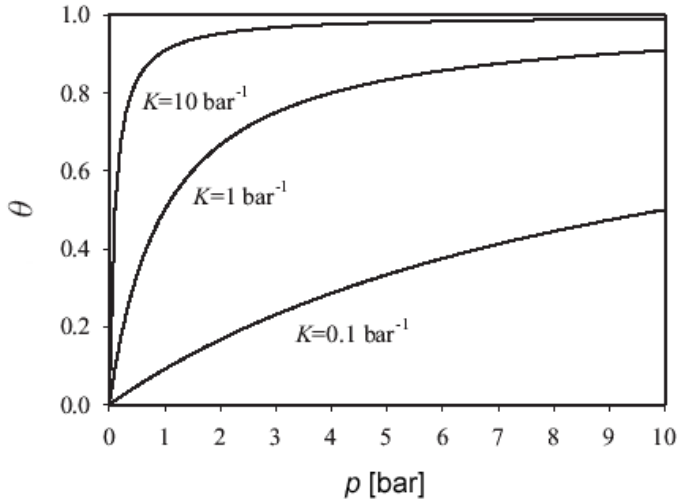

Figure 2.1. Typical shape of Langmuir adsorption isotherm as a plot of coverage versus pressure for three values of the equilibrium constant, K [2].

The Langmuir isotherm can be extended for describing several sorption phenomena on surfaces. For the process with dissociation, the rate of adsorption is proportional to the pressure and to the probability that both atoms will find sites, thus equation contains the square of number of vacant sites. The rate of desorption is proportional to the frequency of encounters of atoms on the surface and is therefore second-order in the number of atoms

present. The condition for no net change leads to the equation of adsorption isotherm with dissociation process:

$$\theta = \frac{(Kp)^{1/2}}{(1+Kp)^{1/2}} \tag{2.6}$$

The extension of the Langmuir adsorption isotherm to include multilayer sorption leads to the BET isotherm, which is frequently used to determine the specific surface area of a material from the sorption of an inert gas such as argon or nitrogen. The BET isotherm is shown in equation (2.7):

$$\frac{p}{V(p_0 - P)} = \frac{1}{CV_{sat}} + \frac{C-1}{CV_{sat}}\frac{p}{p_0} \tag{2.7}$$

where V_{sat} is the saturated volume of monolayer coverage, p_0 is the vapor pressure above layer of sorbate that is more than one molecule thick and which resembles a pure bulk liquid C is a constant which is large when enthalpy of desorption from a monolayer is large compared with the enthalpy of vaporization of the liquid sorbate. The linearized BET isotherm of $p/V(p_0 - p)$ against p/p_0 yields a straight line and the slope and intercept allows the calculation of V_{sat} and C (Figure 2.2).

Once the monolayer coverage has been obtained, the surface area per gram of material can be calculated using following equation:

$$S = V_{sat} N_A A_m \tag{2.8}$$

where S is the total surface area, N_A is Avogadro's number, A_m is area occupied by one sorbate molecule (1 cm^3 of $N_2 \approx 4.374\ m^2$).

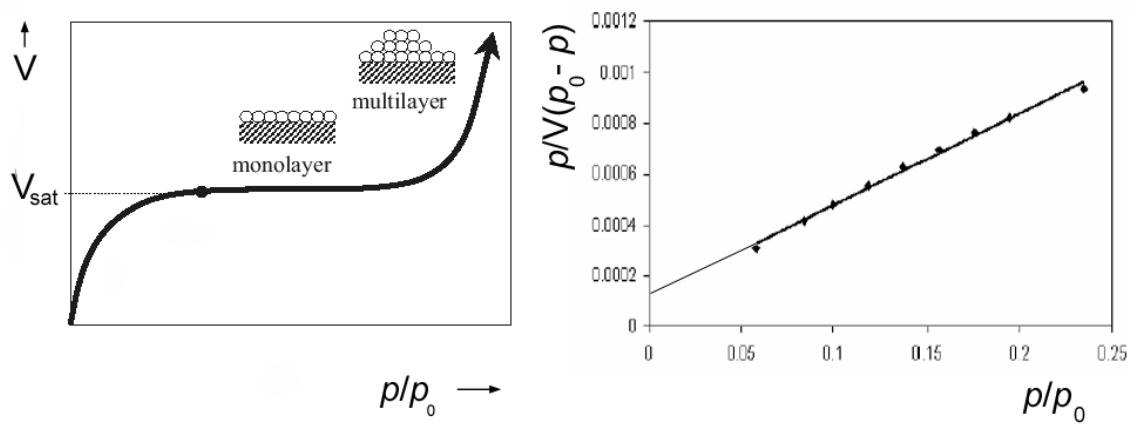

Figure 2.2. BET isotherm (i.e. Type II) in schematic presentation view typically observed for non-porous material (left) [2] and linearized form of BET isotherm used to determine surface area (right) [3].

2.2.1.2. Heat of adsorption

The heat of adsorption can be measured by calorimetric methods. The technique is based on monitoring the changes in the heat flux at constant temperature. The measurement is usually done by a differential scanning calorimeter (DSC) as being one of the most sophisticated methods to determine the enthalpy change. The instrument scans the temperature of the sample and reference material during the analysis and the temperature of the sample changes is significantly relative to that of the reference material if a chemical or physical process involving heat transfer occurs in the sample during the scan. The heat of adsorption is calculated from the integral area of DSC signal, multiplied by sorbate molecular weight and divided to mass difference of each step. The increase area in DSC signal is proportional to the increase in heat of adsorption as presented in the following equation:

$$\Delta H^0 = \int_{T_1}^{T_2} C_p dT \qquad (2.9)$$

where C_p (mJ/K) is the heat capacity at constant pressure, T_1 and T_2 are the temperatures at which the process begins and ends, respectively.

Another way to obtain the heat of adsorption is by using isosteric method which comes from Langmuir isotherms of various applied temperatures. The equation is derived from the Langmuir isotherm:

$$KP = \frac{\theta}{1-\theta} \tag{2.10}$$

Therefore, when θ is constant, the logarithmic equation gives:

$$\ln K + \ln P = const. \tag{2.11}$$

The Gibbs energy $\Delta G = \Delta G^0 + RT \ln K$ is zero at equilibrium, i.e., $\Delta G = 0$. The standard Gibbs energy, ΔG^0 can be described by:

$$\Delta G^0 = \Delta H^0 - T\Delta S^0 \tag{2.12}$$

The equation can be rewritten in the form:

$$\frac{\Delta G^0}{T} = \frac{\Delta H^0}{T} - \Delta S^0 \tag{2.13}$$

The differentiation subsequently derives the equation known as the Gibbs-Helmholtz with the form:

$$\frac{d\left(\Delta G^0/T\right)}{dT} = -\frac{\Delta H^0}{T^2} \tag{2.14}$$

where ΔH^0 is the standard enthalpy at the temperature T.

The differentiation of $\ln P$ with respect to temperature from equation 2.11 with relation to standard Gibbs energy then gives:

$$\frac{d \ln P}{dT} = -\frac{1}{R} \frac{d\left(\Delta G^0 / T\right)}{dT} \tag{2.15}$$

Substituting equation 2.15 into 2.13 gives formula:

$$\frac{d \ln P}{dT} = \frac{\Delta H^0}{RT^2} \tag{2.16}$$

with $d\left(1/T\right)/dT = -1/T^2$ rearranged into $dT = -T^2 d(1/T)$, the substitution into equation 2.16 gives the expression of Clausius Clapeyron equation as presented below. Figure 2.3 shows the applicability of this method for determining enthalpy change of benzene during the sorption with zeolite:

$$\left[\frac{d \ln P}{d\left(1/T\right)}\right]_q = -\frac{\Delta H^0}{R} \tag{2.17}$$

2.2.2. IR spectroscopy

Infrared (IR) spectroscopy is a well-known method for investigating the surface composition of a solid or liquid material. The study involving sorption of gases on the surface may also be carried out within IR spectroscopy since the instrument is applicable towards *in situ* technique. In catalysis, IR spectroscopy is used to identify the sorbed species classifying the chemisorption or physisorption interaction on a catalyst surface. The technique is based on molecule that possesses discrete levels of rotational and

vibrational energy which can be detected after transmission absorption of photons in the range of IR frequencies.

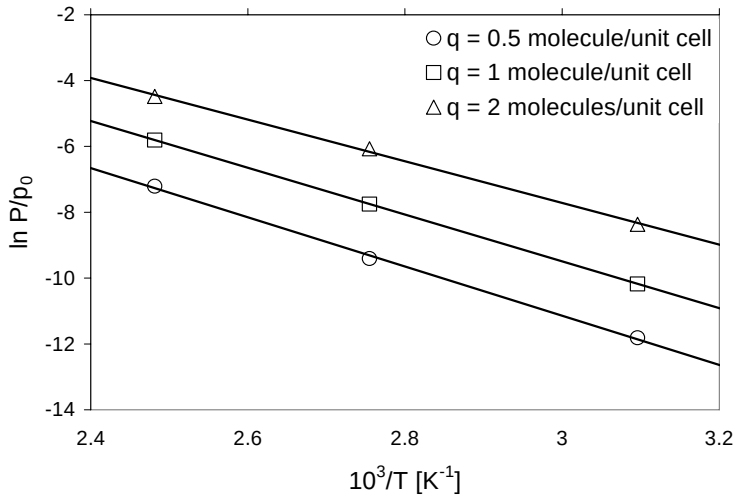

Figure 2.3. The isosteric heat of adsorption can be obtained from the slope of the plot of ln P/p_0 against 1/T as measured from Langmuir isotherm with various temperatures. The sorption of benzene on HZSM-5 gives an average ΔH^0 of 57 kJ/mol.

The IR beam is developed from a radiation source (e.g. SiC glowbar, Hg and Tungsten lamp) and passed to a beam splitter before transmitted into the sample. This electromagnetic spectrum can be divided into three regions, the near-, mid- and far- infrared. The far IR (FIR) has low energy and is lying adjacent to the microwave region (400-10 cm^{-1}), middle IR (MIR) is useful to study the fundamental of vibrations and associated rotational-vibrational structure (4000-400 cm^{-1}), while the near IR (NIR) has high energy and can excite overtone or harmonic vibrations (10000-4000 cm^{-1}) [4, 5].

For the sorption measurement, IR cell with geometry for transmission spectroscopy was designed and attached to a high vacuum system as the apparatus scheme is depicted in Figure 2.4. The partial pressure of sorbate may be introduced into the system and IR spectrum was normally recorded

after an equilibrated pressure is established. The partial pressure of sorbate can be manually varied through a stepwise opening of dosing valve.

The IR study using zeolites as sorbent has been generally focusing on the interactions with hydroxyl groups along with its framework structure. Their stretching and deformation vibrations can be detected in the middle IR range (4000-400 cm^{-1}) in which the spectrum, for instance could significantly separate the hydroxyl groups bands of bridging and terminal site. The terminal silanol and Brønsted bridging hydroxyl groups commonly appear at wavenumber 3745 and 3610 cm^{-1}, respectively. The introduction of basic compounds as probe/sorbate molecule (e.g. linear hydrocarbons and aromatics) may decrease the intensity of those bands since the hydroxyl groups have been active as acidic site. These molecules also exhibited several peaks due to C-H stretching vibration, C-C (or ring) deformation vibrations.

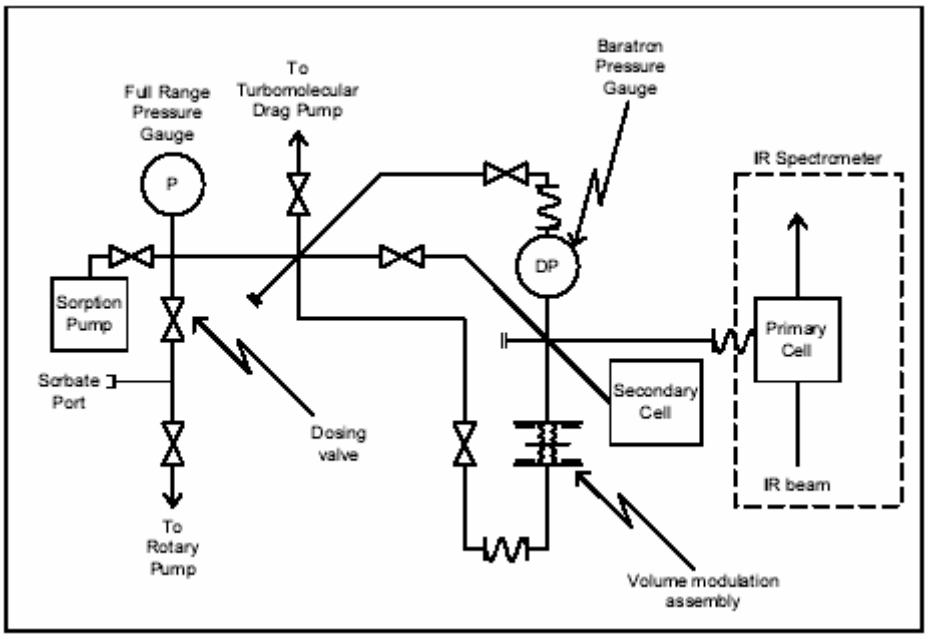

Figure 2.4. Schematic diagram of the apparatus for IR spectroscopy. The setup is also applied for the measurement of frequency response. Note that secondary cell is used for measuring frequency response [6].

In order to perform transmission absorption on zeolites, a sample as initially in powder form must be pressed into a self-supporting wafer. The thickness of wafer cannot be accurately controlled and determined, therefore such a quantitative data shall be extracted from experiments by applying spectral normalization of different types of wafer thickness. For many zeolites, this can be done using the intensity of the lattice vibration overtone bands. In HZSM-5, these bands occur between 2100 and 1740 cm^{-1}. A typical IR spectrum of HZSM-5 showing hydroxyl groups stretching vibration bands as well as the lattice vibration bands can be seen in Figure 2.5, while the wavenumber ranges from the sorption of aromatic in HZSM-5 as implemented for the purpose of integrating considerable band area are tabulated in Table 2.1.

2.3. Transport measurement

2.3.1. Fast time-resolved (rapid scan) IR spectroscopy

To follow the transport processes of aromatic molecules onto the surface of MFI zeolites, kinetic measurement was conducted and implemented on IR spectroscopy. The measurement is based on perturbation of molecules in an equilibrium sorption assuming the reversibility of adsorption-desorption processes. During experiment, the volume was modulated in closed chamber to bring those processes and since the mass transport in micropores occurs typically in the time of milliseconds, the spectral recordings were adjusted and synchronized in a fast-time resolution. Thus, slope from the adsorption uptake of molecules in correspondence to interacted site provides the information on the kinetic properties of molecular transport. The technique is termed as fast time-resolved (rapid scan) IR spectroscopy and originated as well as

developed in the group of Prof. J. A. Lercher. The following sections describe on apparatus setup, spectral recording principle and data analysis.

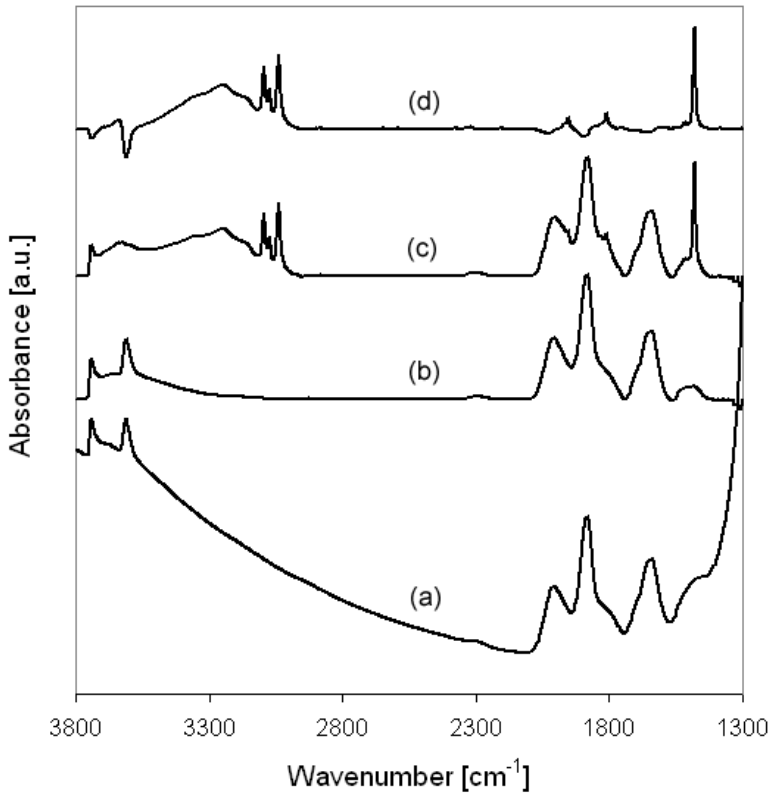

Figure 2.5. IR spectra of activated HZSM-5 as applying (a) non baseline correction, (b) baseline correction and IR spectra of benzene adsorbed on HZSM-5 (ca. P = 1 mbar) as applying (c) non-subtraction, (d) substraction (difference) with respect to activated spectra.

2.3.1.1. Apparatus setup

The setup apparatus of *in situ* IR spectrometer is depicted in Figure 2.4. The additional part on instrument for kinetic measurement involves magnetically driven separator plate that is attached in the middle of sorption chamber of UHV system. This magnet plate is sealed by a pair of flexible UHV metal bellow and used for the generation of periodic variations of the

equilibrium partial pressure of probe molecules, hence changing the total volume of the entire system (Figure 2.6). These periodic pressure/volume modulations allowed the observation of molecular adsorption and desorption processes for a given sample. The total volume of the system can be varied by ±5% resulting, for instance a relative pressure modulation of $\pm 1.0 \times 10^{-2}$ mbar from the equilibrium partial pressure of 2.0×10^{-1} mbar. Only such a small pressure perturbation was applied during the experiments in order to minimize the adiabatic effects resulting from compression and expansion of the gas and from the heat of adsorption during the periodic adsorption and desorption processes.

Table 2 .1. Typical wavenumber range from the sorption of aromatic on HZSM-5 [7].

Sorbate	Wavenumber range [cm^{-1}]			
	ν_{OH} (SiOH)	ν_{OH} (SiOHAl)	ν_{C-H}	δ_{C-C}
Benzene	3700-3764	3577-3640	3006-3121	1422-1517
Toluene			2844-2959	1475-1542
p-Xylene			2819-2970	1481-1539

2.3.1.2. Spectral recording principle

The fast time-resolved (rapid scan) IR spectroscopy is applied by utilizing the possibility of accumulating the reversible adsorption and desorption processes which are induced from the periodic changes in pressure or volume. As the time needed to observe the transport processes is more than 2 orders of magnitude faster than the real time scale, in principle the rates can be calculated by assuming immediate or initial (stepwise) coverage changes. In order to precisely analyze the kinetic data, it is required to collect spectra with high time resolution and an excellent signal-to-noise ratio. Since the mass

transport occurs typically within milliseconds timescale, maximum time resolution had been attempted, while the fast-time spectral recordings shall be performed and depending on the number of interferograms which are significant to obtain acceptable signal-to-noise ratio spectra.

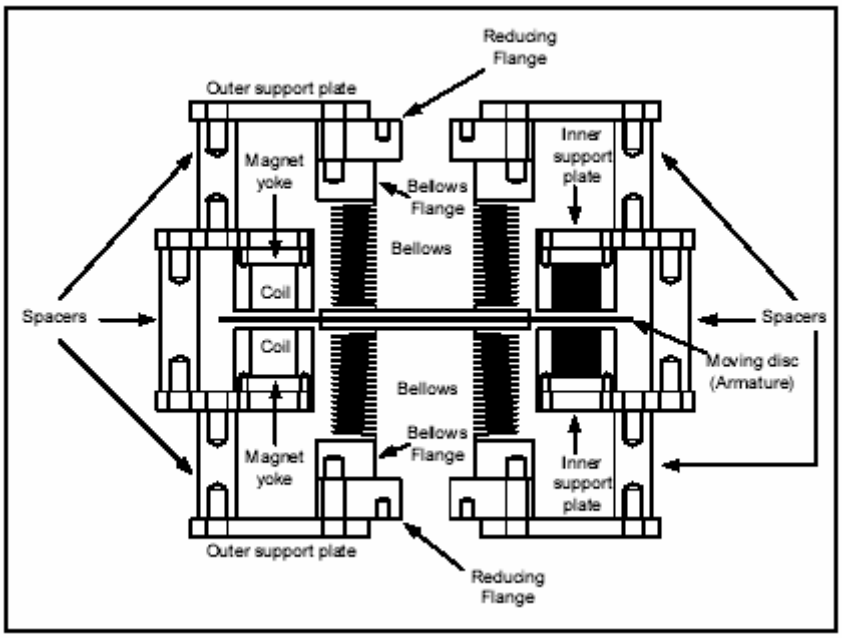

Figure 2.6. Schematic diagram of magnet plate assembly for fast time-resolved (rapid scan) IR spectroscopy and frequency response [6].

It is important to emphasize that the signal-to-noise ratio is increased by co-adding the spectra which were recorded after a certain time and resulting a series of spectra with individual pressure variations. For the performed experiment which results an acceptable data, 4000 interferograms were required with a total time of 60 s for each volume modulation. As the individual interval is divided by 100 spectra, time resolution was 600 ms. For each interval, 10 interferograms were collected with a scan rate of 16.67 scan.s^{-1} and spectral resolution of 8 cm^{-1} which temporarily stored in a buffer file. The volume modulation was repeated 400 times to obtain the required number of interferograms. The spectral co-addition yields a series of fast time-resolved

(rapid scan) spectra with signal-to-noise ratio comparable to that of IR spectra consisting of 4000 interferograms. This experiment is equivalent to a total measurement time for a single spectrum of 240 s. The fast time-resolved (rapid scan) IR spectra (e.g. sorption of benzene on H/ZSM-5) can be seen as three-dimensional graph as depicted in Figure 2.7. The coverage changes of specified site such as in the bridging hydroxyl groups were integrated to result interpretation on molecular adsorption and desorption which corresponds to the kinetic rate properties.

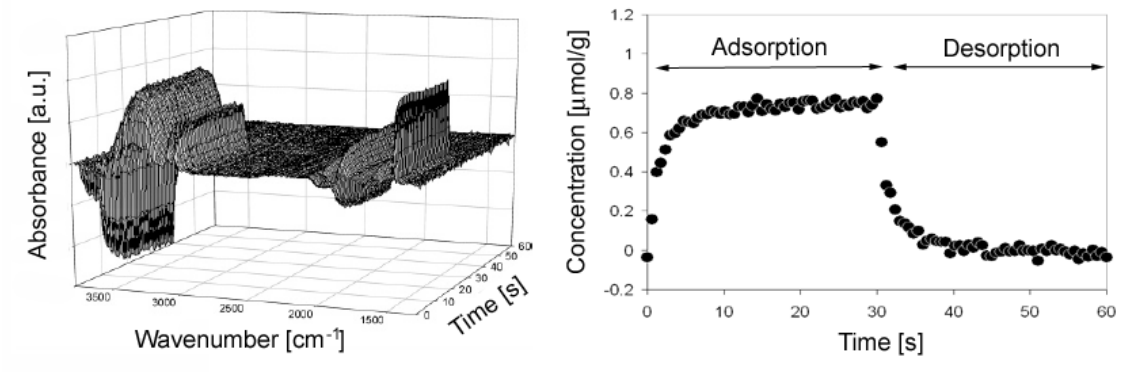

Figure 2.7. Three-dimensional IR spectra as obtained from fast time-resolved (rapid scan) IR spectroscopy (left) and integral result of coverage changes of the bridging hydroxyl groups (right) after benzene adsorbed on HZSM-5 [8].

2.3.1.3. Data analysis

In order to determine the rate of the sorption process, the changes in the coverage of the hydroxyl groups of interest, $\Delta c_{OH}(t)$ during adsorption and desorption in the modulation experiment were fitted using the following exponential equations:

for $0 < t \leq t_p/2$ (adsorption process)

$$\Delta c_{OH}(t) = \Delta c_{OH,eq}\left(1 - e^{-t/\tau_{ad}}\right) \tag{2.18}$$

for $t_p/2 < t < t_p$ (desorption process)

$$\Delta c_{OH}(t) = \Delta c_{OH,eq} e^{-\left[t-\left(t_p/2\right)\right]/\tau_{de}} \tag{2.19}$$

with $\Delta c_{OH,eq}$ being the change of surface concentration of the adsorbing molecules after having reached the new equilibrium after the pressure step. The characteristic time constants of the transport process during the adsorption and desorption are given by τ_{ad} and τ_{de} respectively. As the process is to be first order in the sorbate, it can be assumed that τ is equivalent to $1/k$, so a small time constant τ corresponds to a high rate constant.

2.3.2. Frequency response

Frequency response (FR) is a method to study the kinetic of mass transfer phenomena in gas-surface. The method is able to separate various rate processes which occur simultaneously. In principle, FR is performed based on wide range of frequencies modulations on an ideal gas that is perturbed on solid surface in a closed system. The differences of pressure response between perturbed gas and single gas yields so called “rate spectrum”, where the characteristic functions may derive diffusion coefficients [9, 10].

The sorbate-zeolite system is one of the examples in which at equilibrium, the pressure response differs from that of the single sorbate system. When comparing the sorbate-zeolite and single sorbate system, the increase or decrease of pressure leads to a change in amplitude and the

diffusion of the sorbate molecules in or out of the zeolite micropores delays the attainment of the new equilibrium which results to a phase difference (i.e. phase lag) [11]. By knowing these effects, it should be emphasized that the relaxation processes under such circumstances might involve several possible transport steps such as molecular transport from the gas phase to the surface, the pore entering process and the diffusion into the channels. The example of pressure response applying square and sinusoidal wave can be seen in Figure 2.8.

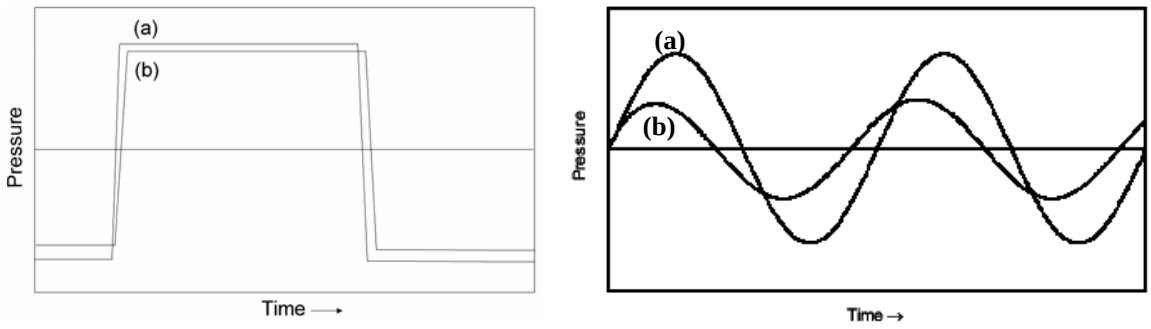

Figure 2.8. Pressure response of a closed system to a square (left) and sinusoidal wave (right) modulation in (a) a cell containing single sorbate and (b) a cell containing both sorbate and zeolite [6].

A change in amplitude and phase as the characteristic functions of frequency response allowed an estimation on diffusivity which can be derived from several transport models. The diffusion coefficient of gaseous sorbate molecules in zeolite pores may be derived based on solution of Fick's law with respect to periodic square or sinusoidal wave of surface concentration modulation. The equations of frequency response were basically derived using complex harmonic notations and expressed as [9]:

$$V(t) = V_{eq}\left(1 - \gamma_V e^{i\omega t}\right) \tag{2.20}$$

$$P(t) = P_{eq}\left(1 + \gamma_P e^{i(\omega t+\phi)}\right) \tag{2.21}$$

$$C(t) = C_{eq}\left(1 + \gamma_C e^{i(\omega t+\phi-\psi)}\right) \tag{2.22}$$

with

$$e^{i\omega t} = \cos\omega t + i\sin\omega t \tag{2.23}$$

where $V(t)$, $P(t)$ and $C(t)$ are the volume, pressure and concentration with the function of time, respectively. γ_V, γ_P, γ_C are the relative amplitude of the volume, pressure and concentration, respectively. ω is the angular frequency, while ϕ and ψ are phase differences where ϕ is termed phase lag. The subscript *eq* stands to condition at equilibrium.

Multiple diffusion processes may also occur in a system. This might due to the presence of multiple sorbents in the solid phase, multiple sorbates in the gas mixtures or multiple state of mobility (e.g. straight and sinusoidal pores of MFI) [12, 13]. When the specific interaction between respective diffusion processes is negligible, treatment of the formula can be extended using only sum of the processes.

2.3.2.1. Diffusion in infinite plane sheet

With the infinite plane sheet model, molecules diffuse only in one direction perpendicular to the surface and Fick's law can be expressed assuming plane sheet of thickness 2L as follows:

$$\partial C/\partial t = \partial/\partial x\left[D(C)\,\partial C/\partial x\right] \tag{2.24}$$

where *x* is the depth coordinate within planar sheet. If the volume modulation is a small percentage of total volume, the concentration gradient will also be small therefore diffusion coefficient can be assumed to be constant. Thus, equation may be rewritten as:

$$\partial C/\partial t = D\left(\partial^2 C/\partial x^2\right) \tag{2.25}$$

Since the system is closed, the material balance during volume modulation leads to:

$$\frac{d}{dt}\left(\frac{PV}{MRT}\right)+\frac{dC}{dt}=0 \tag{2.26}$$

Substituting equation 2.20, 2.21., 2.22 and considering complex equation 2.23 as well as 2.25 into equation 2.26, the characteristic functions of frequency response can be obtained [14]:

$$(\gamma_B/\gamma_S)\cos\phi_{S-B}-1=\sum_{j=1}^{n}K_j\delta_{c,j} \tag{2.27}$$

$$(\gamma_B/\gamma_S)\sin\phi_{S-B}=\sum_{j=1}^{n}K_j\delta_{s,j} \tag{2.28}$$

with

$$\delta_c=\frac{1}{\eta}\left[\frac{\sinh\eta+\sin\eta}{\cosh\eta+\cos\eta}\right] \tag{2.29}$$

$$\delta_s=\frac{1}{\eta}\left[\frac{\sinh\eta-\sin\eta}{\cosh\eta+\cos\eta}\right] \tag{2.30}$$

$$\eta = \sqrt{\omega L^2 / 2D} \tag{2.31}$$

$$K = \frac{\left(RT_0 / V_{eq}\right)}{\left(dQ_{eq} / dP_{eq}\right)} \tag{2.32}$$

where ϕ_{S-B} is the difference between the phase lags in the presence and absence of the zeolite, ω is angular frequency of the volume modulation, D is the diffusion coefficient, L is the thickness of planar sheet, γ_B and γ_S are relative amplitudes of the pressure during the volume change in the absence and in the presence of zeolite, respectively. K is a constant related to the gradient of the adsorption isotherm at the equilibrium partial pressure, P_{eq}. Other parameters included to define K are T_0 the temperature, V_{eq} the system volume, Q_{eq} the equilibrium amount sorbed.

Equation 2.27 and 2.28 are commonly named as in-phase and out-of-phase characteristic function, respectively. The diffusion coefficient is obtained based on the fitting of characteristic functions with the left hand side equation as derived from mass transport model (Figure 2.9). The planar sheet model shows that the characteristic functions are depending on η that comprise D, L and ω.

2.3.2.2. Other diffusion models

Various diffusion models subjected to different characteristic functions for frequency response has been proposed and developed. For example, the models have been applied as diffusion in cylinder, sphere and parallelpiped [10]. Diffusion in sphere has been implemented and become a model for

investigating the three-dimensional channels in zeolites. The diffusion coefficient of krypton on sodium mordenite was investigated and showing fine agreement with the one estimated by theoretical approach [14]. However, neither sphere nor plane model represents the true crystal morphology of porous material. Thus, a model has been developed for diffusion in parallelpiped which can be used to explain cubic, rhombic or coffin-shaped crystals. The diffusivity of n-butane and 2-butane in coffin or parallelpiped-shaped Silicalite-1 was measured using this method [15, 16].

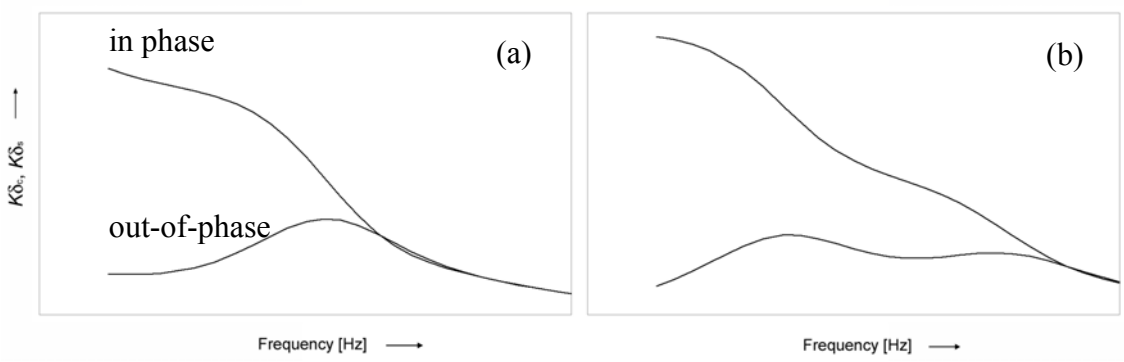

Figure 2.9. Comparison of (a) single and (b) double plane sheet diffusion models typically applied for the sorption of aromatic on zeolites.

References

1. Atkins, P. W, de Paula, J, *Atkins' Physical Chemistry*, Oxford University Press: Oxford, **2002**.
2. Chorkendorff, I., Niemantsverdriet, J. W., *Concepts of Modern Catalysis and Kinetics*, Wiley-VCH: Weinheim, **2003**.
3. Mukti, R. R., *MSc. Thesis*, Universiti Teknologi Malaysia, **2003**.
4. Hunger, M., *Microp. Mesop. Mater.*, **2005**, 82, 241.
5. Lercher, J. A., Grundling, C., Mirth, G. E., *Catal. Today*, **1996**, 27, 353.

6. Heydenrych, H. R., *MSc. Thesis,* University of Cape Town, **2000**.
7. Tanaka, H. *PhD. Thesis*, Tokyo Institute of Technology, **2005**.
8. Jentys, A., Tanaka, H. Lercher, J. A., *J. Phys. Chem. B*, **2005**, 109, 2254.
9. Yasuda, Y., *J. Phys. Chem*., **1976**, 80, 1867.
10. Yasuda, Y., *Heterogen. Chem. Rev*., **1994**, 1, 103.
11. Yasuda, Y., *J. Phys. Chem.*, **1976**, 80, 1870.
12. Song, L. J., Rees, L. V. C., *Microp. Mesop. Mater*., **2000**, 35, 301.
13. Zheng, S., Tanaka, H., Jentys, A., Lercher, J. A., *J. Phys. Chem. B*, **2004**, **108**, 1337.
14. Yasuda, Y., *J. Phys. Chem*., **1982**, 86, 1913.
15. Shen, D. M., Rees, L. V. C., *Zeolites*, **1991**, 11, 684.
16. Oprescu, D., Rees, L. V. C., Shen, D. M., *J. Chem. Soc. Faraday Trans*., **1992**, 88, 2955.

Chapter 3

Energetic and entropic contributions controlling the sorption of benzene in zeolites

3. ENERGETIC AND ENTROPIC CONTRIBUTIONS CONTROLLING THE SORPTION OF BENZENE IN ZEOLITES

3.1. Abstract

The energetic and entropic contributions controlling the sorption of benzene on acidic (HZSM-5) and non-acidic (Silicalite-1) MFI type materials were studied using gravimetry, calorimetry and *in situ* IR spectroscopy to follow the qualitative and quantitative interactions of benzene with the pores and the functional SiOH and SiOHAl groups. The model derived to describe the adsorption isotherms indicates the presence of sterically constrained sorption structures for benzene in MFI type materials. The interaction of benzene with the pore walls controls the sorption energetically, while the localized interaction with the bridging hydroxyl groups contributes only to a minor degree. If benzene is located close to SiOHAl groups perturbed hydroxyl groups are formed. Their wavenumber reflects the local sorption geometry of benzene as well as the acid strength of the hydroxyl group and the base strength of benzene. Two perturbed hydroxyl groups were observed for benzene adsorbed, which are assigned to two orientations of the molecules inside the pores, i.e., with the ring parallel to the pore wall and with the ring being oriented towards the bridging hydroxyl groups. At higher coverage benzene adsorbs at SiOHAl groups additionally in an unconstrained environment, most probably at the pore openings.

3.2. Introduction

Solid acids and bases, such as zeolites, are typically characterized by the type (Brønsted, Lewis), the concentration (extensive factor of acidity) and the strength of the acid/base sites (intensive factor of acidity) [1]. Type and concentration of acid sites are primarily controlled by the location of the Al atoms at framework (tetrahedral positions) and non-framework positions and by the concentration of Al in tetrahedral sites of the zeolite [2], while the strength is at large controlled by the chemical composition and, hence, the polarity of the lattice [3]. The strongest Brønsted acid sites are formed with isolated Al-O tetrahedra. With increasing Al concentration the strength of Brønsted acid sites gradually decreases. Barthomeuf [4] showed that the acid strength starts to decrease markedly as the Al concentration in the lattice exceeds 15 mol % agreeing excellently with theoretical calculations of Jannsens *et al.* [5].

Numerous methods such as temperature programmed desorption of bases [6, 7], sorption of pyridine (followed by IR spectroscopy or gravimetry) [8-10], NMR [11-13], XPS [14-16] and test reactions [17-19] have been used to determine the concentration and type of these acid sites. In contrast to acids in a aqueous environment, in which (hydrated) H_3O^+ is the strongest acid [20, 21], for surface gas reactions solid acids exhibit a wide variety of acid sites with a broad distribution of acid strength. Thus, the interaction and proton transfer of the acid base pair formation has to be probed directly.

Strictly, the acid strength of a surface group is defined by the interaction with a particular and specific base. Depending upon the nature of the acid-base pair this involves proton transfer or not. Thus, acid site concentrations of solids can be measured by sorption of bases ranging from strong bases, such as ammonia or pyridine, to weak bases such as benzene or alkanes with polarizable C-H bonds. If the interactions can be differentiated according to their strength, conceptionally, the acid site distribution can be measured [22]. However, the situation is more complex. The strength of interaction will depend not only on the intrinsic electron pair acceptor (EPA) and donor (EPD)

properties of the participating acid and base groups, it will also depend on the stabilization energy of acid base pair formed in case of proton transfer and – in case of steric constraints – whether or not the optimum EPA-EPD bond length can be established.

In order to avoid complications by proton transfer during ion pair stabilization the more subtle spectroscopic monitoring of the polarization of the OH groups by moderately strong and weak bases has been even more popular than the direct measurement of the interaction strength. For this, one uses the perturbation of the OH groups of the oxide/zeolite, i.e., the disappearance of the band of the free OH group and the appearance of a perturbed OH group at lower wavenumbers. At large, the relation holds that a stronger downward shift points to a stronger interaction of the OH group with the base. For a given base this points to increasing acid strength [23]; while for a given oxide and hydroxyl group it points to an increasing basic strength of the sorbent [24, 25] This approach eliminates the complication of the ion pair stabilization energy, however, sterical constraints play an even larger role as the weaker acid-base interaction makes it even more susceptible to steric influences.

Benzene is one of the most frequently used probe molecule for the evaluation of the acid/base properties of zeolites and in particular for the strength of the Brønsted acidic bridging hydroxyl groups [26-28]. The sorption of benzene was experimentally studied by IR spectroscopy following the changes in the out of plane CH vibrations of benzene [28, 29] as well as the perturbation of the hydroxyl groups [30-35], by neutron scattering using deuterium exchanged benzene [36, 37], by Raman spectroscopy [38] and by measuring gravimetric adsorption isotherms combined with calorimetry [39-41]. We would like to discuss here the significant complexity arising from the local steric constraints, when one uses benzene as probe molecule for a medium pore size (10 membered ring) zeolite, e.g., of MFI type. On this material the interaction of benzene with Brønsted acid sites results in two perturbed

hydroxyl groups, which were assigned to the presence of different types of Brønsted acid sites [30] or to different sorption structures [34].

For MFI type materials, such as ZSM-5 and Silicalite-1, loadings of up to 8 benzene molecules per unit cell have been reported [42]. At loadings up to 4 molecules per unit cell, benzene is located at the channel intersections [43] and with increasing loading also positions in the channel segments are occupied [38]. For loadings below 4 molecules per unit cell, the heat of adsorption for benzene in HZSM-5 is approximately 55-60 kJ/mol. At higher loadings, intermolecular interactions between the benzene adsorbed molecules typically lead to an increase in the heat of adsorption and to reorientations of the molecules within the channels [39].

Theoretical calculations (on DFT level) predict that benzene interacts *via* the π-electrons with the protons of the zeolite. In general, two orientations are suggested, i.e., one, in which the proton points to the benzene ring and the molecule is oriented parallel (or slightly tilted) towards the pore wall [44] and another with an orientation of the acid proton towards a single C atom or a single C-C bond of the ring [45, 46]. The latter sorption structure was identified as a possible transition state in reactions of benzene on the acid sites [44, 45, 47]. Both structures were also reported for the sorption of benzene in mordenite and the formation of two perturbed hydroxyl groups with a shift of $\Delta\nu_{SiOHAl}$= 317 and 287 cm^{-1} was predicted for the sorption of benzene with the ring and with an edge oriented towards the acid hydroxyl group [48]. Note that a study that does not recognize this effect would conclude that two acid sites with quite significant difference in strength should exist.

In this chapter, we focus on the energetic and entropic contributions controlling the sorption of benzene on acidic (HZSM-5) and non-acidic (Silicalite-1) MFI type materials. The heat of adsorption and the loading is used to describe the energetic contribution of the localized interaction between the benzene molecules and the protons. The perturbation of the hydroxyl groups

after sorption of benzene is used to differentiate between the sorption structures and to identify sterically constrained sorption geometries.

3.3. Experimental

3.3.1. Materials

HZSM-5 (Si/Al = 82) and Silicalite-1 (Si/Al = ∞) were used for the experiments. The concentrations of bridging hydroxyl (SiOHAl) and silanol groups (SiOH), determined from ^{1}H-MAS NMR spectroscopy were 0.09 and 0.12 mmol/g for SiOH and SiOHAl groups of HZSM-5 and 0.05 mmol/g for the SiOH groups on Silicalite-1.

3.3.2. Thermogravimetry

The adsorption isotherms for benzene were measured on a Setaram TG-DSC 111 thermoanalyzer. The sample (~20 mg) was activated at 823 K for 1 h (heating rate 10 K.min^{-1}) under vacuum ($p < 10^{-7}$ mbar). Benzene was adsorbed at 323, 363 and 403 K using stepwise pressure increases (steps of 0.01-0.02 mbar) up to 13 mbar and the weight increases as well as the corresponding heat fluxes were measured.

3.3.3. IR spectroscopy

The samples were prepared as a self supporting wafers (weight ~10 mg/cm^2) and activated under vacuum (<10^{-7} mbar) at 823 K (heating rate 10 K.min^{-1}) for 1 h. Benzene, was adsorbed at 323, 343, 363 and 403 K with equilibrium pressures between 10^{-3} and 1 mbar. To directly compare the surface coverage of the adsorbed species all spectra were normalized using

the overtone and combination vibrations of the MFI between 2105 and 1740 cm^{-1} after activation. The coverage of benzene on the SiOH and SiOHAl groups was calculated from the decrease of the intensity of the corresponding OH bands. The intensities of the two (overlapping) perturbed hydroxyl groups at 3350 and 3250 cm^{-1} were determined after a peak deconvolution using a Gauss-Lorenz peak-shape (Gauss/Lorenz ratio = 1:1).

3.4. Results

The adsorption isotherms of benzene on HZSM-5 and Silicalite-1 measured by thermogravimetry at 323, 363 and 403 K and the heat of adsorption as function of the coverage determined by calorimetry are compared in Figure 3.1 and 3.2. With p^* being the partial pressure of benzene normalized to standard conditions (i.e. $p^*=p/p^0$). At all temperatures studied, the sorbed amounts of benzene on HZSM-5 were slightly higher compared to Silicalite-1. At low benzene coverage (<0.5 molecules/unit cell) the heat of adsorption dropped from initial values of above 70 kJ/mol to 60 kJ/mol for HZSM-5 and to 55 kJ/mol on Silicalite-1 and at a coverage above 1 molecules per unit cell the heat of adsorption was the same on both materials (55 kJ/mol). The high heat of adsorption at low coverage results from the interaction of benzene with defect sites and/or very strong Lewis acid sites, which are present in both samples at minor concentrations. The calculation of the isosteric heat of adsorption from the isotherms using coverages of 0.5, 1 and 2 molecules per unit cell (Equation 1) led to a heat of adsorption of 57 kJ/mol and 56 kJ/mol for HZSM-5 and Silicalite-1, respectively, which is in perfect agreement with the values determined by calorimetry.

$$\left(\frac{\Delta \ln p^*}{\Delta \frac{1}{T}} \right)_{q\ const} = -\frac{\Delta H^0_{ads}}{R} \qquad (3.1)$$

In Equation 1 p^* is the partial pressure of benzene normalized to standard conditions (i.e. $p^*=p/p^0$), T the temperature [K], ΔH^0_{ads} the standard heat of adsorption [kJ/mol] and R the gas constant.

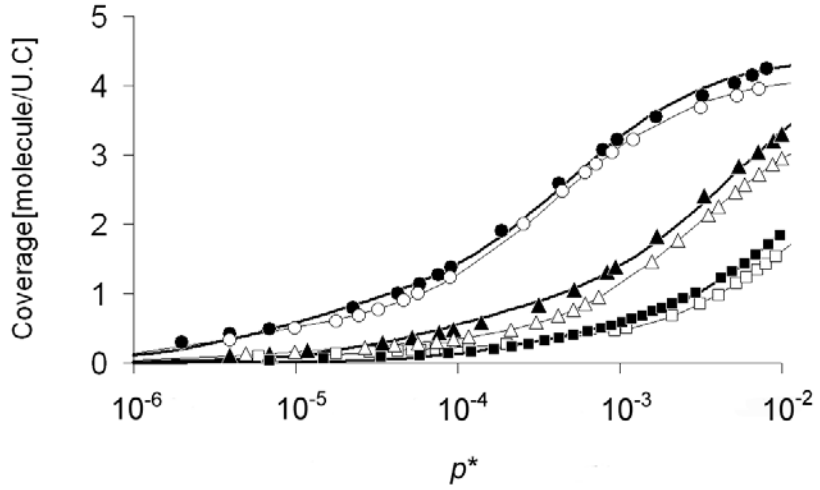

Figure 3.1. Adorption isotherms of benzene from calorimetry on HZSM-5 (full symbols) and Silicalite-1 (open symbols) at (●,○) 323, (▲,Δ) 363 and (■,□) 403 K.

The IR spectra of the activated samples are compared in Figure 3.3. On both materials silanol groups at the outer surface at 3745 cm^{-1} were observed. The broadening of this band at lower wavenumbers indicates the presence of SiOH groups at defect sites, typically observed at 3725 cm^{-1}. For HZSM-5 hydroxyl groups at 3660 and 3610 cm^{-1}, assigned to OH groups on clustered extra-framework aluminum oxide species and to SiOHAl groups (Brønsted acid sites), respectively, were observed.

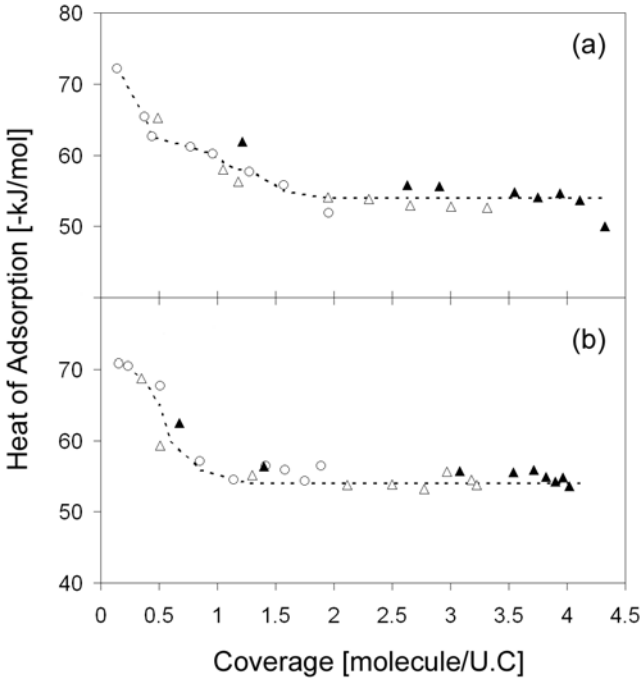

Figure 3.2. Differential heat of adsorption of (a) HZSM-5 and (b) Silicalite-1 from calorimetry at (▲) 323, (Δ) 363 and (○) 403 K.

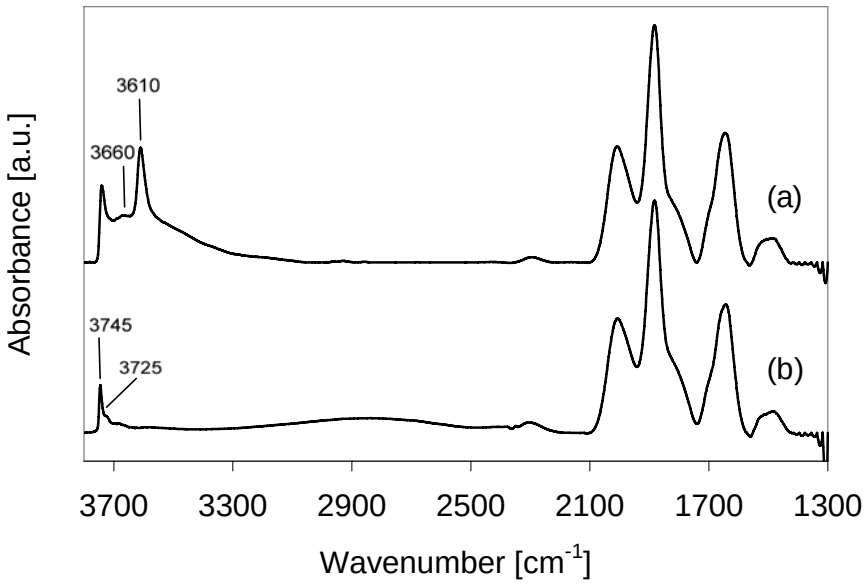

Figure 3.3. IR spectra of activated (a) HZSM-5 and (b) Silicalite-1.

The changes in the IR spectra after sorption of benzene with partial pressures between 10^{-3} and 1 mbar at 323 and 403 K are compared in Figures 3.4 and 3.5 for HZSM-5 and at 323 K for Silicalite-1 in Figure 3.6. The spectra show the differences between the IR spectra after sorption of benzene and the activated samples. Therefore, only the changes in the spectra are observed, i.e., bands decreasing in intensity are negative, band increasing in intensity are positive. For HZSM-5, the intensities of hydroxyl groups at 3745, 3725, 3660 and 3610 cm^{-1} decreased during the sorption of benzene. Bands of adsorbed benzene were observed at 3092, 3074, 3039 (CH stretching vibrations), at 1969, 1952, 1855 1830 and 1810 cm^{-1} (out of plane CH deformation vibrations, region enlarged in the insert) and at 1477 cm^{-1} (C-C stretching vibration) [49]. On both materials CH out of plane deformation vibrations at 1954 and 1815 cm^{-1}, characteristic for liquid benzene, were observed at high loadings. The band at 1855 cm^{-1}, also observed with both materials, is assigned to the interaction of benzene with the zeolite pore walls and the bands at 1969 and 1830 cm^{-1}, observed only on HZSM-5, result from the strong polarization of the π-electrons of the aromatic ring during the interaction with the protons of the zeolite [28]. The sorption of benzene on the hydroxyl groups of HZSM-5 led to a perturbed hydroxyl band at approximately 3610 cm^{-1} and to three (overlapping) perturbed hydroxyl bands at 3350, 3250 and 3170 cm^{-1}, resulting from the hydrogen bonding interaction between the aromatic ring and the SiOH or SiOHAl groups, respectively. The perturbed hydroxyl group at 3170 cm^{-1} was only observed for benzene partial pressures exceeding 10^{-1} mbar and at temperature lower than 403 K. The appearance of up to three perturbed groups at $\Delta\nu_{SiOHAl}$= 250, 350 and 440 cm^{-1} from a single bridging hydroxyl group either indicates the presence of (energetically and/or geometrically) different sorption structures for benzene in HZSM-5 on a particular type of hydroxyl group [30] or an inhomogeneous acid strength of the SiOHAl groups [50, 51]. On Silicalite-1 the intensity of the SiOH groups decreased after sorption of benzene and a perturbed hydroxyl group at 3600 cm^{-1} was formed.

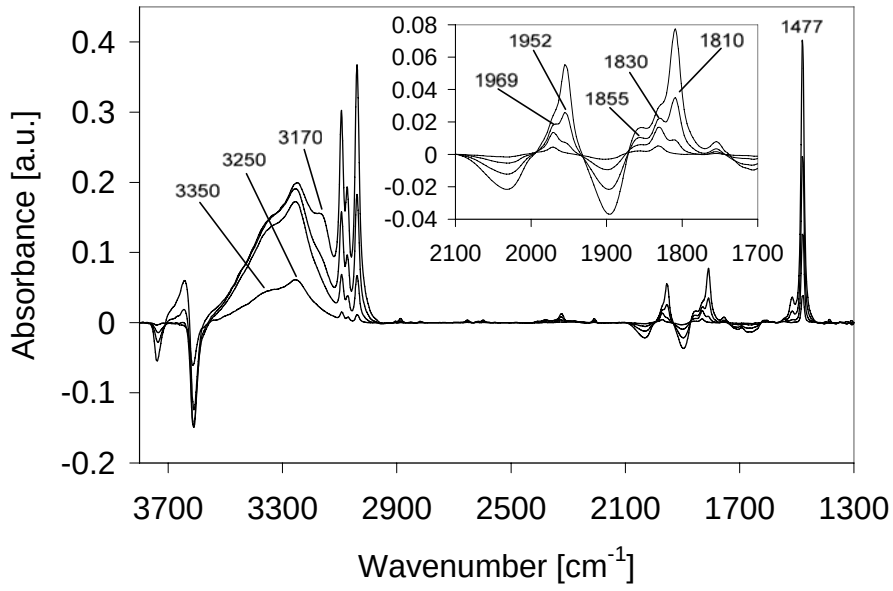

Figure 3.4. Differences in the IR spectra after sorption of benzene on HZSM-5 with partial pressures of 10^{-3}, 10^{-2}, 10^{-1} and 1 mbar at 323 K.

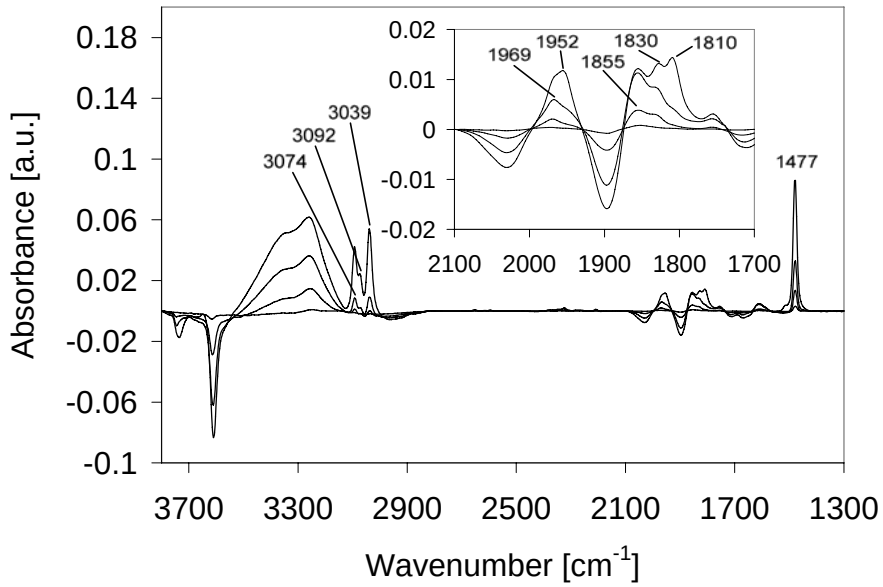

Figure 3.5. Differences in the IR spectra after sorption of benzene on HZSM-5 with partial pressures of 10^{-3}, 10^{-2}, 10^{-1} and 1 mbar at 403 K.

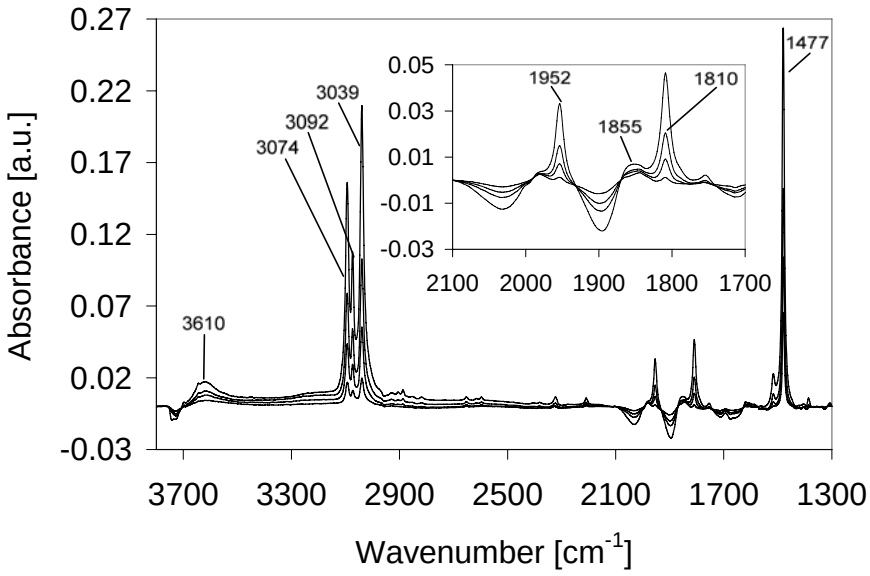

Figure 3.6. Differences in the IR spectra after sorption of benzene on Silicalite-1 with partial pressures of 10^{-3}, 10^{-2}, 10^{-1} and 1 mbar at 323 K.

The coverage of the SiOH and SiOHAl groups with benzene was quantitatively determined by integration of the (negative) intensity of the IR bands at 3745 and 3610 cm^{-1}, assuming that the molar extinction coefficient of the OH groups is independent of the coverage. As the bands at 3745 and 3725 cm^{-1} strongly overlap, IR bands of the SiOH groups on the outer surface and on defect sites were integrated together. As the perturbed hydroxyl group of the SiOH vibration overlaps with the free hydroxyl band of the SiOHAl groups (at 3610 cm^{-1}), the spectra of benzene on Silicalite-1 (at the corresponding temperature and scaled to the same intensity of the band at 3745 cm^{-1}) were subtracted from the spectra of benzene on HZSM-5 before the integration of the band at 3610 cm^{-1}.

The isotherms of benzene on the SiOH and SiOHAl groups of HZSM-5 and on the SiOH groups of Silicate-1 in the pressure range up to 1 mbar were described with a with a dual-site Langmuir model (Equation 2).

$$q = \sum_{j=1}^{n} q_j^{sat} \frac{K_j \cdot p^*}{1 + K_j \cdot p^*} \tag{3.2}$$

in which K_j denotes the thermodynamic equilibrium constant for the sorption process j, q_j^{sat} is the maximum sorption capacity for process j [molecules/unit cell] and p^* is the partial pressure of benzene normalized to standard conditions (i.e. $p^*=p/p^0$). The adsorption isotherms for benzene on the SiOHAl groups of HZSM-5 at 323, 363 and 403 K together with the contributions of the individual sorption processes are shown in Figure 3.7, the values for K_j and q_j^{sat} are summarized in Table 3.1.

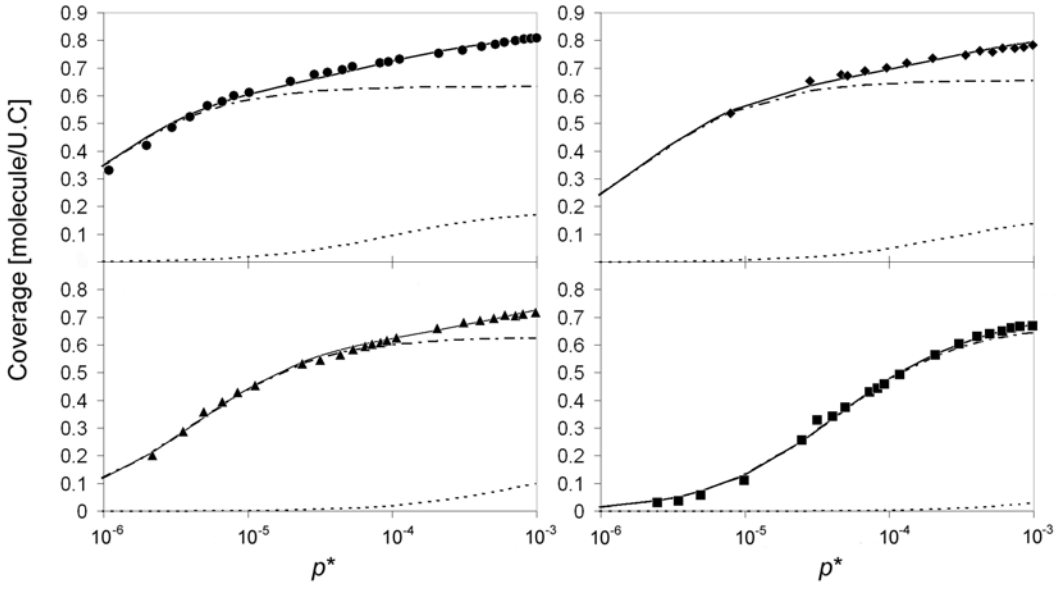

Figure 3.7. Adsorption isotherms of benzene on SiOHAl groups of HZSM-5 at (●) 323, (♦) 343, (▲) 363 and (■) 403 K; (— ·· — ·· —) K_1, (·····) K_2 and (——) sum of K_1 and K_2.

Table 3.1. Sorption equilibrium constants determined from adsorption isotherms measured by infrared spectroscopy.

Material	T [K]	q_1^{sat} [molec./ U.C.]	K_1	q_2^{sat} [molec./ U.C.]	K_2
SiOHAl HZSM-5	323	0.63	1.22×10^6	0.18	1.07×10^4
	343	0.65	5.91×10^5	0.17	4.00×10^3
	363	0.62	2.35×10^5	0.17	1.32×10^3
	403	0.67	2.34×10^4	0.14	2.57×10^2

The enthalpic and entropic contributions of the sorption of benzene on HZSM-5 and Silicalite-1 were estimated from Equation 3 using the equilibrium constants K_j determined for the sorption in the temperature range between 323 and 403 K.

$$K_j = e^{\frac{\Delta S^0}{R}} \cdot e^{-\frac{\Delta H^0}{RT}} \tag{3.3}$$

The changes in standard entropy ΔS^0 and in standard enthalpy ΔH^0 can be calculated from the correlation of $\ln(K_j)$ *vs.* T^{-1} (shown in Figure 3.8) according to Equation 4.

$$\ln(K_j) = \frac{\Delta S^0}{R} - \frac{\Delta H^0}{RT} \tag{3.4}$$

The values for ΔS^0 and ΔH^0 for the sorption of benzene on the SiOH and SiOHAl groups of HZSM-5 and for ΔH^0on the SiOH groups of Silicalite-1 are summarized in Table 3.2. For HZSM-5 two sorption structures with an

equivalent heat of adsorption of 53 kJ/mol) and a different decrease in entropy (49 and 80 J/mol.K) were identified. For the sorption of benzene on the SiOH groups (isotherms are not shown, the values for ΔH^0 and ΔS^0 are included in Table 3.2) two sorption processes were observed. The predominant sorption process with a heat of adsorption of 23 kJ/mol and a decrease in entropy of 5.9 J/mol.K was assigned to the interaction of benzene with the SiOH groups. Additionally, a minor contribution (q^{sat} = 0.025 – 0.06 molecules/U.C.) was observed, which is assigned to the sorption of benzene on strong Lewis acid sites. As a secondary effect a lateral interaction between the benzene molecules adsorbed and neighboring SiOH was formed, which resulted in a sharp decrease in the intensity of the SiOH groups at $p/p_o < 10^{-5}$. For the SiOH groups on Silicalite-1 the heat of adsorption and the decrease in entropy was the same as for the SiOH groups of the HZSM-5 sample.

Table 3.2. Standard enthalpy and standard entropy changes for benzene adsorbed on the hydroxyl groups of HZSM-5 and Silicatite-1.

Material	ΔH_1 [kJ mol^{-1}]	ΔH_2 [kJ mol^{-1}]	ΔS_1 [J mol^{-1} K^{-1}]	ΔS_2 [J mol^{-1} K^{-1}]
SiOHAl HZSM-5	-54	-51	-47	-80
SiOH HZSM-5	-24	-	-5.9	-
SiOH Silicalite-1	-23	-	-5.5	-

3.5. Discussion

The sorption of molecules inside the pores of molecular sieves can be described by at least two energetic contributions. One results from the directed interaction between electron pair acceptor sites such as Brønsted acidic SiOHAl groups or accessible metal cations in the zeolite and the electron pair donor (basic) function of the molecules. The other contribution results from the non-directed van der Waals interactions between the sorbate and the zeolite pore walls.

For the sorption of *n*-hexane in HZSM-5 and Silicalite-1 heats of adsorption of 83 and 71 kJ/mol, respectively, were reported [52] and confirmed in a later study [53] (i.e., 67 and 73 kJ/mol for Silicalite-1 using a model also based on dual Langmuir isotherms). This indicates that the direct interaction of the alkane with the strong Brønsted acid sites contributes only about 12 kJ/mol and that heat of adsorption linearly increases with the size of the alkane. Although benzene and hexane have the same number of C atoms, the lower heat of adsorption of benzene (approximately 60 kJ/mol) indicates that benzene interacts less ideally with the MFI pores than the more flexible alkane. Nevertheless, the sorption of benzene is almost completely controlled by the interaction with the pore walls, shown by the almost identical (gravimetric) uptake of HZSM-5 and Silicalite-1 and by the small difference between the heat of adsorption for benzene in HZSM-5 and Silicalite-1 (60 *vs.* 55 kJ/mol). This small difference also suggests that the interaction with benzene at localized sites is much more constrained than with n-alkanes.

Let us now discuss the downward shift of the SiOHAl groups. The two bands of perturbed hydroxyl groups observed in the IR spectra after sorption of benzene on HZSM-5 at 3350 and 3250 cm^{-1} indicate the presence of at least two energetically different sorption structures for benzene on SiOHAl groups. In principle, the different wavenumbers of the perturbed hydroxyl groups either

indicate the presence of Brønsted acid sites with different acid strength or a different steric constraint for the benzene molecules being adsorbed. Conceptually, it is possible to discriminate between both effects by comparing $\Delta\nu_{SiOH}$ of (amorphous) SiOH with $\Delta\nu_{SiOHAl}$ of the SiOHAl groups for a particular probe molecule in a so-called Bellamy-Hallam-Williams plot, where both effects will result in a deviation from the linear relation [54, 55]. For a series of molecules with increasing diameter adsorbed on HZSM-5 and H/MCM-22 smaller values of $\Delta\nu_{SiOHAl}$ were observed for molecules with a diameter similar to the pore size [32, 33]. Therefore, a sterically constrained sorption will lead to a higher frequency of the perturbed hydroxyl group (i.e., a smaller $\Delta\nu_{SiOHAl}$) for the same value of $\Delta\nu_{SiOH}$, while more acidic bridging hydroxyl group will lead to a lower frequency of the perturbed group (i.e., to a larger $\Delta\nu_{SiOHAl}$). Combining the data reported in ref. [32] with the values observed for $\Delta\nu_{SiOHAl}$ (see Figure 3.9) it can be clearly seen that a deviation to lower values of $\Delta\nu_{SiOHAl}$ for both perturbed hydroxyl groups (i.e. 260 and 360 cm^{-1}) occurs, which indicates two sterically constrained sorption structures for benzene in HZSM-5. Thus, the downward shift of the OH bands was markedly smaller than what would be expected given the base strength of benzene and the acid strength of the SiOHAl groups (i.e., ideally the band of the perturbed OH group of HZSM-5 should be found at 3180 cm^{-1}) [32]. The third (minor) band of perturbed hydroxyl groups at $\Delta\nu_{SiOHAl}$ = 440 cm^{-1} observed on HZSM-5 at pressures above 10^{-1} mbar is at the frequency expected for a sterically non-constrained sorption of benzene on SiOHAl groups. The simultaneous appearance of the CH out of plane deformation vibrations at the position of liquid benzene suggests that these molecules are sorbed on bridging hydroxyl groups present in a sterically non-constrained environment, e.g., at the pore openings.

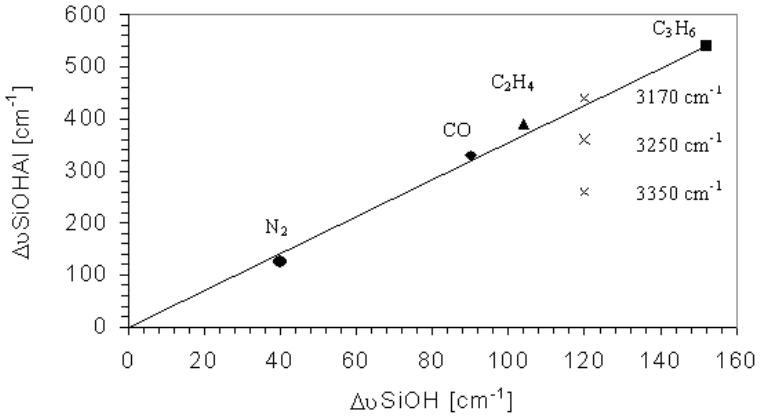

Figure 3.9. Bellamy Hallam Williams plot; data taken from ref. [32] shown as full symbols, (×) data from present work.

The adsorption isotherms of benzene on the SiOHAl and the SiOH groups of HZSM-5 up to loading of 4 molecules/unit cell can be perfectly fitted using a dual-site Langmuir adsorption isotherm. For the sorption of benzene on the bridging hydroxyl groups of HZSM-5 inside the pores the heats of adsorption for both contributions were similar indicating an identical enthalpy of interaction for the sorption structures. The different standard adsorption entropies (ΔS^o = -49 and -80 J/mol.K), reveal that two sorption structures with different geometrical requirements exist. It should be noted, that the coverage of the site with the lesser sterical constraint is about 4 times higher than the coverage of the more constrained sorption site (see Table 3.1). The ratio between the intensities of the two perturbed hydroxyl groups at 3250 and 3350 cm^{-1} (as determined by deconvolution) did not vary as a function of pressure and temperature, which indicates that the occupation of the sorption sites and the orientation of benzene does not depend on the coverage up to 4 molecules per unit in HZSM-5.

Note that at loadings below 4 molecules/unit cell neutron scattering [37, 43] and Raman [38] studies agree that benzene is preferentially adsorbed in the intersections between the straight and the sinusoidal channels and only at

higher coverage positions in the straight and sinusoidal channels are occupied. The MFI structure contains 24 unique positions for the tetrahedral atoms (Si and Al atoms), which are randomly substituted with Al atoms [56]. All positions are accessible *via* the intersections, therefore, preferential adsorption sites for benzene resulting from the location of the Al^{3+} atoms within the MFI structure can be excluded. As the sorption of benzene inside the pores is energetically controlled to the largest extent by the interaction of benzene with the pore walls, the question arises to what extent the direct interaction between benzene and the bridging hydroxyl groups controls the sorption structure.

A perturbed hydroxyl group is observed, if benzene is located sufficiently close to SiOHAl groups and the hydrogen bonding interaction established perturbs the stretching vibrations of the zeolite hydroxyl groups. For a given strength of a bridging OH group the maximum perturbation occurs if the (equilibrium) distance between benzene and the SiOHAl hydroxyl group can be established. The lower values for $\Delta\nu_{SiOHAl}$ suggest that the constrained environment inside the MFI channels induces repulsive interactions, which does not allow reaching the minimum equilibrium distance between benzene and the hydroxyl groups. The formation of two perturbed hydroxyl groups indicates the presence of two well-defined sorption geometries for benzene inside HZSM-5.

It is interesting to explore now to what extent the localized interaction with the OH groups influences the sorption structure. The small contribution may certainly influence, but not direct the overall sorption structure. Using previously postulated structures from theoretical calculations and neutron scattering studies, we would like to speculate that one perturbed hydroxyl group results from the (symmetric) interaction of benzene *via* the π-electrons from the benzene ring with the bridging hydroxyl groups and the other from the interaction with a polarized C-H group similar to the interactions with a C-H group of alkanes. The closer the distance between the SiOHAl group and the C atoms of benzene, the lower the frequency of the perturbed hydroxyl group (i.e.,

the lesser the deviation from the frequency expected from the basic character of benzene). For benzene in HZSM-5 a smaller distance was reported for the orientation of the OH groups towards the corner of the aromatic ring [44], while for benzene in mordenite (a zeolite containing larger pores) the orientation towards the center of the ring led to a shorter distance between benzene and the SiOHAl groups [48]. A schematic drawing of the two possible sorption structures for benzene in the intersections of HZSM-5 is depicted in Figure 3.10. Note it was proposed from neutron scattering that two sorption structures, both oriented with the C-C bond towards the pore wall at a different angle, exist [43].

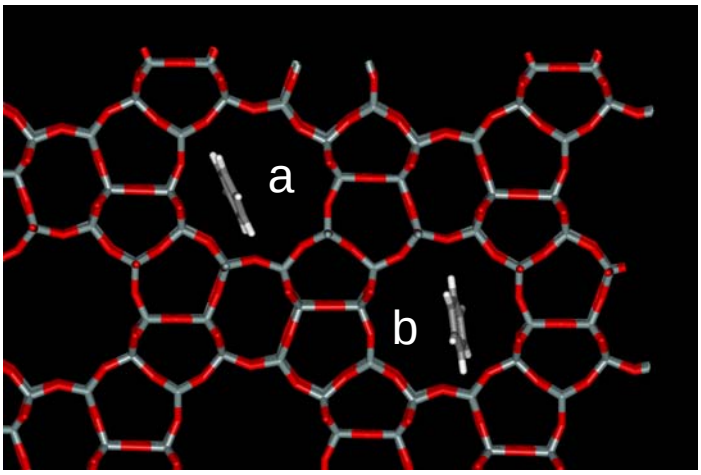

Figure 3.10. Sorption structure of benzene in Silicalite-1 (a) with the aromatic ring and (b) with a corner oriented towards the pore walls.

The existence of a sorption structure of the aromatic ring system towards the SiOHAl groups is further supported by the appearance of the band assigned to the out of plane vibration for benzene with strongly polarized π-electrons resulting from the interaction with a proton of the zeolite. A schematic picture of the sorption of benzene inside the MFI structure (calculated using the sorption module of Cerius[2] (version 4.8) and the open

force field to describe the sorption of benzene in Silicate-1) with a loading of 4 molecules/unit cell is shown in Figure 3.11. Most of the benzene molecules were found to be oriented towards the pore walls with a corner or an edge of the aromatic ring, while only a minor fraction of benzene was interacting with the pore wall via the aromatic ring system. This is in perfect agreement with the higher occupation of the less constrained sorption site (e.g., the site with the larger shift between the free and perturbed hydroxyl group and the smaller decrease in entropy after sorption).

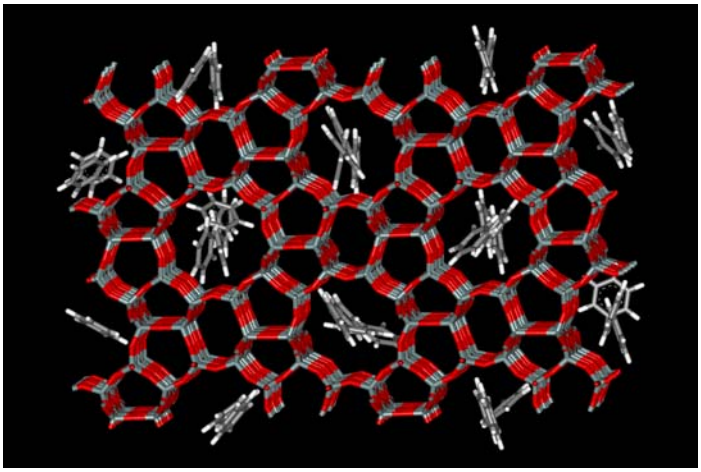

Figure 3.11. Sorption of benzene in Silicalite-1 with a loading of 4 molecules/unit cell (The picture shows a simulation of the sorption of benzene in a model structure consisting of 8 unit cells).

The third perturbed hydroxyl group at the position expected for an unconstrained interaction between benzene and the SiOHAl groups, indicates the sorption of benzene on Brønsted acid sites located close to the pore openings. Due to absence of interactions of benzene with the pore walls the interaction is weaker and, therefore, these sites are only occupied at a higher partial pressure. In contrast to the sorption inside the pores this sorption structure is primarily controlled by the interaction of benzene with the SiOHAl groups and consequently the benzene molecules are adsorbed at the

energetically favored distance to the bridging hydroxyl groups. Therefore, the perturbed hydroxyl group was observed at the position expected from the acid/base interaction of benzene on SiOHAl groups. The formation of out of plane vibrations at the position of liquid benzene indicates that the weak interaction with the sorption sites, i.e., the small energetic difference between sites at the pore month and on the external surface, leads to multilayer sorption.

The formation of up to three perturbed hydroxyl groups during sorption of benzene demonstrates the strong influence of the geometry and the dimensions of the pore system on the orientation of the benzene molecules within the pores and their distance to the bridging hydroxyl groups of the zeolite. For the characterization of the strength of acid sites these results have the important consequence that the orientation of the probe molecules inside the pores with respect to the (random) positions of the bridging hydroxyl groups primarily controls the perturbation of the hydroxyl groups, while the localized effect resulting from the acid strength of the SiOHAl groups (the property being studied) has only a minor contribution to the position of the perturbed hydroxyl band. Therefore, the perturbation of hydroxyl groups can only be used to study the acid character of sites in materials having the same structure, while a comparison of the acid sites in materials with different pore geometry might be easily misleading.

For the sorption of benzene on the SiOH groups of HZSM-5 and Silicalite-1 one predominant sorption structure was observed. As the stretching frequencies of the SiOH groups located on the outer surface (3745 cm^{-1}) and at defects inside the pores (3725 cm^{-1}) are strongly overlapping (see Figure 3.6) the sum of both contributions was used for the determination of the changes in standard entropy and enthalpy. As already discussed the sorption inside the pores is controlled by the interaction of benzene with the pore walls and, consequently, the heat of adsorption of benzene on SiOH inside the pores should be similar to that of the sorption on SiOHAl groups. While the heat of adsorption measured by DSC on the HZSM-5 and the Silicate-1 sample were

almost identical (i.e. 60 and 55 kJ/mol), the heat of adsorption for benzene determined from the uptake on the SiOH groups was significantly lower (23 kJ/mol). In contrast to the SiOHAl group, SiOH groups can be located inside the pores as well as on the outer surface of the zeolite crystals. The lower heat of adsorption and the lower decrease in entropy (~ -6 J/mol.K) indicates that the majority of the SiOH groups is located at the external surface of the particles. Additionally benzene adsorbed on strong Lewis acid sites (presumably not reaching the adsorption desorption equilibrium under the conditions studied) establish lateral interactions with SiOH groups located in the close vicinity, which resulted in a sharp increase in the adsorption isotherms of benzene on the SIOH groups at low partial pressures ($p/p_o<10^{-5}$).

3.6. Conclusions

The sorption of benzene on HZSM-5 and Silicalite-1 was studied by calorimetry and IR spectroscopy and adsorption isotherms for the integral uptake (by gravimetry) and for the individual coverage of the SiOH and SiOHAl groups (from IR spectroscopy) were reported. The sorption of benzene is described by a complex multi site Langmuir model and from the individual equilibrium constants, the heat of adsorption and the decrease of entropy for the adsorbed molecules were determined for the different sorption sites. The sorption of benzene on HZSM-5 is energetically controlled by the interaction of the molecules with the pore walls, while the localized interaction with the bridging hydroxyl groups is only a minor energetic contribution. Generally the sorption of benzene inside the pores of HZSM-5 leads to a sterically constrained sorption structure. If benzene is located close to SiOHAl groups perturbed hydroxyl groups are formed, their frequency reflecting more the local constraints of benzene at the sorption sites than the true acid base interaction. Two major orientations of benzene in contact with SiOHAl groups can be

differentiated. One exists in an orientation with the ring parallel to the pore walls and one with a specific C atom or C-C bond oriented towards the SiOHAl groups. The similar heat of adsorption confirms the random orientation of benzene at the acid sites, while the different decrease in entropy and the formation of two perturbed hydroxyl groups reveals that the steric constraint and, thus, the distance between the benzene molecules and the bridging hydroxyl groups is different. The perturbation of the hydroxyl groups is, therefore, primarily determined by the orientation of the benzene molecules inside the channels and the random position of the Al atoms on the framework positions, while the acid character of the SiOHAl groups results only in a minor difference in the stretching frequency of the perturbed hydroxyl groups.

3.7. Acknowledgments

Partial support for this project from the “Bayerische Forschungsstiftung” and the “Verband der Chemischen Industrie” is gratefully acknowledged.

References

1. Haw, J. F., *Phys. Chem. Chem. Phys.*, **2002**, 4, 5431.
2. Ward, J. W., *J. Catal.*, **1967**, 9, 225.
3. Barthomeuf, D., *Mater. Chem. Phys.*, **1987**, 17, 49.
4. Barthomeuf, D., *J. Phys. Chem*. **1993**, 97, 10092.
5. Janssens, G. O. A., Toufar, H., Baekelandt, B. G., Mortier, W. J., Schoonheydt, R. A., *J. Phys. Chem.*, **1996**, 100, 14443.
6. Corma, A., Fornes, V., Melo, F. V., Herrero, J., *Zeolites*, **1987**, 7, 559.
7. Gorte, R. J., *Catal. Today*, **1996**, 28, 405.
8. Lavalley, J. C., *Catal. Today*, **1996**, 27, 377.

9. Auroux, A., Datka, J., *Appl. Catal. A*, **1997**, 165, 473.
10. Busca, G., *Phys. Chem. Chem. Phys*., **1999**, 1, 723.
11. Hunger, M., Ernst, S., Steuernagel, S., Weitkamp, J., *Microp. Mater*., **1996**, 6, 349.
12. Heeribout, L., Semmer, V., Batamack, P., Doremieux-Morin, C., Fraissard, J., *Microp. Mesop. Mater*., **1998**, 21, 565.
13. Nicholas, J. B., Xu, T., Haw, J. F., *Top. Catal*., **1998**, 6, 141.
14. Stoch, J., Lercher, J. A., Ceckiewicz, S., *Zeolites*, **1992**, 12, 81.
15. Stocker, M., *Microp. Mater*., **1996**, 6, 235.
16. Kaliaguine, S., *Stud. Surf. Sci. Catal*., **1996**, 102, 191.
17. Benesi, H. A., Winquist, B. H. C., *Adv. Catal*., **1978**, 27, 97.
18. Haag, W. O., Dessau, R. M., *Proceedings 8th International Congress on Catalysis Berlin*; Dechema: Frankfurt, **1984**.
19. Bourdillon, G., Gueguen, C., Guisnet, M. R., *Appl. Catal*., **1990**, 61, 123.
20. Umansky, B., Engelhardt, J., Hall, W. K., *J. Catal*., **1991**, 127, 128.
21. Zecchina, A., Lamberti, C., Bordiga, S., *Catal. Today*, **1998**, 41, 169.
22. Auroux, A., *Catal. Lett*. **1997**, 4, 71.
23. Lercher, J. A., Noller, H., *J. Catal*. **1982**, 77, 152.
24. Hair, M. L., Hertl, W., *J. Phys. Chem*., **1970**, 74, 91.
25. Sauer, J., Schroder, K. P., Termath, V., *Coll. Czech. Chem. Commun*. **1998**, 63, 1394.
26. Barthomeuf, D., Ha, B.-H, *J. Chem. Soc. Faraday Trans*., **1973**, 69, 2147.
27. Barthomeuf, D., Ha, B.-H, *J. Chem. Soc. Faraday Trans*., **1973**, 69, 2158.
28. Su, B. L., Barthomeuf, D., *J. Catal*., **1993**, 139, 81.
29. Su, B. L., Barthomeuf, D., *Zeolites*, **1995**, 15, 470.
30. Jentys, A., Lercher, J. A., *Stud. Surf. Sci. Catal*., **1989**, 46, 585.
31. Onida, B., Bonelli, B., Borello, L., Fiorilli, S., Geobaldo, F., Garrone, E., *Stud. Surf. Sci. Catal*. **2002**, 142, 143.
32. Onida, B., Bonelli, B., Borello, L., Fiorilli, S., Geobaldo, F., Garrone, E., *J. Phys. Chem. B*, **2002**, 106, 10518.

33. Onida, B, Geobaldo, F., Testa, F., Aiello, R., Garrone, E., *J. Phys. Chem. B*, **2002**, 106, 1684.
34. Trombetta, M., Armaroli, T., Alejandre, A. G., Gonzalez, H., Solis, J. R., Busca, G., *Catal. Today*, **2001**, 65, 285.
35. Trombetta, M., Armaroli, T., Alejandre, A. G., Solis, J. R., Busca, G., *Appl. Catal. A*, **2000**, 192, 125.
36. Vigné-Maeder, F., Jobic, H., *Chem. Phys. Lett*., **1990**, 169, 31.
37. Floquet, N., Coulomb, J. P., Weber, G., Bertrand, O., Bellat, J. P., *J. Phys. Chem. B*, **2003**, 107, 685.
38. Huang, Y. N., Havenga, E. A., *J. Phys. Chem. B*, **2000**, 104, 5084.
39. Pope, C. G., *J. Phys. Chem*., **1986**, 90, 835.
40. Thamm, H., *J. Phys. Chem*., **1987**, 91, 8.
41. Coker, E. N., Jia, C. J., Karge, H. G., Langmuir, 2000, 16, 1205.
42. Rudzinski, W., Narkiewicz-Michalek, J., Szabelski, P., Chiang, A. S. T., *Langmuir*, **1997**, 13, 1095.
43. Goyal, R., Fitch, A. N., Jobic, H., *J. Phys. Chem. B*, **2000**, 104, 2878.
44. Nicholas, J. B., *Top. Catal*., **1997**, 4, 157.
45. Zaragoza, I. P., Martinez-Magadan, J. M., Santamaria, R., Dixon, D., Castro, M., *Int. J. Quant. Chem*., **2000**, 80, 125.
46. Ryder, J. A., Chakraborty, A. K., Bell, A. T., *J. Phys. Chem. B*, **2000**, 104, 6998.
47. Clark, L. A., Sierka, M., Sauer, J., *J. Am. Chem. Soc*., **2003**, 125, 2136.
48. Demuth, T., Benco, L., Hafner, J., Toulhoat, H., Hutschka, F., *J. Chem. Phys*., **2001**, 114, 3703.
49. Primet, M., Garbowski, E., Mathieu, M. V., Imelik, B., *J. Chem. Soc. Faraday Trans*., **1980**, 76, 1942.
50. Datka, J., Marschmeyer, S., Neubauer, T., Meusinger, J., Papp, H., Schutze, F. W., Szpyt, I., *J. Phys. Chem*., **1996**, 100, 14451.
51. Datka, J., Gil, B., *J. Molec. Structure*, **2001**, 596, 41.
52. Eder, F., Lercher, J. A., *Zeolites*, **1997**, 18, 75.

53. Zhu, W., Kapteijn, F., van der Linden, B., Moulijn, J. A., *Phys. Chem. Chem. Phys.*, **2001**, 3, 1755.
54. Pimentel, G. C., McClellan, A. L., *The Hydrogen Bond*; Freeman, W. G.: San Francisco, **1960**.
55. Knözinger, H., *The H-bond: recent advances in theory and experiment*; North Holland: Amsterdam, **1976**.
56. Schöder, K. P., Sauer, J., Leslie, M., Catlow, C. R. A., *Zeolites*, **1992**, 12, 20.

Chapter 4

Orientation of alkyl-substituted aromatic molecules during sorption in the pores of zeolite HZSM-5

4. ORIENTATION OF ALKYL-SUBSTITUTED AROMATIC MOLECULES DURING SORPTION IN THE PORES OF ZEOLITE HZSM-5

4.1. Abstract

Two energetic contributions of the sorption of benzene, toluene and *p*-xylene on MFI zeolites process are identified. One is the non-specific interaction with the pore walls, the other is the specific directed interaction with the Brønsted acidic SiOHAl groups. Although the energetic contribution of the non-specific interaction is about ten times lager than the directed interaction, this minor contribution is sufficient to direct the aromatic molecules at low coverage to sorption sites at intersections containing SiOHAl groups and only at higher loadings intersections without bridging hydroxyl groups are occupied. The adsorption of benzene on the SiOHAl groups is described by a dual site Langmuir isotherm related to two orientations of the aromatic molecule, differing in the decrease of entropy, but with the same heat of adsorption. The two sorption structures are manifested by the appearance of two perturbed hydroxyl groups in the IR spectra of the zeolite in contact with the aromatic molecule. At low coverage also for toluene two sorption structures with different steric constraints are differentiated while at higher coverage only the less constrained structure dominates. In contrast for *p*-xylene the Langmuir model was inadequate to describe the adsorption isotherm on the SiOHAl groups, which reflects the strongly confined sorption structure resulting from the two alkyl groups. For all three molecules, the initial preferential adsorption at the intersections causes the molecules to be spatially well separated, randomly oriented with respect to SiOHAl groups. With increasing coverage

the molecules arrange into the geometrically less constrained sorption structures.

4.2. Introduction

Zeolites and crystalline microporous solids are frequently used materials in the (petro-) chemical industry for selective sorption and shape selective catalysis, as the similar size of the pores and of the (reacting/sorbing) molecules allows controlling the access of the reactants to the active sites. Substituted aromatic molecules, for example, are being separated with zeolitic sorbents and catalytically converted in large scale technical processes using the principles of shape selectivity [1,2]. However, the steric constraints may also decrease the rate of access of molecules to the sorption sites if the minimum kinetic diameter is close to or above the effective diameter of the pore openings. In order to understand and improve the shape selective properties of catalytically active materials the elementary steps of sorption and diffusion have been addressed theoretically and experimentally [3-6].

For the sorption of alkyl substituted benzene isomers in medium pore zeolites (such as HZSM-5) the investigations can be generally divided into a macroscopic and a microscopic point of view. The macroscopic description is typically based on measuring the adsorption isotherm by gravimetric or site specific spectroscopic methods and the interpretation is based on a thermodynamic and/or geometric description of the uptake, allowing, e.g., the determination of energetic and entropic contributions [7-10]. On the other hand, the microscopic approach provides a detailed description of the interaction between the molecules and the functional groups of the zeolite on an atomistic level using spectroscopic techniques such as NMR [11,12], neutron diffraction [13,14], Raman [15,16] and IR spectroscopy [17].

Zeolites of the MFI structure type can be synthesized with Si/Al ratios between ~10 [18,19] and ∞ [20,21]. The substitution of Al into the zeolite framework generates bridging SiOHAl groups, which act as strongly Brønsted acid sites. The framework of MFI consists of two intersecting channel systems forming a 10-membered ring pore structure. The sinusoidal channels are parallel to the [100] axis with elliptical pore apertures of 5.1 × 5.5 Å, the straight channels are parallel to the [010] axis with an (almost circular) aperture of 5.3 × 5.6 Å [22]. Within the unit cell (U.C.) of the MFI structure 4 intersections between straight and sinusoidal channels exist.

Chiang *et al*. and Rudziński *et al*. [23,24] differentiated three types of sites (i.e., straight channels, sinusoidal channels and intersections) for the sorption of benzene and *p*-xylene from isotherms and the corresponding heat of adsorption. Using Raman spectroscopy and neutron diffraction [13,16,25] it has been shown that benzene sorbs at the intersections at low loadings (1 - 4 molecules/U.C.), at the sinusoidal channels at intermediate loadings (5-6 molecules/U.C.) and that it relocates from the sinusoidal channels into the midsections of the straight channels at high loadings (7-8 molecules/U.C.). This relocation of the molecules inside the pores leads to a deviation from the Langmuir type isotherm observed up to a loading of 4 molecules/U.C. At higher loadings a second step in the isotherm is typically observed. Olson *et al.* [26] and Talu *et al.* [27] proposed that the phase transition of the MFI zeolite causes the step in the adsorption isotherm at a coverage above 4 molecules/unit cell. Later, this was confirmed by Snurr *et al*. [28] by a simulation the transition of the $P2_1/n$-*P*nma (monoclinic/ORTHO) to the *P*nma-$P2_12_12_1$ (orthorhombic/PARA) symmetry in the polymorphic framework of MFI and by Takaishi experimentally for p-xylene [29]. The presence of different locations for adsorbed benzene and *p*-xylene molecules in the zeolite before and after the phase transition were also described by NMR [30] and by the characteristic heat of adsorption [28,29,31].

The interaction of benzene with silanol groups (SiOH) and Brønsted acidic bridging hydroxyl groups (SiOHAl) of HZSM-5 has been studied extensively using vibrational spectroscopy [32-35]. The hydrogen bonding between the electron donor function of the aromatic molecules and the hydroxyl groups of the zeolite leads to a shift of the frequency of the OH stretching vibration to lower wavenumbers. In general, the difference in the frequencies of the OH stretching vibrations before and after sorption of the aromatic molecules ($\Delta\nu_{OH}$) reflects the strength of the electron donor-acceptor interaction as well as the local geometry of the molecules at the sorption sites. While the evaluation of the strength of the electron donor-acceptor interaction from the difference between the perturbed and the unperturbed OH vibration frequencies was frequently described as probe for the acid strength [36-39], the effects of steric constraints on the hydroxyl group perturbation were described by Onida *et al.* [40,41]. In principle, the strength of the EPD-EPA interaction is directly proportional to perturbation of the OH group and, therefore, the correlation of $\Delta\nu_{SiOH}$ (of amorphous silica) versus $\Delta\nu_{SiOHAl}$ (of a zeolite) for the a series of molecules should lead to a linear relation, the so-called Bellamy-Hallam-Williams (BHW) plot [42]. The slope of this graph is a measure for the acid strength of the zeolite, if steric constraints for the sorbates are absent (e.g. alkanes, N_2, CO). For larger molecules, such as benzene, a deviation to smaller shifts for $\Delta\nu_{SiOHAl}$ was reported, and a detailed study of the energetic and entropic contributions indicated a sterically constrained geometry for the sorption. Frequently, more than one band of perturbed hydroxyl group was seen after sorption of alkyl-substituted benzene molecules, which was assigned to different geometric locations/orientations of the molecules within the pores of the zeolite or to the presence of hydroxyl groups with non-uniform acid strength [43,44].

Recently, we have studied the energetic and entropic contributions for the sorption of benzene in acidic and non-acidic MFI materials [45 or Chapter 3]. IR spectroscopy indicated the presence of three perturbed hydroxyl groups,

which are assigned to two orientations of benzene inside the pores and to one at the pore mouth opening. The adsorption isotherms for benzene on SiOHAl groups inside the pores follow a dual-site Langmuir model. In present communication, we would like to extend this model to the sorption of alkyl-substituted benzene molecules to evaluate the role of the additional alkyl groups on the energetic and entropic contributions and on the local orientation within the pores.

4.3. Experimental

4.3.1. Materials

The sorption of benzene, toluene and p-xylene, all in spectroscopic grade obtained from Merck, was studied on HZSM-5 (Si/Al = 82) and Silicalite-1 (Si/Al = ∞). The concentrations of silanol groups (SiOH) and bridging hydroxyl groups (SiOHAl), determined by ^{1}H MAS NMR spectroscopy, were 0.09 and 0.12 mmol/g for SiOH and SiOHAl groups of HZSM-5 (equivalent to 0.7 SiOHAl groups per U.C.) and 0.05 mmol/g for the SiOH groups on Silicalite-1.

4.3.2. Thermogravimetry

The gravimetric sorption capacities of the molecules on the zeolite samples were measured on a Setaram TG-DSC 111 thermoanalyzer. The sample (~20 mg) was activated at 823 K for 1 h (heating rate 10 K.min^{-1}) under vacuum ($p < 10^{-7}$ mbar). During equilibration with the sorbate at 323, 363 and 403 K using pressure steps of 0.01-0.02 mbar up to 13 mbar the weight increase and the thermal flux were measured.

4.3.3. IR spectroscopy

The samples were compacted to self supporting wafers (weight ~10 mg/cm^2) and activated under vacuum (p <10^{-7} mbar) at 823 K (heating rate 10 K.min^{-1}) for 1 h. The sorption was carried out at 323, 343, 363 and 403 K using equilibrium pressures between 10^{-3} and 1 mbar. To directly compare the surface coverage of the adsorbed species all spectra were normalized using the overtone and combination vibrations of the MFI materials between 2105 and 1740 cm^{-1}. The coverage of SiOHAl group was determined from the intensity of the OH band at 3610 cm^{-1}. The intensities of the two (overlapping) perturbed hydroxyl groups after sorption were determined by a peak deconvolution using a Gauss-Lorentz peak-shape (Gauss/Lorentz ratio = 1:1).

4.4. Results

The adsorption isotherms of benzene, toluene and *p*-xylene on HZSM-5 and Silicalite-1 at 323, 363, 403 K measured by gravimetry are compared in Figure 4.1. In the case of benzene and *p*-xylene the uptake with HZSM-5 was slightly higher than with Silicalite-1, while for toluene the same sorption capacity for the acidic and non acidic samples was observed. For all equilibrium partial pressures and temperatures studied the uptake of *p*-xylene was the highest followed by toluene and benzene. The heat of adsorption for the series of molecules on HZSM-5 and Silicalite-1 as a function of the coverage is compared in Figure 4.2. In all cases, the heat of adsorption strongly decreased up to a coverage of 0.7 -1 molecules/U.C and reached a broad region with a constant value of 55, 80 and 96 kJ/mol, for benzene, toluene and *p*-xylene on HZSM-5 respectively, up to coverage of 4 molecules/U.C. For Silicalite-1, the heat of adsorption was about 3 to 5 kJ/mol lower compared to the acidic HZSM-5 sample. The distinct decrease in the

heat of adsorption observed at low coverage for benzene compared to toluene and p-xylene indicates that benzene can reach highly reactive defect sites, which are not accessible for the larger molecules due the repulsive interaction of the $–CH_3$ groups and the pore walls.

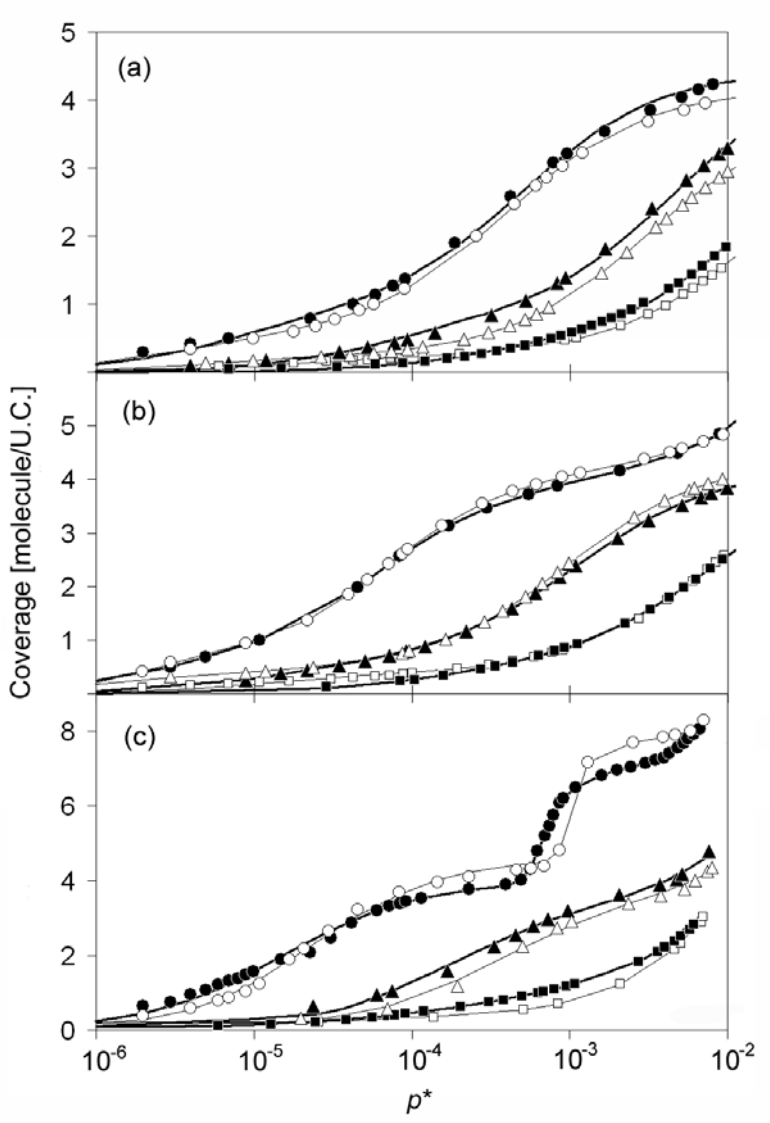

Figure 4.1. Gravimetric adsorption isotherms of (a) benzene, (b) toluene and (c) *p*-xylene on HZSM-5 (closed symbols) and Silicalite-1 (open symbol) at (●,○) 323, (▲,Δ) 363 and (■,□) 403 K.

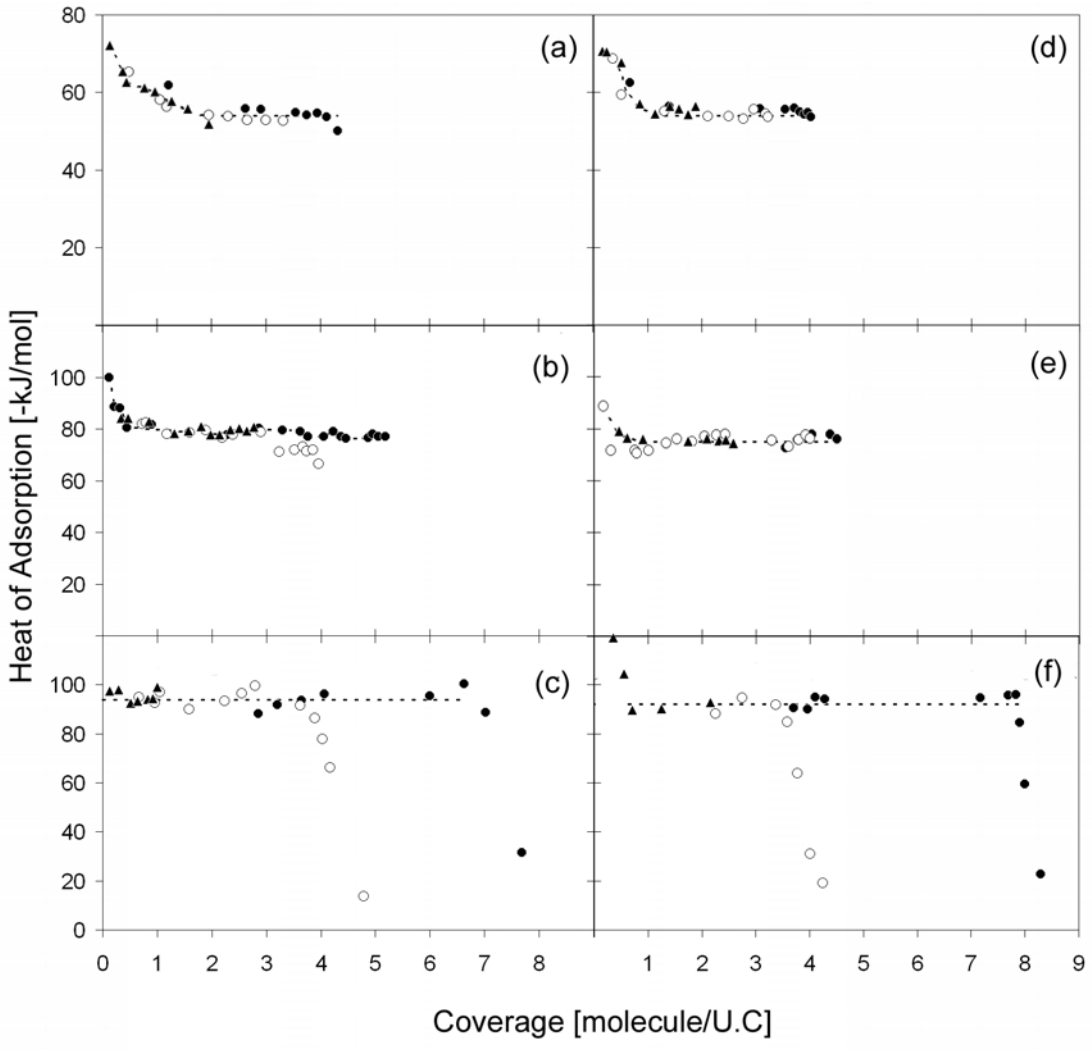

Figure 4.2. Differential heat of adsorption of (a, d) benzene, (b, e) toluene, (c, f) *p*-xylene on HZSM-5 and Silicalite-1 measured from calorimetry at (●) 323, (○) 363 and (▲) 403 K.

The electron donor-acceptor interaction between the molecules and the hydroxyl groups of the zeolite was studied by IR spectroscopy. The changes in the IR spectra after sorption of 1 mbar benzene, toluene and *p*-xylene at 403 K on HZSM-5 are shown in Figure 4.3. The interaction of the aromatic molecules with HZSM-5 led to a decrease in the intensity of the silanol groups at 3745

cm^{-1} as well as of the bridging hydroxyl groups at 3610 cm^{-1} [32,34,35] and to the formation of two perturbed hydroxyl groups at 3350 and 3250 cm^{-1}. In general, the increasingly more basic character of the alkyl substituted aromatic molecule (benzene < toluene < p-xylene) leads to a lower wavenumber of two perturbed hydroxyl groups. The wavenumber difference between the unperturbed SiOHAl group and the perturbed hydroxyl groups ($\Delta\nu_{SiOHAl}$) reflects the strength of the electron donor-acceptor interaction and in this particular case the basic strength of the electron donor species [36,39] as well as the steric constraints at the sorption sites [40]. The deconvolution of the perturbed hydroxyl groups into individual bands using Gauss-Lorentz functions is shown in Figure 4.4. In contrast to benzene, where the two perturbed hydroxyl groups were present in a constant ratio at all pressures and temperatures studied (i.e., p=10^{-3}-1 mbar T=323-403 K), for toluene and *p*-xylene two perturbed hydroxyl groups were only present at low coverage, while at high coverage and particularly at low temperature only one perturbed hydroxyl group was observed.

The correlation between $\Delta\nu_{SiOHAl}$ versus $\Delta\nu_{SiOH}$ (determined from the sorption on non porous amorphous silica) for a series of molecules allows identifying the presence of steric constraints. The data reported here together with data for N_2 and C_3H_6 published in the literature [40] are shown in Figure 4.5. For HZSM-5 the small molecules (N_2, C_3H_6) are reported to be on the linear correlation, while the deviation to smaller shifts of $\Delta\nu_{SiOHAl}$ with respect to $\Delta\nu_{SiOH}$ for benzene, toluene and *p*-xylene clearly reveals the presence of steric constraints for the molecules adsorbed on the SiOHAl groups inside the pores of HZSM-5. Following the coverage of the SiOHAl and SiOH groups after sorption of benzene, toluene and *p*-xylene by IR spectroscopy allows to differentiate between molecules adsorbed inside the pores (SiOHAl groups) and on the outer surface (SiOH groups) of the HZSM-5 crystals. The coverage of the SiOHAl groups after sorption of benzene, toluene and p-xylene is shown

in Figure 4.6. The correlation of the gravimetric uptake and the coverage of the Brønsted acid sites is shown in Figure 4.7. The linear correlation with a slope of one up to a concentration of 0.5 molecules per U.C. indicates that the aromatic molecules are preferentially adsorbed on the SiOHAl groups at low coverage and only at higher loadings molecules are also located at intersections without SiOHAl groups. Note that the linear trends observed in the correlation of the gravimetric uptake and the intensity of ring deformation vibration of *p*-xylene (1515 cm^{-1}), which is proportional to the total amount of *p*-xylene adsorbed on the zeolite sample, shown in Figure 4.8, clearly proves that the sorption equilibrium was established at all temperatures and pressure studied.

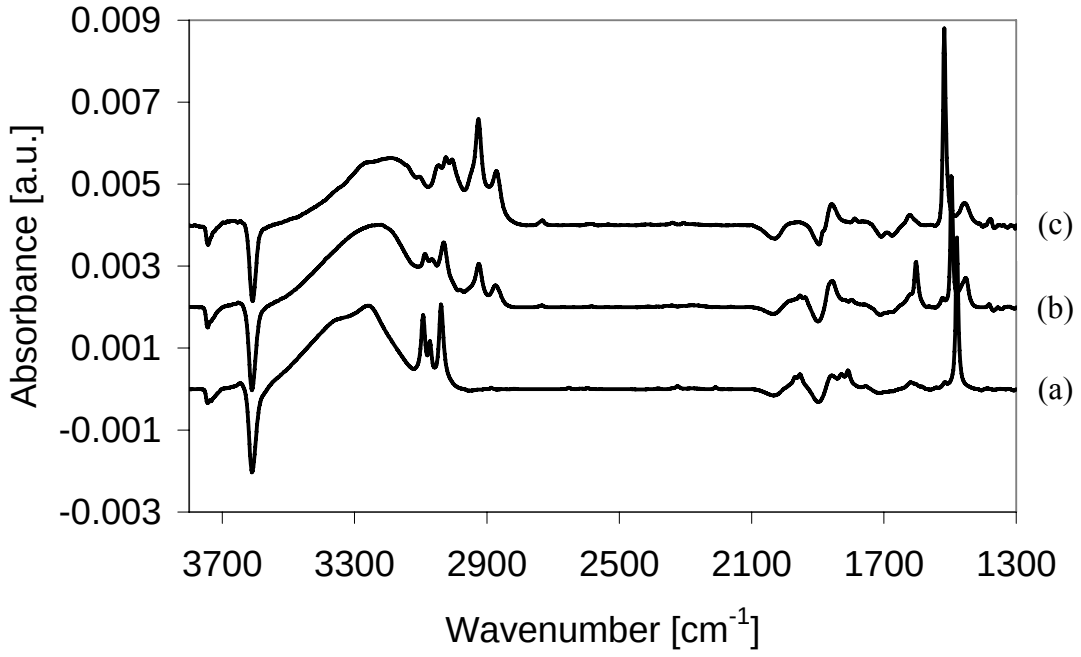

Figure 4.3. Changes of IR spectra after sorption of (a) benzene, (b) toluene and (c) *p*-xylene on HZSM-5 at 1 mbar at 403 K.

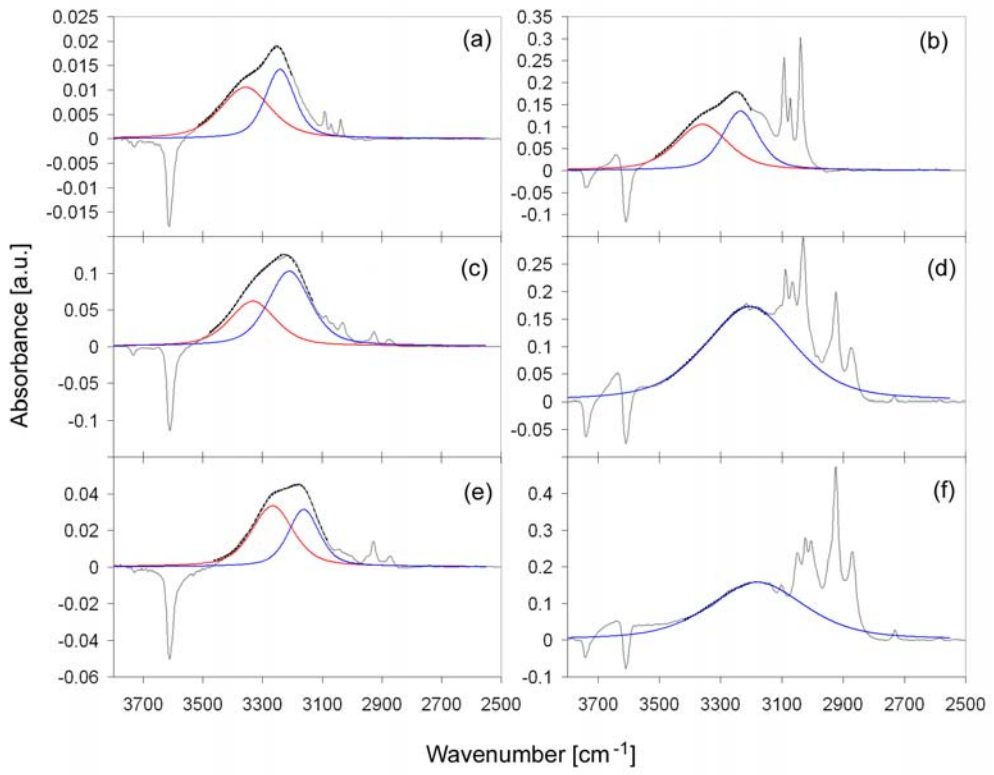

Figure 4.4. Band deconvolution of perturbed hydroxyl groups after sorption of (a, b) benzene, (c, d) toluene and (e, f) *p*-xylene with partial pressures of 10^{-3} and 1 mbar at 343 K.

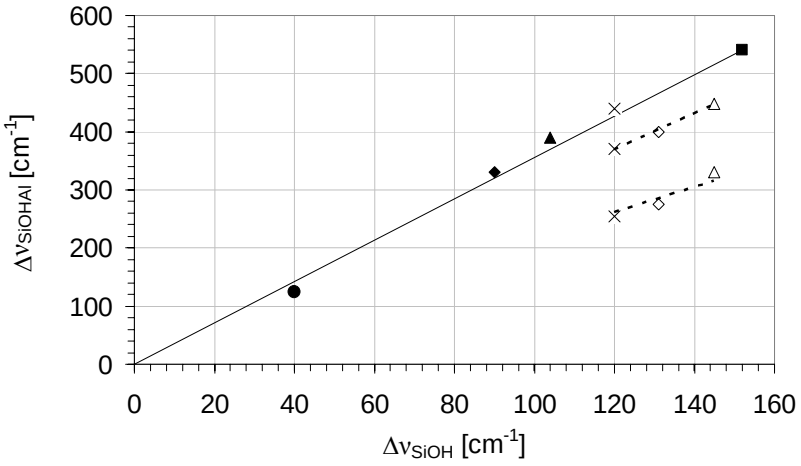

Figure 4.5. Bellamy-Hallam-Williams plot (● N_2, ♦ CO, ▲ C_2H_4, ■ C_3H_6) from ref. [40], (× C_6H_6) from ref. [45] and (◊ C_7H_8), (Δ C_8H_{10}) of present work.

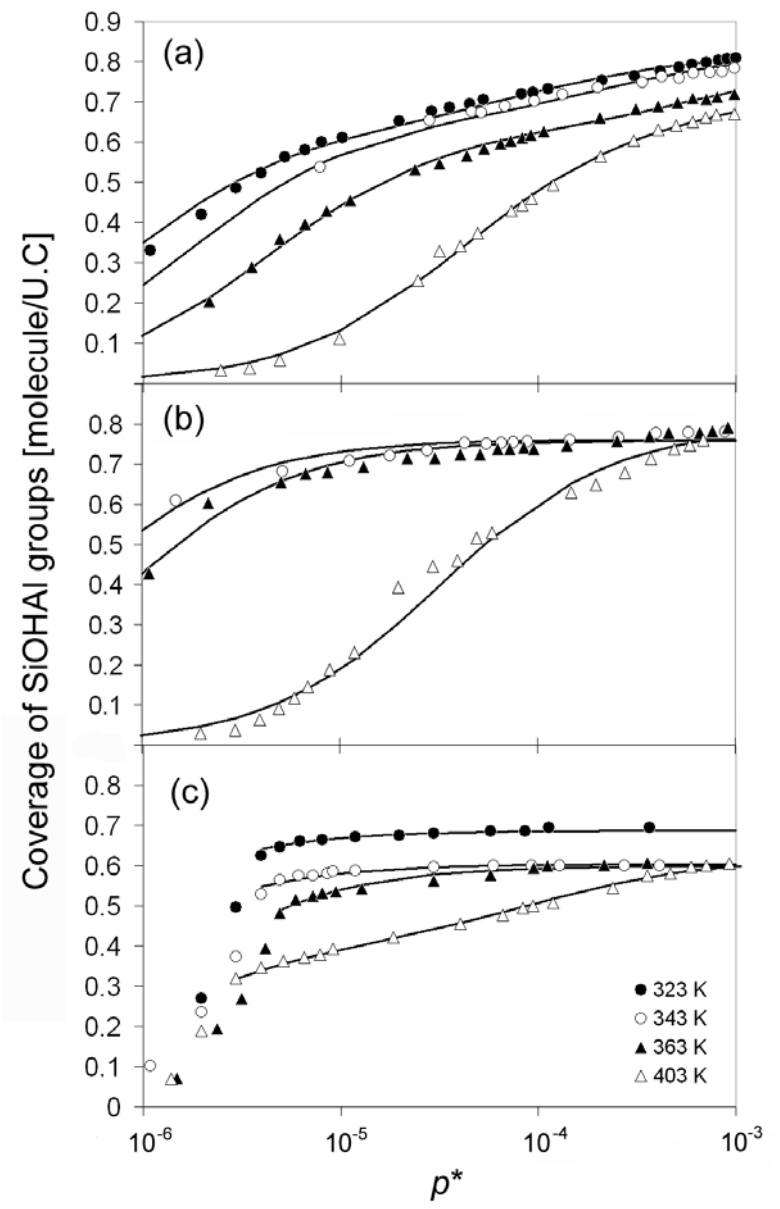

Figure 4.6. Adsorption isotherms of (a) benzene, (b) toluene and (c) *p*-xylene on SiOHAl groups of HZSM-5.

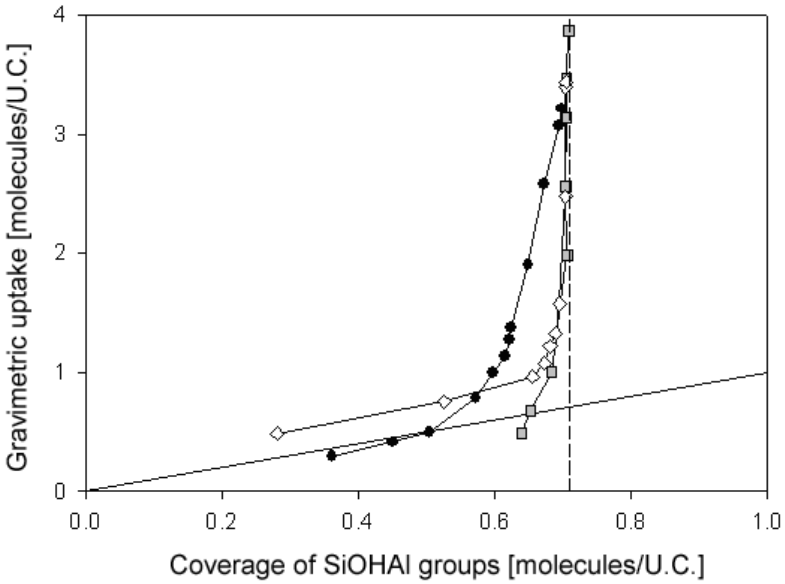

Figure 4.7. Correlation between the total coverage determined from gravimetry and the coverage of the SiOHAl groups determined by IR spectroscopy for (●) benzene, (■) toluene and (◇) p-xylene. The full line indicates the 1:1 ratio and the dashed line the concentration of Brønsted acid sites of the HZSM-5.

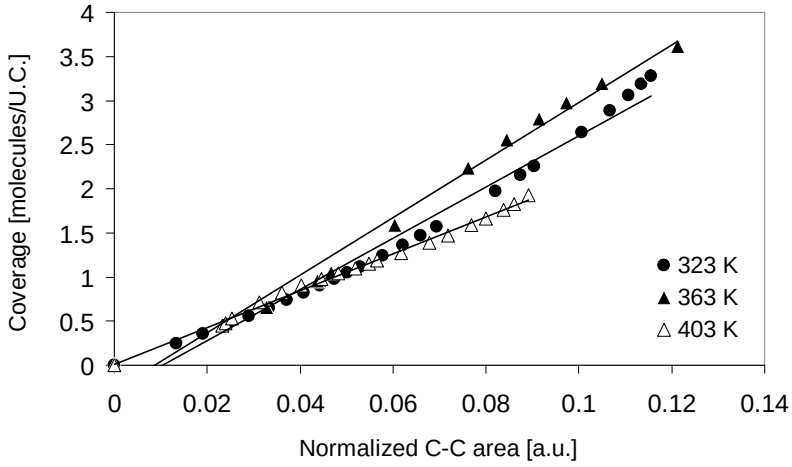

Figure 4.8. Correlation between *p*-xylene coverage determined from gravimetry and normalized area of *p*-xylene ring deformation vibration band.

Although the shape and character of the gravimetric adsorption isotherms were similar for the three molecules adsorbed on HZSM-5 (see Figure 4.1), distinct differences were observed in the site specific adsorption isotherms on the bridging hydroxyl groups (see Figure 4.6). For benzene the adsorption isotherms can be described by dual-site Langmuir model [45]:

$$q = \sum_{j=1}^{2} q_j^{sat} \frac{K_j \cdot p^*}{1 + K_j \cdot p^*} \qquad (4.1)$$

where K_j denotes the thermodynamic equilibrium constant for the sorption process *j*, q_j^{sat} is the maximum coverage of the particular sorption site *j* [molecules/unit cell] and *p** is the partial pressure being normalized to standard conditions (i.e. $p^* = p/p^0$). For toluene, a single-site Langmuir model was sufficient to fit the adsorption isotherm on the SiOHAl groups, while for *p*-xylene the fit with a Langmuir isotherm was not successful, because after a sharp initial uptake at low pressure the adsorption isotherm immediately reached saturation. The use of the dual- and single-site Langmuir model for benzene and toluene is verified by the correlation coefficient (R^2), which is 0.99 for benzene and 0.96 - 0.99 for toluene, while for p-xylene only 0.63 - 0.88 could be reached by applying the Langmuir model.

From the temperature dependence of the equilibrium constants calculated from the Langmuir isotherms the changes in the standard enthalpy and entropy (ΔH^0 and ΔS^0) for the molecules adsorbed can be calculated according to Equation 4.2.

$$K = e^{\frac{\Delta S^0}{R}} \cdot e^{-\frac{\Delta H^0}{RT}} \qquad (4.2)$$

The values for K_j and q_j^{sat} for the sorption of benzene and toluene are summarized in Table 4.1 and the values for ΔH^0 and ΔS^0 for the sorption on the SiOHAl groups of HZSM-5 are summarized in Table 4.2.

Table 4.1. Sorption equilibrium constants determined from adsorption isotherms measured by infrared spectroscopy.

Sorbate	T [K]	q_1^{sat} [molecules/ U.C.]	K_1	q_2^{sat} [molecules/ U.C.]	K_2
Benzene	323	0.63	1.22×10^6	0.18	1.07×10^4
	343	0.65	5.91×10^5	0.17	4.00×10^3
	363	0.62	2.35×10^5	0.17	1.32×10^3
	403	0.67	2.34×10^3	0.14	2.57×10^2
Toluene	343	0.76	2.35×10^6	-	-
	363	0.76	1.29×10^6		
	403	0.79	3.14×10^4		

4.5. Discussion

The sorption of benzene, toluene and *p*-xylene on both MFI type materials reaches a plateau at a coverage of 4 molecules/U.C, which results from the sorption at the intersections between sinusoidal and straight channels. As we have already described for benzene [45], also for toluene and p-xylene only a slightly higher uptake and a slightly higher heat of adsorption was observed for the acidic HZSM-5 compared to the non acidic Silicalite-1 sample. (The almost identical uptake of toluene on both materials can only result from the limits of accuracy of the TGA experiment.) Only for *p*-xylene an

uptake above 4 molecules/U.C was observed in the temperature and pressure range studied indicating the reorientation of the molecules from the intersections to sites in the sinusoidal and straight channels. Note that for the sorption of p-xylene on HZSM-5 a phase transition from the monoclinic *P*nma to the orthorhombic $P2_12_12_1$ phase was reported in the literature at a coverage of 4 molecules/U.C [29], which was accompanied by a change in the heat of adsorption of 2 kJ/mol.

Table 4.2. Standard enthalpy and standard entropy changes for aromatic molecules.

Sorbate	Sorption	ΔH_1^o [kJ/mol]	ΔH_2^o [kJ/mol]	ΔS_1^o [J/mol K]	ΔS_2^o [J/mol K]
Benzene	Gravimetry	-51	-50	-60	-92
	IR / SiOHAl	-54	-51	-47	-80
Toluene	Gravimetry	-77	-	-119	-101
	IR / SiOHAl	-86	-	-125	-
p-Xylene	Gravimetry	-94	-	-197	-
	IR / SiOHAl	-	-	-	-

It is interesting to note that also for these molecules, although having a higher basicity compared to benzene, the main energetic contribution is also the non-specific interaction with the pore walls. Moreover, the additional energetic contribution per -CH_3 group to the heat of adsorption for toluene (25 kJ/mol) is larger compared to *p*-xylene (20 kJ/mol), which shows that the geometrically more demanding *p*-xylene molecules experience a stronger repulsive interaction from the zeolite pores when being adsorbed at the intersections. The differences in the heat of adsorption between the acidic and the non acidic materials allow estimating the energetic contribution of the localized interaction between the aromatic molecules and the SiOHAl groups

(3-5 kJ/mol). Although this is more than an order of magnitude lower compared to the non-localized interaction this additional energetic contribution leads to a preferential adsorption of the molecules in intersections containing SiOHAl groups. As the HZSM-5 sample used contains (in average) 0.7 SiOHAl groups per unit cell, the molecules are well separated at low loadings (assuming a statistical distribution of Al within the material) and only at higher pressure neighboring intersections are occupied. Therefore, the gravimetric uptakes and the coverage of the bridging hydroxyl groups show a different trend as function of the sorbate partial pressure, while linear correlations between the gravimetric uptakes and the intensities of the ring deformation vibrations (both directly measure the concentration of adsorbed molecules) were observed.

The formation of two (or more) perturbed hydroxyl groups after sorption of weakly basic molecules (electron donor) can either result from the presence of sorption sites with distinctively different acid strength [38], or from the sorption at sites with different geometrical constraints [40]. For benzene sorption, two perturbed hydroxyl groups at low coverage and a third one at high coverage were observed. The perturbed hydroxyl groups at 3350 and 3250 cm^{-1} were assigned to the sorption of benzene with the ring and a C-C bond oriented towards the bridging hydroxyl groups of the zeolite, respectively [45]. The orientation with the ring towards the SiOHAl groups leads to the formation of the perturbed hydroxyl groups at 3350 cm^{-1}, which is the orientation with the sterically more constrained geometry with the larger decrease in entropy [45]. Typically the width of the perturbed hydroxyl groups increases with increasing $\Delta\nu_{SiOHAl}$ [46]. The broader perturbed hydroxyl group at the higher frequency (i.e. the smaller $\Delta\nu_{SiOHAl}$) further supports the assignment band to the sterically more constrained sorption structure. The shift in the wavenumber for the third perturbed hydroxyl band at 3170 cm^{-1} indicates that this group results from the sorption of benzene in an almost unconstrained environment at the pore openings. For the methyl-substituted benzene

molecules only at low coverage two perturbed hydroxyl bands at 3335 and 3210 cm^{-1} as well as at 3280 and 3160 cm^{-1} for toluene and *p*-xylene, respectively, were observed. However, with increasing coverage only the perturbed hydroxyl band of the less constrained sorption structure (i.e., at 3210 and 3160 cm^{-1} for toluene and *p*-xylene, respectively) remained. This indicates that at low coverage ($<10^{-1}$ mbar) also toluene and *p*-xylene can be adsorbed in two orientations at the intersections with respect to the SiOHAl groups. At this partial pressure the preferential adsorption at intersections containing SiOHAl groups leads to spatially well separated molecules which can be randomly oriented with respect to the bridging hydroxyl groups. However, at higher partial pressures also neighboring intersections (i.e. without SiOHAl groups) are occupied and we would like to speculate that the intermolecular interactions lead to a long range ordering of the molecules in the less constrained sorption geometry within the MFI structure.

It is interesting to note that this effect is only observed for the sterically more demanding molecules. A model based on the geometric properties of the MFI structure and of p-xylene (shown in Figure 4.9) indicates the close proximity of the adsorbate molecules located at the intersections at a coverage of 4 molecules/U.C. It appears that the close proximity of the $-CH_3$ groups directs the sorption of the alkyl substituted molecules into the less constraint sorption geometry within the pores, which is presumably the orientation with a single C atoms or a C-C bond towards the SiOHAl groups.

Similar to benzene, a small fraction of toluene and p-xylene should adsorb on bridging hydroxyl groups at the pore openings in an (almost) unconstrained environment. The perturbed hydroxyl bands of the SiOHAl groups for this type of interaction should appear at 3150 and 3090 cm^{-1} for toluene and p-xylene, respectively (i.e., $\Delta\nu_{SiOHAl}$ = 460 and 520 cm^{-1} based on the data presented in Figure 4.5), where they strongly overlap with the C-H stretching vibrations in the region 3080 – 2970 cm^{-1}. For toluene a shoulder at ~ 3115 cm^{-1} was observed (see Figure 4.4 d), but an unambiguous assignment

to the perturbed hydroxyl group of an unconstrained sorption can not be made.

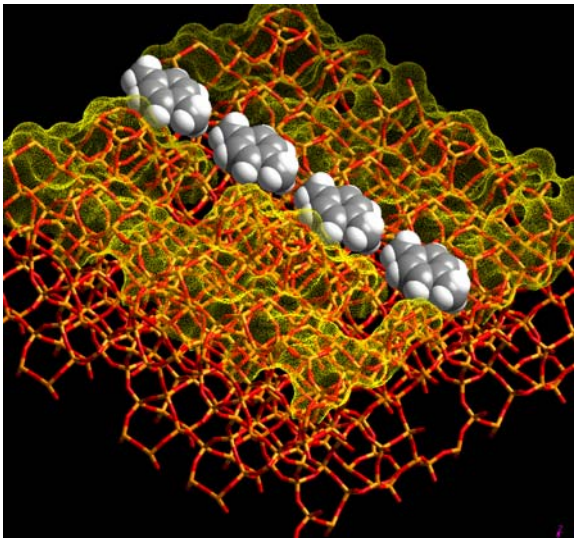

Figure 4.9. Graphical model for *p*-xylene adsorbed at the intersections of MFI (loading 4 molecules per unit cell). The molecules are shown with their van der Waals radii.

The difference in $\Delta\nu_{SiOHAl}$ with respect to the unconstrained sorption decreases in the order *p*-xylene, toluene and benzene (see Figure 4.5), which follows the decrease in standard entropy after sorption and is in line with the larger sterical constraints of the alkyl substituted molecules. For benzene two orientations with different decrease in entropy (47 and 80 J/mol·K) and similar enthalpy (~ 54 kJ/mol) were identified from the site specific adsorption isotherms on the SiOHAl groups. The larger decrease in entropy (125 J/mol·K) and enthalpy (80 kJ/mol) observed for toluene shows that the presence of the additional -CH_3 group leads to a stronger interaction and to the sorption in a sterically more constrained geometry compared to benzene. For *p*-xylene the Langmuir model is inadequate to describe the adsorption isotherms on the SiOHAl groups. This might be a consequence of the strongly confined sorption

structure resulting from the two alkyl groups in para-position, which only allows an orientation along the straight channels. Note that this is in perfect agreement with the almost twice as large decrease in the standard entropy determined from the gravimetric adsorption isotherms for p-xylene compared to toluene (see Table 4.2.).

In general, the decrease in entropy after sorption of the molecules inside the pores can be understood as a loss of vibrational, rotational or translational degrees of freedom. As a result of the close fit of the molecules inside the pores one can assume that the molecules are partially hindered in their rotational and vibrational modes, while the diffusion through the pores allows translational motion. The rotational partition function of non-linear molecules per degree of freedom is given by [47]:

$$q_r = \frac{1}{\sigma}\left(\frac{8\pi^2 k_B T}{h^2}\right)^{\frac{3}{2}} \sqrt{\pi . I_x I_y I_z} \tag{4.3}$$

where σ is the molecule symmetry number and I is moment of inertia along the three Cartesian coordinates and *r* the interatomic distance:

$$I = \left(\frac{m_1 . m_2}{m_1 + m_2}\right) r^2 \tag{4.4}$$

The rotational contribution to the entropy can be calculated from:

$$S_r = R\left[\ln q_r + T\left(\frac{\partial \ln q}{\partial T}\right)_V\right] \tag{4.5}$$

Which leads after substitution of Equation 4.3 into Equation 4.5 to:

$$S_r = R\left(\ln q_r + \frac{3}{2}\right) \tag{4.6}$$

The decrease in entropy per rotational degree of freedom for benzene, toluene and p-xylene is summarized in Table 4.3. The sorption of benzene with the aromatic ring oriented towards the SiOHAl groups leads to a decrease in entropy of 80 J/mol.K, which indicates that the molecules looses approximately one degree of rotational freedom (90 J/mol.K), while the orientation with the C-C bond oriented towards the SiOHAl group leads to a decrease in entropy of 47 J/mol.K, which corresponds to the loss of approximately half a degree of freedom for the rotation. For toluene both sorption structures led to the same decrease in entropy of 125 J/mol.K, which is close to one degree of freedom for the rotation (111 J/mol.K). This indicates that the additional $-CH_3$ group in toluene hinders the rotation around one axis in both orientations, while for benzene the (symmetric) molecule looses only ½ degree of rotational freedom for the sorption with the C-C bond oriented towards to SiOHAl groups. For *p*-xylene the decrease of entropy of 197 J/mol.K, calculated from the gravimetric isotherm corresponds to the loss of almost two degrees of freedom for the rotation (109 J/mol.K). The increasingly hindered rotation in presence of the additional $-CH_3$ groups is in prefect agreement with the larger deviation for $\Delta\nu_{SiOHAl}$ observed in the IR spectra (see Figure 4.5) and indicates that the presence of the $-CH_3$ groups leads to a more ordered sorption structure, which might also explain why the reorientation from the intersections to positions in the channels is observed at the lowest partial pressure for p-xylene within the series of molecules studied.

Table 4.3. Moments of inertia, partition functions and rotational entropies of aromatic molecules calculated by statistical thermodynamics.

Molecules	I_{xyz} [kg.m^2]	q_r		S_r [J/mol.K]	
		323 K	403 K	323 K	403 K
Benzene	2.90×10^{-45}	8.26×10^3	1.15×10^4	87	90
	1.45×10^{-45}				
	1.45×10^{-45}				
Toluene	4.74×10^{-45}	9.70×10^4	1.35×10^5	108	111
	3.30×10^{-45}				
	1.49×10^{-45}				
p-xylene	7.20×10^{-45}	8.11×10^4	1.13×10^5	106	109
	5.74×10^{-45}				
	1.58×10^{-45}				

4.6. Conclusion

The main energetic contribution of the sorption of benzene, toluene, *p*-xylene on HZSM-5 and Silicalite-1 is the non-specific interaction with the pore walls. The specific interaction with the Brønsted acidic SiOHAl groups is about an order of magnitude lower. However, this additional energetic contribution leads to the preferential occupation of intersections containing SiOHAl groups. For benzene sorption two energetically equal, but entropically different sorption structures were identified. The toluene sorption on the SiOHAl groups can be described with one adsorption isotherm. Also in this case, two statistically distributed sorption structures with different sterical constraints are observed at low coverage by IR spectroscopy. For p-xylene, the sharp initial uptake is followed by a rapid saturation of the sorption of the SiOHAl groups. The

Langmuir model is inadequate to describe this sorption. Similar to toluene also two randomly populated orientations are observed at low coverage, while at higher coverage the molecules are concluded to be adsorbed in a less constrained orientation. The sterical effects of the additional $-CH_3$ groups leads to a further loss of rotational entropy, and to an ordering of the molecules inside the pores. The preferential adsorption at intersection results in spatially well separated molecules which can be randomly oriented with respect to SiOHAl groups.

4.7. Acknowledgments

The authors acknowledge fruitful discussions in the framework of the network of excellence IDECAT.

References

1 Corma, A., *J. Catal.*, **2003**, 216, 298.

2 Mohanty, S., McCormick, A. V., *Chem. Eng. J.*, **1999**, 74, 1.

3 Karge, H. G., *C. R. Chimie* **2005**, 8, 303.

4 Kärger, J., *Adsorption*, **2003**, 9, 29.

5 Broadbelt, L. J., Snurr, R. Q., *Appl. Catal. A*, **2000**, 200, 23.

6 Kärger, J., Ruthven, D. M., *Diffusion and Adsorption in Porous Solids*. In *Handbook of Porous Solids*; Schüth, F., Sing, K. S., Weitkamp, J., (Eds.); Wiley-VCH: Weinheim, 2002, Vol. 4, 2089.

7 Song, L. J., Sun, Z. L., Ban, H. Y., Dai, M., Rees, L. V. C., *Adsorption*, **2005**, 11, 325.

8 Shah, D. B., Chokchalacha, S., Hayhurst, D. T., *J. Chem. Soc. Faraday Trans.*, **1993**, 89, 3161.

9 McCullen, S. B., Reischman, P. T., Olson, D. H., *Zeolites*, **1993**, 13, 640.

10 Zhu, W., Kapteijn, F., Moulijn, J. A., *Phys. Chem. Chem. Phys.*, **2000**, 2, 1989.

11 Portsmouth, R. L., Gladden, L. F., *Chem. Eng. Res. Design*, **1992**, 70, 186.

12 Pfeifer, H., Kärger, J., *J. Mol. Liquids*, **1992**, 54, 253.

13 Floquet, N., Coulomb, J. P., Weber, G., Bertrand, O., Bellatt, J. P., *J. Phys. Chem. B*, **2003**, 107, 685.

14 Jobic, H., *Curr. Opin. Solid State Mater. Sci.*, **2002**, 6, 415.

15 Ashtekar, S., McLeod, A. S., Mantle, M. D., Barrie, P. J., Gladden, L. F., *J. Phys. Chem. B*, **2000**, 104, 5281.

16 Huang, Y. N., Havenga, E. A., *J. Phys. Chem. B*, **2000**, 104, 5084.

17 Niessen, W., Karge, H. G., *Microp. Mater.*, **1993**, 1, 1.

18 Nastro, A., Coflella, C., Aiello, R., *Stud. Surf. Sci. Catal.*, **1985**, 24, 19.

19 Berak, J. M., Mostowcz, R., *Stud. Surf. Sci. Catal.*, **1985**, 24.

20 Guth, J.-L., Kessler, H., Wey, R., *Stud. Surf. Sci. Catal.*, **1986**, 28, 121.

21 Flanigen, E. M., Bennett, J. M., Grose, R. W., Cohen, J. P., Patton, R. L., Kirchner, R. M., Smith, J. V., *Nature*, **1978**, 271, 512.

22 Kokotailo, G. T., Lawton, S. L., Olson, D. H., Olson, D. H., Meier, W. M., *Nature*, **1978**, 272, 437.

23 Narkiewicz-Michalek, J., Szabelski, P., Rudzinski, W., Chiang, A. S. T., *Langmuir*, **1999**, 15, 6091.

24 Rudzinski, W., Narkiewicz-Michalek, J., Szabelski, P., Chiang, A. S. T., *Langmuir*, **1997**, 13, 1095.

25 Huang, Y. N., Havenga, E. A., *Chem. Mat.*, **2001**, 13, 738.

26 Olson, D. H., Kokotailo, G. T., Lawton, S. L., Meier, W. M., *J. Phys. Chem.*, **1981**, 85, 2238.

27 Talu, O., Guo, C. J., Hayhurst, D. T., *J. Phys. Chem.*, **1989**, 93, 7294.

28 Snurr, R. Q., Bell, A. T., Theodorou, D. N., *J. Phys. Chem.*, **1993**, 97, 13742.

29 Takaishi, T., Tsutsumi, K., Chubachi, K., Matsumoto, A., *J. Chem. Soc., Faraday Trans.*, **1998**, 94, 601.

30 Portsmouth, R. L., Duer, M. J., Gladden, L. F., *J. Chem. Soc. Faraday Trans.*, **1995**, 91, 559.

31 Lee, C. K., Chiang, A. S. T., *J. Chem. Soc. Faraday Trans.*, **1996**, 92, 3445.

32 Armaroli, T., Bevilacqua, M., Trombetta, M., Alejandre, A. G., Ramirez, J., Busca, G., *Appl. Catal. A*, **2001**, 220, 181.

33 Armaroli, T., Trombetta, M., Alejandre, A. G., Solis, J. R., Busca, G., *Phys. Chem. Chem. Phys.*, **2000**, 2, 3341.

34 Trombetta, M., Alejandre, A. G., Solis, J. R., Busca, G., *Appl. Catal. A*, **2000**, 198, 81.

35 Trombetta, M., Armaroli, T., Alejandre, A. G., Gonzalez, H., Solis, J. R., Busca, G., *Catal. Today*, **2001**, 65, 285.

36 Lercher, J., A.; Noller, H., *J. Catal.*, **1982**, 77, 152.

37 Su, B. L., Norberg, V., *Coll. Surf. A*, **2001**, 187, 311.

38 Hair, M. L., Hertl, W., *J. Phys. Chem.* **1970**, 74, 91.

39 Su, B. L., Barthomeuf, D., *J. Catal.* **1993**, 139, 81.

40 Onida, B., Bonelli, B., Borello, L., Fiorilli, S., Geobaldo, F., Garrone, E., *J. Phys. Chem. B*, **2002**, 106, 10518.

41 Onida, B., Geobaldo, F., Testa, F., Aiello, R., Garrone, E., *J. Phys. Chem. B*, **2002**, 106, 1684.

42 Bellamy, L. J., Hallam, H. E., Williams, R. L., *J. Chem. Soc. Faraday Trans.*, **1958**, 54, 1120.

43 Datka, J., Gil, B., *Catal. Today*, **2001**, 70, 131.

44 Datka, J., Gil, B., Weglarski, *Microp. Mesop. Mater.*, **1998**, 21, 75.

45 Jentys, A., Mukti, R. R., Tanaka, H., Lercher, J. A., *Microp. Mesop. Mater.* **2006**, 90, 284.

46 Makarova, M. A., Ojo, A. F., Karim, K., Hunger, M., Dwyer, J. *J. Phys. Chem.*, **1994**, 98, 3619.

47 Chorkendorff, I., Niemantsverdriet, J. W., *Concepts of Modern Catalysis and Kinetics*; Wiley, **2003**.

Chapter 5

Surface transport processes and sticking probability of aromatic in HZSM-5

5. SURFACE TRANSPORT PROCESSES AND STICKING PROBABILITY OF AROMATIC IN HZSM-5

5.1. Abstract

The surface transport processes and sticking probabilities for a series of aromatic molecules (i.e. benzene, toluene, *p*-xylene and o-xylene) on HZSM-5 and SiO_2 (Aerosil) were studied by fast time-resolved (rapid scan) IR spectroscopy. The transport of the molecules from the gas phase to the sites inside the pores of the zeolite follows a series of steps including a weakly bound (pre-adsorbed) state formed after the collision of the molecules with the surface, which is controlled by the sticking probability of the molecules on the surface. For benzene, toluene and p-xylene the sticking probabilities on HZSM-5 and SiO_2 were found to be in the order of 10^{-7}. Using statistical thermodynamic calculations the low sticking probabilities were related to the loss of rotational degrees of freedom of the molecules in the pre-adsorbed state. The existence of external mass transport resistances was studied by comparing the transport diffusivities of the aromatic molecules on the samples prepared as self-supporting wafers and as dispersed powder samples. The identical diffusion processes for both preparation methods, the similar BET surface area and the dimensions of the interparticle space confirmed that the sample preparation in form of wafers does not lead to a retardation of diffusion processes.

5.2. Introduction

The study of molecular sorption and transport of reactants into nano-sized porous materials, where sorption and reaction sites reside, has been a

critical issue in catalysis and the complex interactions and mass transfer processes of gas phase molecules can be considered as the first step in the reactions over heterogeneous catalysts. The understanding of the entire surface processes including the adsorption on the outer surface and the diffusion into the active sites is essential when tailoring the shape selective properties of catalytically active materials, e.g., by the modification of the surface [1,2].

The diffusion of aromatic molecules in zeolites have been addressed in great detail by experimental [2-16] and theoretical [17-22] methods, while the elementary steps prior to the diffusion inside the pores have been the focus of our recent investigations [23-26]. As molecules with a kinetic diameter similar to that of the pore aperture can not directly enter into the pores [27], processes on the outer surface will control the concentration gradients of the reactants and thus the diffusion processes. Closely related to this point is the presence of surface barriers, which were reported to directly influence the transport diffusion [9,28]. As these processes are fast and only a small fraction of the molecules are typically involved, a fast spectroscopic technique with an excellent signal to noise ratio is required. We have already described the sequence of transport steps of aromatic molecules in HZSM-5 using fast time-resolved (rapid scan) IR spectroscopy [26], a method able to monitor the micro kinetic processes on the surface within time scale of milliseconds. A series of consecutive steps including the collision of molecules with the surface, the sorption in a weakly bound surface state (i.e., a pre-adsorbed state) with a high two-dimensional mobility of molecules on the outer surface and finally the parallel transport to silanol groups at the surface and to bridging hydroxyl groups inside the pores was identified [26].

The sorption of a molecule on a surface can be described with the sticking probability, which is the probability that a molecule is captured on the (particle) surface after the collision from the gas phase. From the collision frequencies and the uptake rates of aromatic molecules on the silanol groups

of ZSM-5 and Aerosil sticking probabilities in the order of 10^{-7} were estimated [26]. Simon et al. [29] challenged those numbers by reporting a sticking probability close to one for n-butane on Silicalite-1 determined from PFG-NMR and molecular dynamics simulations. The authors suggested that the low numbers observed in our work are presumably due to the presence of mass transport limitations of the molecules through the bed of zeolite particles (i.e. external diffusion limitations). To follow up with this argument, we confirmed experimentally the absence of such limitations and could be further shown by statistical thermodynamics that such a low sticking probability is expected when the molecules loose (rotational) entropy during the sorption [23]. In a reply to these arguments the sticking probability for benzene in Silicalite-1 was re-estimated by Kärger et al. [30] based on the Fick's first law and was reported to be in the order of 10^{-4}, while for ethane in zeolite NaX, the number was in the order of 10^{-2}. The pore sizes of 10-membered ring zeolites such as HZSM-5 and Silicalite-1 are in the same order as the kinetic diameters of aromatic molecules. The reason for lower sticking probability of aromatic molecules in Silicalite-1 compared to n-alkanes in zeolite NaX results from the different gas phase molecular geometry of the smaller n-alkane, which leads to a faster and entropically less demanding reorientation when entering the pores [31].

Due to the focal interest on studying the mass transport processes of reactant molecules from the gas phase to the sites inside the pores, the impact of different steric environments on the sticking probability as well as its boundary conditions for the transport of aromatic in HZSM-5 are described. Additional confirmation is provided that IR experiments are not disturbed by artifacts such as local exothermicity or external mass transfer limitations when using samples prepared as self-supporting wafers. The present work attempts to contribute to the complete description of surface transport processes and to the thermodynamic description of the sticking probability of aromatic molecules in zeolites.

5.3. Experimental

5.3.1. Materials

The surface processes of aromatic molecules (i.e. benzene, toluene, p-xylene) were studied on HZSM-5 with a Si/Al ratio of 82. The particle size of the zeolite was 0.5 μm, MAS-MNR indicated the absence of octahedral Al. The concentrations of the terminal silanol groups (SiOH) and the bridging hydroxyl groups (SiOHAl, Brønsted acid sites) of HZSM-5 were 0.09 and 0.12 mmol/g, respectively determined by ^{1}H MAS NMR spectroscopy. Benzene, toluene and *p*-xylene in spectroscopic grade were obtained from Sigma-Aldrich.

5.3.2. Fast time-resolved (rapid scan) IR spectroscopy

The detailed measurement principle, instrument setup and signal-to-noise ratio requirements of fast time-resolved (rapid scan) IR spectroscopy are already described in ref [26]. The samples were prepared as self-supporting wafers with weight of approximately 25 mg/cm^2 and inserted in a vacuum cell with a geometry optimized for transmission IR spectroscopy. All IR spectra were recorded with a resolution of 8 cm^{-1}. The samples were activated under vacuum (<10^{-7} mbar) at 823 K (heating increment 10 K.min^{-1}) for 1 h. All sorption and transport experiments were carried out at 403 K. After the sorption equilibrium was established, the volume of the system was modulated (±5%) by a magnetically driven pair of vacuum bellows and synchronized with the recording of the IR spectra [26]. The changes in the coverage of the SiOHAl groups with benzene, toluene or p-xylene were studied at equilibrium partial pressures of 2×10^{-1}, 6×10^{-2} and 2×10^{-2} mbar, while for the coverage changes of the SiOH groups an equilibrium partial pressure of 1 mbar was used. To directly compare the surface coverage of the adsorbed species, all spectra were normalized using the lattice vibrations in the spectrum of the activated

zeolite between 2105 and 1740 cm^{-1}. The coverage changes of the SiOHAl and SiOH groups were converted from the changes in integral intensity of the corresponding IR bands to concentrations assuming that the molar extinction coefficients for the stretching vibrations of the corresponding hydroxyl groups are independent from the coverage.

5.3.3. Diffusion coefficients

The diffusion coefficients of the transport diffusivity for benzene, toluene and p-xylene were determined using the frequency response method [2,3,32]. Approximately 30 mg of the sample, either in the form of powder or pressed as a self-supporting pellets and subsequently crushed into small platelets, were activated in a quartz tube following the same conditions as described for the rapid scan IR experiments. The aromatic compounds were introduced into the system with an equilibrium partial pressure of 2×10^{-1} mbar at 403 K. After the sorption equilibrium was established, the volume of the system was modulated with a square-wave function in a frequency range between 0.001 and 1 Hz. The response of the pressure to the volume perturbation was recorded with a Baratron pressure transducer.

From the solution of Fick's second law for the diffusion of a single species in a solid (planar sheet) when subjected to a periodic, sinusoidal pressure modulation, the transport diffusivity can be determined from frequency response method [32]:

$$\text{in phase: } (\gamma_B / \gamma_S)\cos\phi_{S-B} - 1 = \sum_{j=1}^{n} K_j \delta_{c,j} \qquad (5.1)$$

$$\text{out-of-phase: } (\gamma_B / \gamma_S)\sin\phi_{S-B} = \sum_{j=1}^{n} K_j \delta_{s,j} \qquad (5.2)$$

$$\delta_c = (1/\eta)\left[\left(\sinh\eta + \sin\eta\right)/\left(\cosh\eta + \cos\eta\right)\right] \quad (5.3)$$

$$\delta_s = (1/\eta)\left[\left(\sinh\eta - \sin\eta\right)/\left(\cosh\eta - \cos\eta\right)\right] \quad (5.4)$$

$$\eta = \sqrt{\omega L^2 / 2D} \quad (5.5)$$

where ϕ_{S-B} is the difference between the phases of the pressure response in the presence and absence of the zeolite, ω is angular frequency of the volume modulation, D is the transport diffusion coefficient, L is the diameter/length of zeolite crystals, γ_B and γ_S are relative amplitudes of the pressure during the volume change in the absence and in the presence of zeolite, respectively. K is a constant related to the gradient of the sorption isotherm at the certain equilibrium partial pressure.

5.4. Results

5.4.1. Kinetics of surface transport processes of aromatic in HZSM-5

The sorption of aromatic molecules on HZSM-5 leads to a decrease in the intensity of the bands for the stretching vibrations of both hydroxyl groups (SiOHAl and SiOH groups) and to the formation of two bands assigned to perturbed bridging hydroxyl groups and one assigned to the perturbed silanol groups [6,33]. As the stretching vibration of the bridging hydroxyl groups at 3610 cm^{-1} is overlapped by the perturbed hydroxyl groups resulting form the sorption on the SiOH groups ($\Delta\nu$=120 cm^{-1}), the spectrum of the sorption of the same molecule on Silicalite-1 at the same temperature and pressure was subtracted before the integration. The changes in the coverage of the hydroxyl groups during the pressure modulation of benzene over HZSM-5 are shown in

Figure 5.1. The first spectrum of each series (at t = 0 s) was subtracted from the spectra of the series of time-resolved spectra, thus, bands increasing in intensity are pointing upwards whereas bands decreasing in intensity are pointing downwards.

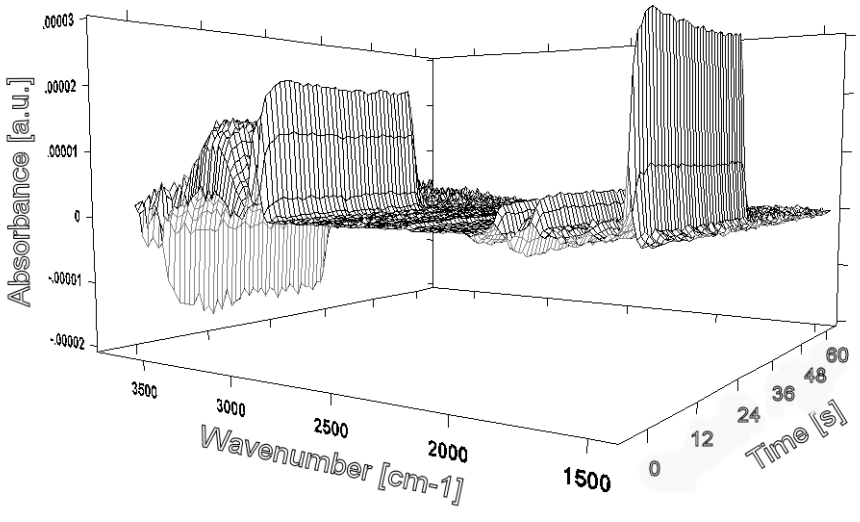

Figure 5.1. Fast time-resolved (rapid scan) IR spectra of benzene sorption on HZSM-5 during a pressure modulation of 2×10^{-2} mbar at equilibrium partial pressure of 2×10^{-1} mbar.

The changes in coverage of the SiOH and SiOHAl groups with benzene were followed from the intensity of the bands at 3745 and 3610 cm^{-1}, respectively. The SiOHAl groups are located inside the pores, while the SiOH groups terminate the crystals on the outer surface. The changes in the coverage of the SiOHAl and SiOH groups as function of the pressure modulation during the sorption of benzene, toluene and p-xylene are shown in Figure 5.2. The partial pressure of the aromatic molecules was selected to be in the steep region of the isotherm in order to observe the maximum change in the coverage during the pressure modulations.

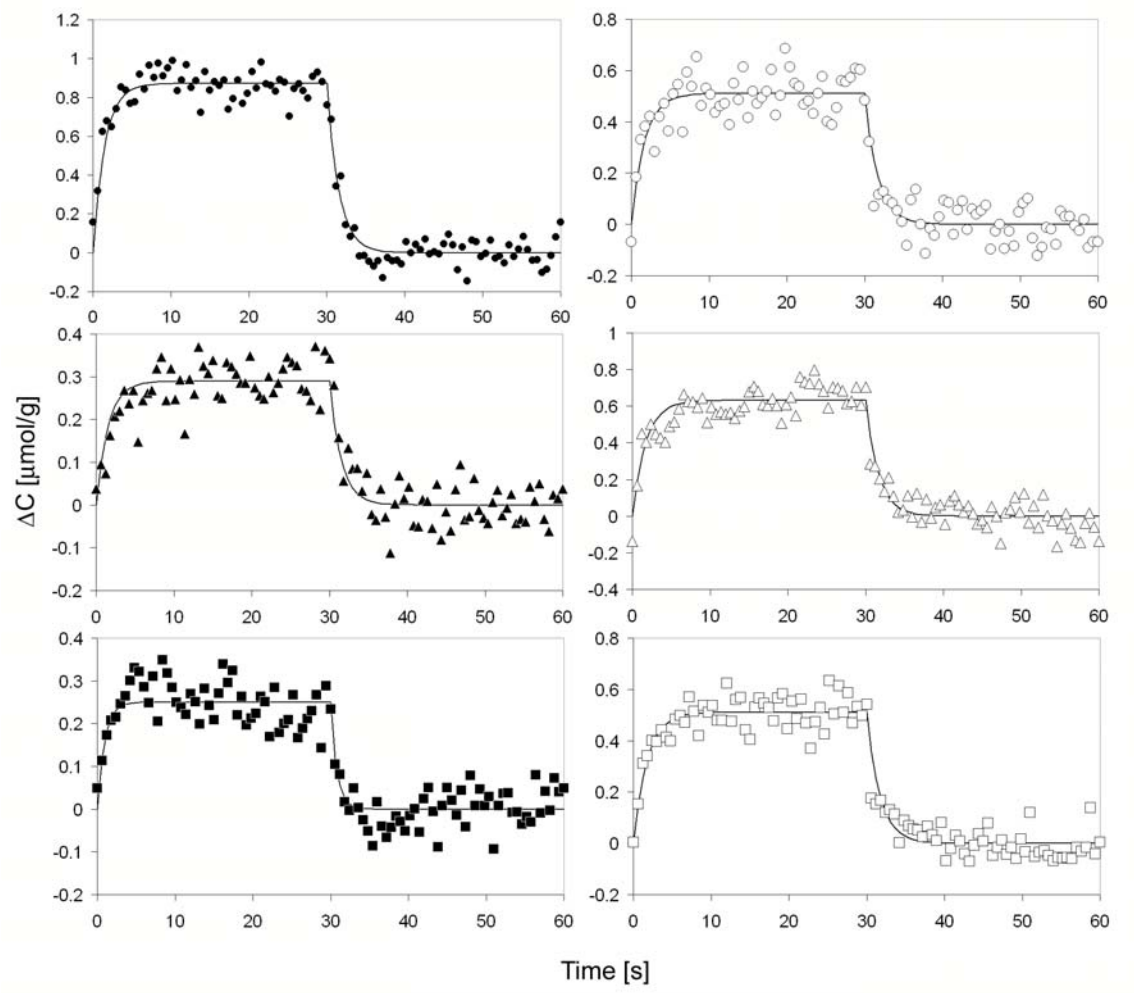

Figure 5.2. Changes in the coverage of SiOHAl groups marked in solid symbols (left) and SiOH groups marked in open symbols(right) for sorption of (•, ○) benzene, (▲, Δ) toluene and (■, □) p-xylene on HZSM-5.

The changes of the coverage of the hydroxyl groups after the stepwise increase of the partial pressure were fitted with an exponential function and the rate of the sorption process (i.e., dc/dt) for the adsorption and desorption part of the modulation experiment was determined from:

for $0 < t \leq t_p/2$ (adsorption process)

$$\Delta c_{OH}(t) = \Delta c_{OH,eq}\left(1 - e^{-t/\tau_{ad}}\right) \tag{5.6}$$

for $t_p/2 < t < t_p$ (desorption process)

$$\Delta c_{OH}(t) = \Delta c_{OH,eq} e^{-\left[t-(t_p/2)\right]/\tau_{de}} \tag{5.7}$$

with $\Delta c_{OH,eq}$ being the change of the surface concentration of the molecules after reaching the equilibrium and t_p the time period of the pressure modulation. The characteristic time constants of the transport process during the adsorption and desorption are given by τ_{ad} and τ_{de}, respectively. As the process is assumed to be first order, τ is equivalent to $1/k$, i.e., a small time constant corresponds to a large rate constant thus indicating a fast sorption process.

The corresponding time and rate constants for the adsorption and desorption processes are compiled in Table 5.1 and Table 5.2. For both HZSM-5 samples (the data for the HZSM-5 sample with Si/Al = 45 is included from ref [26]) the adsorption rate on the SiOHAl groups was faster compared to the SiOH groups, when the molecules were able to enter into the pores.

Table 5.1. Time and rate constants for the sorption of aromatic molecules on SiOHAl groups of HZSM-5.

Sorption Sites	Sorbate	τ_{ad} [s]	τ_{de} [s]	τ [s]	k [s^{-1}]
SiOHAl HZSM-5 (Si/Al=82)	Benzene	1.50	1.52	1.51	0.66
	Toluene	1.50	1.50	1.50	0.66
	p-Xylene	0.93	0.80	0.86	1.16
SiOHAl HZSM-5 (Si/Al=45)*	Benzene	1.99	2.18	2.08	0.48
	Toluene	1.72	1.89	1.81	0.55
	p-Xylene	1.62	1.50	1.56	0.64

* Results taken from ref. [26].

Table 5.2. Time and rate constants for the sorption of aromatic molecules on SiOH groups of HZSM-5 and amorphous silica.

Sorption Sites	Sorbate	τ_{ad} [s]	τ_{de} [s]	τ [s]	k [s^{-1}]
SiOH HZSM-5 (Si/Al=82)	Benzene	1.70	1.70	1.70	0.59
	Toluene	1.70	1.65	1.67	0.59
	p-Xylene	1.75	1.70	1.72	0.58
SiOH HZSM-5 (Si/Al=45)*	Benzene	3.25	3.77	3.51	0.28
	Toluene	2.84	2.70	2.77	0.36
	p-Xylene	2.00	2.10	2.05	0.49
	o-Xylene	0.50	0.60	0.55	1.82
SiOH Aerosil*	Benzene	1.70	1.64	1.67	0.60
	Toluene	1.49	1.57	1.53	0.66
	p-Xylene	0.60	0.60	0.60	1.67
	o-Xylene	0.70	0.70	0.70	1.43

* Results taken from ref. [26].

5.4.2. Sticking probability of aromatic molecules on HZSM-5 and Aerosil

Following the model of a pre-adsorbed state on the outer surface for the transport of the aromatic molecules into the pores of HZSM-5, the sum of the uptake rates on the SiOH and SiOHAl groups has to be used for the calculation of the sticking probability. Note that on Aerosil the SiOH groups were the only sorption sites and thus the sticking probability was calculated from the adsorption rate on the silanol groups [34]. Assuming a fully established sorption equilibrium, the rate of adsorption (r_{ad}) can be expressed by:

$$r_{ad} = \alpha \cdot \frac{\langle u \rangle}{4} \cdot n \tag{5.8}$$

with

$$\langle u \rangle = \sqrt{\frac{8 \cdot R \cdot T}{\pi \cdot M}} \tag{5.9}$$

and

$$n = \frac{N}{V} = \frac{p}{R \cdot T} \cdot N_A \tag{5.10}$$

in which α denotes the sticking probability, $\langle u \rangle$ the mean gas velocity, n the number of molecules per volume, T the temperature, p the pressure and N the total number of molecules, N_A the Avogadro's number V the volume and M the molecular mass. The adsorption rate (r_{ad}) changes as function of the pressure dependency of $\langle u \rangle$ and can be determined from the initial slope (i.e. at t=0) of the coverage changes after a pressure step (Equation 5.6).

$$\Delta r_{ad} = \frac{d\left(\Delta c_{OH}(t)\right)}{dt} = \frac{\Delta c_{OH,eq}}{\tau_{ad}} e^{-t/\tau_{ad}} \quad at\ t = 0 \rightarrow \Delta r_{ad} = \frac{\Delta c_{OH,eq}}{\tau_{ad}} \tag{5.11}$$

The changes in sorption rate can be also calculated through the changes of the surface concentration ($\Delta c_{OH,eq}$) of the SiOHAl and SiOH groups as described in Equation 5.7.

$$\Delta r_{ad} = \frac{\Delta c_{OH,eq}}{\tau_{ad}} = \frac{\Delta c_{OH}(t)}{\tau_{ad}\left(1 - e^{-t/\tau_{ad}}\right)} \tag{5.12}$$

From the changes in adsorption rate and collision frequency (determined by the type of molecules adsorbed, the pressure and temperature) before and after the volume modulation, the sticking probability can be derived as follows:

$$\Delta r_{ad} = \alpha \cdot \frac{\langle u \rangle}{4} \cdot \frac{p_2}{R \cdot T} \cdot N_A - \alpha \cdot \frac{\langle u \rangle}{4} \cdot \frac{p_1}{R \cdot T} \cdot N_A \tag{5.13}$$

and

$$\alpha = \frac{\Delta r_{ad}}{\frac{\langle u \rangle}{4} \cdot \frac{N_A}{RT} \cdot (p_2 - p_1)} \tag{5.14}$$

Using the expression of the adsorption rate (Equation 5.7), the sticking probability is proportional to the changes in surface coverage:

$$\alpha = \frac{\Delta c_{OH}(t)}{\tau_{ad} \frac{\langle u \rangle}{4} \cdot \frac{N_A}{RT} \cdot (p_2 - p_1)\left(1 - e^{-t/\tau_{ad}}\right)} \tag{5.15}$$

Table 5.3 summarizes the sticking probability of benzene, toluene, p-xylene and o-xylene calculated for HZSM-5 and Aerosil.

5.4.3. Transport diffusivity of aromatic in HZSM-5

In order to observe the potential influence of the preparation method on sorption and transport, the diffusion coefficients were determined for the

sample prepared as a pellet (prepared with a pressure of 5.2×10^6 Pa) and in form of the powder using the frequency response technique. The characteristic functions of the frequency response method for the diffusion of benzene, toluene and p-xylene in HZSM-5 for both preparation methods (powder and as self-supporting pellet) are compared in Figure 5.3 and the diffusion coefficients are summarized in Table 5.4.

Table 5.3. Sticking probabilities of aromatic molecules in HZSM-5 and amorphous silica.

Sorbate	α	
	HZSM-5 (Si/Al=45)	Aerosil
Benzene	1.92×10^{-7}	1.00×10^{-7}
Toluene	1.64×10^{-7}	1.59×10^{-7}
p-Xylene	1.56×10^{-7}	4.72×10^{-7}
o-Xylene	4.00×10^{-7}	4.59×10^{-7}

Two diffusion processes were observed for the transport of benzene, toluene and p-xylene in HZSM-5 for both sample preparation methods, which can be explained with different transport pathways of the molecules in the HZSM-5 channels. Based on the similar diffusivities (about one order of magnitude) and on the presence of the two processes for all three molecules studied we assign the two maxima to the diffusion in the straight and sinusoidal channels of ZSM-5 [2]. The transport within the inter-particle space should be significantly faster than the transport inside the pores and for this case a maximum in the characteristic function (δ_s) at higher frequencies should be observed. As this can be excluded from the data reported, the influence of

the sample preparation can be neglected in the sorption and diffusion of aromatic molecules on HZSM-5.

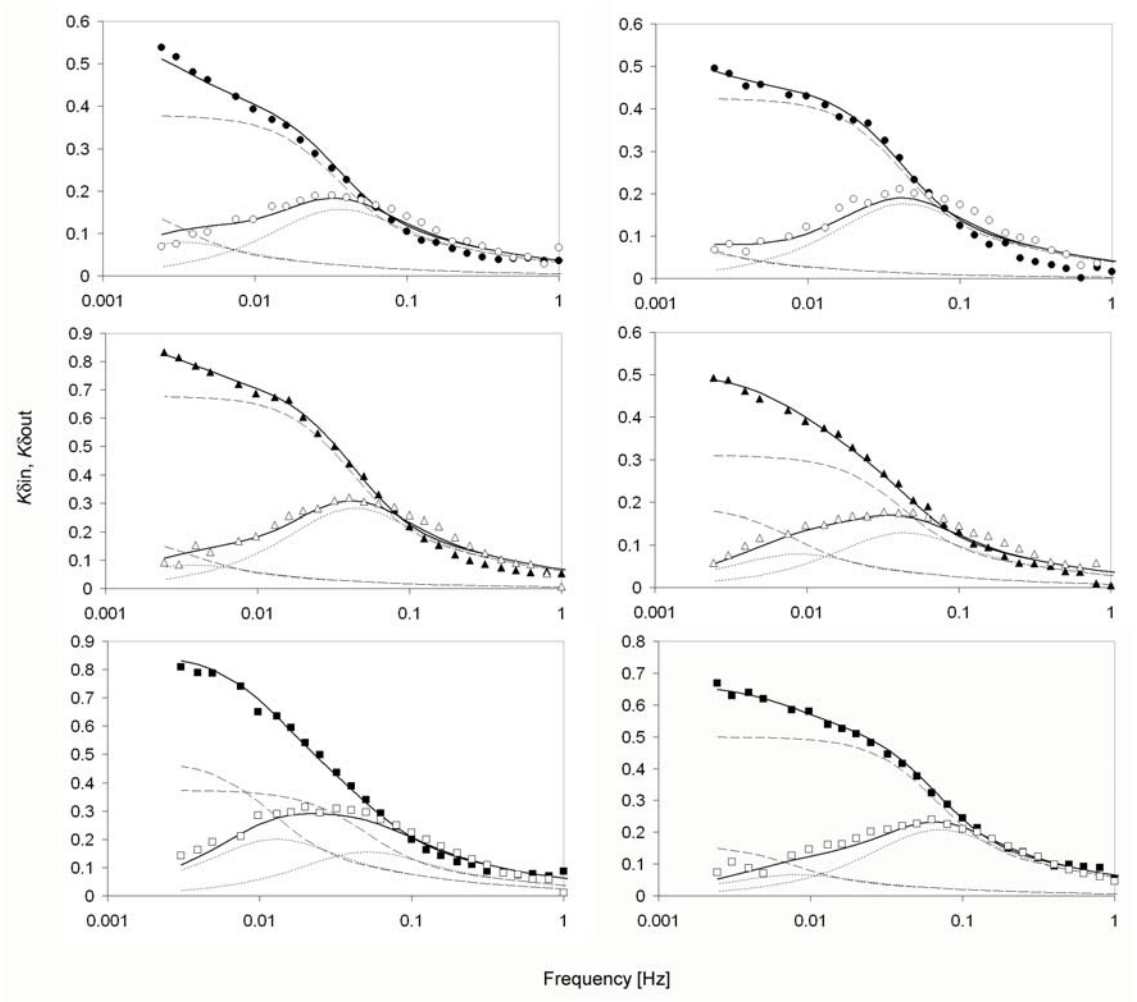

Figure 5.3. Frequency response data for (●, ○) benzene, (▲, Δ) toluene and (■, □) p-xylene diffusion in HZSM-5; in-phase function marked in solid symbol and out-of-phase function marked in open symbols; the sample measured as powder (left) and as pellet (right).

Table 5.4. Transport diffusivities of aromatic molecules in HZSM-5 estimated from the frequency response method.

Sample form	Sorbate	D_0^1	D_0^2	K_1	K_2
		$\times 10^{15}$ [$m^2.s^{-1}$]			
Powder	Benzene	1.40	0.12	0.37	0.19
	Toluene	1.70	0.14	0.67	0.19
	p-Xylene	2.00	0.50	0.37	0.48
Pellet	Benzene	1.67	0.06	0.42	0.15
	Toluene	1.70	0.34	0.31	0.19
	p-Xylene	2.70	0.31	0.49	0.16

5.5. Discussion

We have already shown that the transport of molecules to the hydroxyl groups of zeolites is preceded by the sorption into a weakly (pre-)adsorbed and highly (two-dimensionally) mobile state, followed by the diffusion of the molecules to the SiOH and SiOHAl groups [26]. For the series of aromatic molecules studied, the heat of adsorption increases from benzene over toluene to p-xylene due to the additional contribution of ~ 20 kJ/mol per -CH_3 group [35 or Chapter 4], which leads to an increase of the uptake rate on the SiOHAl groups (i.e. benzene<toluene<p-xylene).

The sticking probability of aromatic molecules (~ 10^{-7}) is about six orders of magnitude lower compared to the typical sticking probabilities of hydrogen, nitrogen, oxygen, carbon monoxide and ethylene on metals and metal oxides, which is typically between 0.1 and 1 [36]. Additionally, for the sorption of n-butane on molecular sieves (Silicalte-1) molecular dynamics simulations [29,37]

predicted a sticking probability close to 1. Although the sorption of n-butane is energetically and geometrically entirely different to the sorption of aromatic molecules with respect to the entropic contributions [24 or Chapter 3, 31, 35] such a difference in the sticking probabilities would not be expected at first sight. Based on these results and on diffusion measurements by PFG-NMR for n-alkanes in NaX, Simon et al. [29] mentioned that the very low sticking probabilities observed for the experiments using pressed samples might result from mass transfer limitations in the inter-crystalline space of the pellets. To verify the absence of such artifacts and, moreover, to confirm that the preparation of samples as self-supporting wafers (typically for transmission IR spectroscopy) in general does not lead to mass transfer limitations, frequency response experiments on the same sample prepared as a wafer and in powder form were carried out. This technique allows differentiating two diffusion processes with a difference in the diffusion coefficient of about half an order of magnitude and is thus extremely sensitive to differentiate between transport processes. For all aromatic compounds studied two diffusion processes were observed independent of the sample preparation as powder or pellet, which clearly confirms that pressing the HZSM-5 sample with a pressure of 5.2 MPa does not induce to any additional transport resistances. The two diffusion coefficients were in the order of 10^{-15} to 10^{-17} $m^2.s^{-1}$, which is in agreement to the values obtained from previous studies (see Table 5.4) [38-40].

Another way to prove the absence of the external transport limitations in the wafer is to compare the overall transport diffusion with the intracrystalline diffusion. The intracrystalline diffusion coefficient (or so called long-range diffusion coefficient) can be calculated from [41]:

$$D_{intra} = p_{inter} \cdot D_{inter} \tag{5.16}$$

with p_{inter} and D_{inter} denoting the fraction of molecules in the inter-particle space and their diffusivity. The inter-particle space between individual crystals was

estimated from scanning electron microscopy (SEM) micrographs shown for the HZSM-5 sample in powder and pellet form (pressed at 5.2 MPa) in Figure 5.4. The comparison of the two samples confirmed that pressing of the wafers does not induce changes in the crystal morphologies. The inter-particle space between the individual HZSM-5 crystals (size 0.1-0.5 μm) was in the order of 0.05-0.1 μm, therefore, the diffusion in the inter-particle space can be described as Knudsen diffusion [42] with a diffusion coefficient for benzene of 3×10^{-5} $m^2.s^{-1}$. From the gravimetric adsorption isotherm, p_{inter} was determined to be 8.1×10^{-5} for benzene at a partial pressure of 2×10^{-1} mbar and 403 K, which leads to an intracrystalline diffusion coefficient for benzene of 10^{-9} $m^2.s^{-1}$. Compared to the overall transport diffusion for benzene, determined by the frequency response method (~10^{-15} $m^2.s^{-1}$) this process is significantly faster (about 5 orders of magnitude), which also confirms that external mass transfer limitations of the molecules in the interparticle space do not exist for benzene (and the other aromatic molecules studied) on the pressed samples. In agreement with the microscopy it should also be mentioned that the BET-surface area of the sample in powder form and pressed as a pellet was nearly identical, i.e. 362 and 398 m^2/g, respectively.

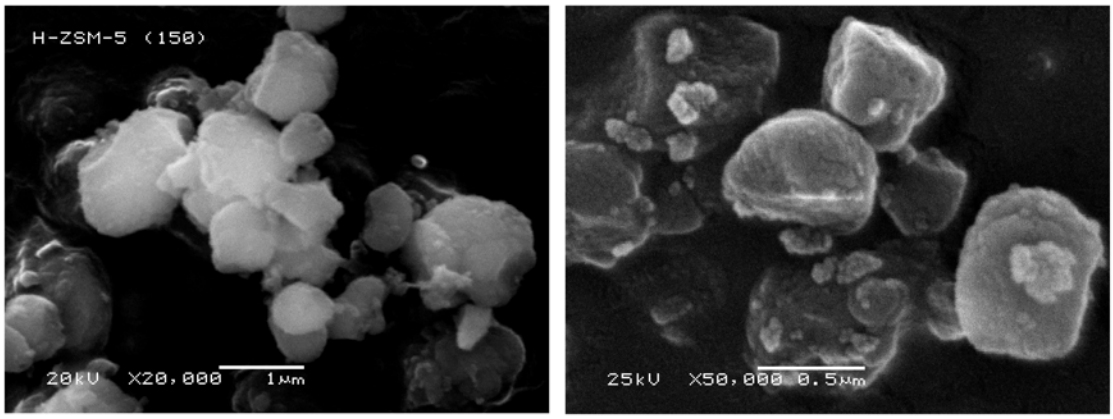

Figure 5.4. SEM micrograph of HZSM-5 with sample in the form of (a) powder and (b) pellet.

From the decrease of entropy, i.e., the loss of molecular degrees of freedom, the theoretical sticking probability in pre-adsorbed state ($\alpha^{\#}$) can be derived using statistical thermodynamics:

$$\alpha^{\#} = \frac{q_{rot}^{\#} \cdot q_{vib}^{\#}}{q_{rot}^{gas} \cdot q_{vib}^{gas}} \tag{5.17}$$

where $q_{rot}^{gas}, q_{rot}^{\#}, q_{vib}^{gas}, q_{vib}^{\#}$ represent the rotational and vibrational partition functions of the molecule in the gas phase (unhindered) and in the pre-adsorbed state (hindered). If only rotations of the molecule are (partially) hindered in the weakly sorbed state, $\alpha^{\#}$ can be related to the decrease of molecular rotational entropy in the pre-adsorbed state. The rotational partition function of a molecule is given by assuming free rotation around the principal axes (x, y, z) as presented in Equation 5.18.

$$q_{rot} = \frac{1}{\sigma}\left(\frac{8\pi^2 k_B T}{h^2}\right)^{\frac{3}{2}} \sqrt{\pi \cdot I_x \cdot I_y \cdot I_z} \tag{5.18}$$

with σ the total molecule symmetry number ($\sigma = \sigma_x \cdot \sigma_y \cdot \sigma_z$), k_B the Boltzmann constant, h the Planck constant and I_x, I_y, I_z the moment of inertia along the three Cartesian coordinates. The rotational partition functions and the resulting sticking probabilities for benzene, toluene and p-xylene on HZSM-5 and Aerosil are compared in Table 5.5. The experimental and theoretical sticking probabilities differ by about one to two orders of magnitude, which can be explained as the experimental sticking probability also includes the trapping coefficient of the sorbent. The trapping coefficient (χ) describes the probability of a molecule to be trapped into pre-adsorbed state due to exothermic collision on the external surface [43]. By comparing the experimental and

theoretical sticking probability, the trapping coefficient can be calculated following Equation 5.19 (see Table 5.5).

$$\alpha = \chi.\alpha^{\#} \tag{5.19}$$

For larger molecules such as p-xylene, the trapping coefficient has a higher value compared to benzene molecules. Generally a high number corresponds to a long residence time of the molecule on the external surface in the pre-adsorbed state allowing the generation of the heat of adsorption.

Table 5.5. Rotational partition function, sticking probability in the pre-adsorbed state and trapping coefficient of aromatic molecules in amorphous silica calculated by statistical thermodynamics

Sorbate	q_{rot}	$\alpha^{\#}$	χ (Aerosil)
Benzene	1.15×10^{4}	8.69×10^{-5}	1.15×10^{-3}
Toluene	1.35×10^{5}	7.40×10^{-6}	2.15×10^{-2}
p-Xylene	1.13×10^{5}	8.85×10^{-6}	5.33×10^{-2}
o-Xylene	2.21×10^{5}	4.52×10^{-6}	1.01×10^{-1}

5.6. Conclusions

The surface transport and sticking probability of aromatic molecules in HZSM-5 were studied by fast time-resolved (rapid scan) IR spectroscopy. The sticking probabilities of the aromatic molecules on HZSM-5 and Aerosil were in the order of 10^{-7}, which supports the previously proposed existence of a pre-adsorbed state in the sorption process. The comparison between HZSM-5 samples prepared as self-supporting wafer and in powder form clearly

confirmed the absence of artifices resulting from the pressing of the zeolite, which could induce mass transfer limitations in the inter particle space. Statistical thermodynamics revealed that the low sticking probability in the pre-adsorbed state is related to the total loss of all rotational degrees of freedom.

5.7. Acknowledgment

The authors are grateful to Dipl.-Ing. Martin Neukamm for conducting SEM measurements.

References

1 Zheng, S., Heydenrych, H., Jentys, A., Lercher, J. A., *J. Phys. Chem. B*, **2002**, 106, 9552.

2 Zheng, S., Tanaka, H., Jentys, A., Lercher, J. A., *J. Phys. Chem. B*, **2004**, 108, 1337.

3 Song, L. J, Sun, Z. L., Ban, H. Y., Dai, M., Rees, L. V. C., *Phys. Chem. Chem. Phys*., **2004**, 6, 4722

4 Song, L. J., Sun, Z. L., Ban, H. Y., Dai, M., Rees., L. V. C., *Adsorption*, **2005**, 11, 325.

5 Olson, D. H., Kokotailo, G. T., Lawton, S. L., *J. Phys. Chem*., **1981**, 85, 2238.

6 Jentys, A, Lercher, J. A., *Stud. Surf. Sci. Catal.*, **1989**, 46, 585.

7 Ruthven, D. M., Kaul, B. K., *Ind. Eng. Chem. Res*., **1993**, 32, 2053.

8 Ruthven, D. M., Kaul, B. K., *Ind. Eng. Chem. Res*., **1993**, 32, 2047.

9 Kärger, J., Caro, J., *J. Chem. Soc. Faraday Trans*., **1977**, 73, 1363.

10 Kärger, J., Pfeifer, H., Wutscherk, T., Ernst, S., Weitkamp, J., Fraissard, J., *J. Phys. Chem*., **1992**, 96, 5059.

11 Pampel, A., Engelke, F., Galvosas, P., Krause, C., Stallmach, F., Michel, D., Kärger, J., *Microp. Mesop. Mater.*, **2006**, 90, 271.

12 Su, B. L., Barthomeuf, D., *J. Catal*., **1993**, 139, 81.

13 Su, B. L., Barthomeuf, D., *Appl. Catal. A*, **1995**, 124, 81.

14 Su, B. L., Barthomeuf, D., *Zeolites*, **1995**, 15, 470.

15 Su, B. L., Manoli, J. M., Potvin, C., Barthomeuf, D., *J. Chem. Soc. Faraday Trans*., **1993**, 89, 857.

16 de Mallmann, A., Barthomeuf, D., *J. Phys. Chem*., **1989**, 93, 5636.

17 Chempath, S., Snurr, R. Q., Low, J. J., *AIChE J.*, **2004**, 50, 463.

18 Chempath, S., Snurr, R. Q., Denayer, J. F. M., Baron, G. V., *Stud. Surf. Sci. Catal.*, **2004**, 154, 1983.

19 Snurr, R. Q., Bell, A. T., Theodorou, D. N., *J. Phys. Chem*., **1994**, 98, 11948.

20 Snurr, R. Q., Bell, A. T., Theodorou, D. N., *J. Phys. Chem*., **1993**, 97, 13742.

21 Mohanty, S., Davis, H. T., McCormick, A. V., *Chem. Eng. Sci*., **2000**, 55, 2779.

22 Mohanty, S., Davis, H. T., McCormick, A. V., *AIChE J.*, **2000**, 46, 1662.

23 Jentys, A., Mukti, R. R., Lercher, J. A., *J. Phys. Chem. B*, **2006**, 110, 17691.

24 Jentys, A., Mukti, R. R., Tanaka, H., Lercher, J. A., *Microp.Mesop. Mater*., 2006, 90, 284

25 Jentys, A.; Tanaka, H.; Lercher, J. A. *Studies Surface Science and Catalysis* **2004**, *154*, 2041.

26 Jentys, A., Tanaka, H., Lercher, J. A., *J. Phys. Chem. B*, **2005**, 109, 2254.

27 Kärger, J., Ruthven, D. M., *Handbook of Porous Solids*, **2002**, 4**,** 2089.

28 Kärger, J., Bullow, M., Millward, B. R., Thomas, J. H., *Zeolites*, **1986**, 6, 146.

29 Simon, J. -M., Bellat, J. -P, Vasenkov, S., Kärger, J., *J. Phys. Chem. B*, **2005**, 109, 13523.

30 Kärger, J., Vasenkov, S., *J. Phys. Chem. B*, **2006**, 110, 17694.

31 Pieterse, J. A. Z., Veefkind-Reyes, S,. Seshan, K., Lercher, J. A., *J. Phys. Chem. B*, **2000**, 104, 5715.

32 Yasuda, Y., *Heterog. Chem. Rev*., **1994**, 1, 103.

33 Armaroli, T., Bevilacqua, M., Trombetta, M., Alejandre, A. G., Ramirez, J., Busca, G., *Appl. Catal. A*, **2001**, 220, 181.

34 *Compendium of Chemical Terminology IUPAC*; Research Triangle Park NC, **1997**.

35 Mukti, R. R., Jentys, A., Lercher, J. A., *J. Phys. Chem. C*, **2007**, 111, 3973.

36 Trapnell, B. M. W., *Chemisorption*; Butterworth: London,1964.

37 Tsai, M.-H., *Comput. Phys. Commun*., **2002**, 147, 130.

38 Zheng, S., Heydenrych, H., Röger, P, Jentys, A., Lercher, J. A., *Stud. Surf. Sci. Catal*., **2001**, 135, 214.

39 Karge, H. G., *C. R. Chimie*, **2005**, 8, 303.

40 Niessen, W., Karge, H. G., *Microp. Mater*., **1993**, 1, 1.

41 Kärger, J., Vasenkov, S., *Microp. Mesop. Mater*., **2005**, 85, 195.

42 Takahashi, R., Sato, S., Sodesawa, T., Arai, K., Yabuki, M., *J. Catal.*, **2005**, 229, 24.

43 van Santen, R. A., Niemantsverdriet, J. W., *Chemical Kinetics and Catalysis*; Plenum Press: New York, **1995**.

Chapter 6

Summary

6. Summary

6.1. Summary

The ability of understanding and describing molecular sorption and transport on porous materials is essential for designing and tailoring novel catalytically active materials. MFI zeolites with ten-membered ring pores are ideal materials for selective sorption and catalytic reactions with aromatic molecules. Using these zeolites, separation of para xylene out of xylene mixtures is possible, which is an important intermediate in the production of polyester fibers, resins and films. For utilizing shape selectivity of zeolites in catalytic reactions the fundamental understanding of sorption and transport has to be improved with respect to the thermodynamics, diffusion and kinetic aspects.

The aim of this thesis was to study the sorption and transport of aromatic molecules in acidic (HZSM-5) and non acidic (Silicalite-1) MFI zeolites using gravimetry, calorimetry, IR spectroscopy and frequency response method. The sorptive properties were described starting with benzene and the model introduced was extended to the alkyl substituted aromatic molecules (i.e. toluene and p-xylene). Due to the close fit between the kinetic diameter of the aromatic molecules and the pore dimensions the sorption was mainly controlled by the entropy. The micro-kinetic pathways of sorption and transport of the molecules inside the pores were studied by fast time-resolved (rapid scan) IR spectroscopy, which allowed measuring the kinetic rate of processes within the timescale of milliseconds.

The sorption of benzene on the bridging hydroxyl groups (SiOHAl) as well as on the terminal hydroxyl (SiOH) groups studied by IR spectroscopy was described by a dual-site Langmuir model, where the heat of adsorption and the decrease of entropy were determined from the temperature dependence of the

equilibrium constants. Calorimetry showed that the heat of adsorption of benzene in the acidic MFI (HZSM-5) is only 5 kJ/mol higher compared to the non acidic MFI (Silicalite-1), which indicates that the sorption of benzene in MFI zeolites is energetically controlled by the interaction of the molecules with the pore walls, while the localized interaction with the SiOHAl groups is only a minor energetic contribution.

The sorption of benzene inside the pores led to sterically constrained sorption structures indicated by the decrease of the entropy. Two perturbed hydroxyl groups after the adsorption of the aromatic molecules on the SiOHAl groups were observed reflecting two orientations of benzene inside the pores i.e., an orientation with the ring parallel to the pore walls and one with a specific C atom or C-C bond oriented towards the SiOHAl groups. The strength of the electron pair acceptor-donor (EPA-EPD) interaction in principle is directly proportional to perturbation of the hydroxyl groups and, therefore, if benzene is located close to SiOHAl groups the frequency from perturbed hydroxyl groups reflects the local constraints of benzene at the sorption sites. The additional energetic contribution for the sorption in acidic MFI leads to the preferential occupation at intersections. The extended investigation on toluene and p-xylene supports this evidence and shows even more complex interactions. As for the sorption of benzene, two orientations could also be identified for the sorption of toluene. For p-xylene, the sharp initial uptake was followed by a rapid saturation of the sorption of the SiOHAl groups, thus the Langmuir model is inadequate to describe this sorption process. Similar to toluene also for p-xylene two randomly populated orientations were observed at low coverage, while at higher coverage the molecules are concluded to be adsorbed in a less constrained orientation. The steric effects of the additional –CH_3 groups led to a further loss of rotational entropy and to an ordering of the molecules inside the pores. The preferential adsorption at intersection results in spatially well separated molecules which are randomly oriented with respect to the position of the SiOHAl groups. In a so called Bellamy-Hallam-Williams

(BHW) plot, the two steric constraint sorption structures can be detected from the deviation in the linear relation between $\Delta\nu_{SiOH}$ (of amorphous silica) and $\Delta\nu_{SiOHAl}$ (of a zeolite) using a series of molecules (e.g. alkanes, N_2, CO). The slope of this graph is a measure for the acid strength of the zeolite and for larger molecules such as aromatic, deviations to smaller shifts for $\Delta\nu_{SiOHAl}$ indicate the existence of geometrical constraints for the molecules during sorption in the pore of the zeolites.

The surface transport routes of benzene, toluene and p-xylene in HZSM-5 were directly followed by fast time-resolved (rapid scan) IR spectroscopy. The postulated micro-kinetic pathway is concluded to proceed via the physisorption in a weakly bound state (pre-adsorbed state) allowing high two-dimensional mobility of molecules on the surface, subsequently followed by parallel sorption processes on the surface SiOH groups and on the SiOHAl groups inside the pores. From these experiments the sticking probability of the aromatic could be directly calculated using the sorption rates on the SiOH groups in case of Aerosil (amorphous silica) and from the sum of sorption rates on the SiOH and SiOHAl groups in the case of HZSM-5 (porous material). The sticking probabilities of the series of aromatic molecules in HZSM-5 and Aerosil were in the order of 10^{-7}, which confirmed the presence of a pre-adsorbed state. The reason for the low sticking probability of aromatic molecules compared to n-alkanes is the different size and geometry of the molecules, where steric constraints in the sorption geometry further limit the molecular motions thus leading a higher loss in entropy. Statistical thermodynamics revealed that the low sticking probability in the pre-adsorbed state is related to the total loss of all rotational entropy.

In summary, the sterically constrained sorption of aromatic molecules on MFI zeolites has been understood from the point of molecular interactions, orientations and the transport to the zeolite surface. The non-specific interaction of the aromatic molecules with the pore walls is the main energetic contribution, while the directed interaction of the aromatic molecules with the

acidic sites has a minor contribution, which is, however, sufficient to preferentially direct the aromatic molecules to sorption sites at intersections at low coverage. For sorption of benzene, the two perturbed hydroxyl groups are assigned to two orientations of the molecules inside the pores, being equal in their energetic but different in their entropic contributions. In addition, a third perturbed hydroxyl group band was observed at high coverage which can be assigned to the non-constrained sorption (e.g. pore openings). In the case of toluene and p-xylene, only a single perturbed hydroxyl band appears at high coverage indicating the preference for the geometrically less constrained sorption structure. The study of the transport of aromatic molecules to the surface of zeolite was described via a pre-adsorbed state and the sticking probabilities derived for the aromatic molecules on amorphous and porous material has led to the understanding of sorption phenomena on highly steric constraints environment. The loss of entropy (i.e. mostly from the rotational contributions) along with the subsequent increase of heat of adsorption from benzene to the alkyl substituted aromatic molecules contributes to the further understanding of the energetic and kinetic effects in shape selective reactions of aromatic molecules on MFI zeolites.

6.2. Zusammenfassung

Um neue katalytisch aktive Materialien zu designen und maßgeschneidert herzustellen, hat das Verständnis und die Beschreibung der Prozesse der Adsorption und des Transports von Molekülen in porösen Materialien wesentliche Bedeutung. Zeolithe des MFI-Typs, welche über zehngliedrige Porenöffnungen verfügen, stellen aufgrund der Porendurchmesser ideale poröse Materialien für die selektive Sorption und katalytische Reaktion von aromatischen Molekülen dar. Mit diesen Zeolithen ist die Abtrennung von p-Xylol, einem wichtigen Zwischenprodukt für die Herstellung von Polyesterfasern, -harzen und -filmen, aus Mischungen der Xylol Isomere möglich. Um die formselektiven Eigenschaften zeolithischer Katalysatoren gezielt für katalytische Reaktionen zu nutzen muss das grundlegende Verständnis für die Prozesse der Sorption und des Transports hinsichtlich thermodynamischer, kinetischer und diffusionsbedingter Aspekte deutlich verbessert werden.

Das Ziel dieser Arbeit war es, die Sorption und die Transporteigenschaften aromatischer Moleküle in aciden (HZSM-5) und nicht-aciden (Silicalite-1) Zeolithen des MFI-Typs mittels der experimentellen Methoden der Gravimetrie, Kalorimetrie, Infrarot-Spektroskopie und der Frequency Response zu erforschen. Die Eigenschaften der Sorption wurden beginnend beim Benzol beschrieben und das dabei eingeführte Sorptionsmodell auf die alkyl-substituierten aromatischen Moleküle (d.h. Toluol und p-Xylol) erweitert. Aufgrund der guten Übereinstimmung des kinetischen Durchmessers der aromatischen Moleküle und der Porendurchmesser des Zeoliths werden die Sorptionseigenschaften hauptsächlich entropisch kontrolliert. Die mikrokinetischen Pfade der Sorption und des Transports von Molekülen in den Poren wurden mittels zeitaufgelöster Rapid–Scan-IR-Spektroskopie untersucht. Diese Messmethode erlaubt es die

Raten der ablaufenden kinetischen Prozesse mit einer Zeitauflsung von Millisekunden zu bestimmen.

Die Sorption von Benzol an den verbrückten Hydroxyl- (SiOHAl) und Silanolgruppen (SiOH) des Zeoliths, die mittels IR-Spektroskopie untersucht wurde, konnte über einen „dual-site Langmuir“ Modellansatz beschrieben werden. Aus den dabei erhaltenen Gleichgewichts-konstanten der Adsorption von Benzol und deren Temperaturabhängigkeit wurden die Adsorptionswärme und Entropieabnahme bei der Adsorption bestimmt. Mittels Kalorimetrie konnte gezeigt werden, dass sich die Adsorptionswärme für Benzol im aciden MFI-Typ Zeolith HZSM-5 und dem nicht aciden Vertreter Silicalite-1 nur um 5 kJ/mol unterscheidet. Dieses Resultat verdeutlicht, dass die Adsorption von Benzol in MFI-Typ Zeolithen energetisch durch die Wechselwirkung der aromatischen Moleküle mit den Porenwänden gesteuert wird, wohingegen die lokalisierte Wechselwirkung mit den SiOHAl Gruppen nur einen geringeren energetischen Beitrag zu beiträgt.

Die Abnahme der Entropie bei der Sorption legt nahe, das die Sorption des Benzols innerhalb der Poren zu sterisch gehinderten Sorptionstrukturen führt. Nach Adsorption der aromatischen Moleküle an den SiOHAl Gruppen werden zwei gestörte Hydroxyl-Gruppen beobachtet, welche die beiden möglichen Orientierungen von Benzol innerhalb der Poren, eine mit dem aromatischen Ring parallel zu den Porenwänden und die andere mit einem spezifischen C-Atom oder einer C-C Bindung in Richtung der SIOHAl Gruppen, widerspiegeln. Prinzipiell ist die Stärke der Elektronakzeptor-Donor (EPA-EPD) Wechselwirkung direkt proportional zur Stärke der Störung der Hydroxyl-Gruppen. Daher reflektiert folglich die Wellenzahl der gestörten Hydroxyl-Gruppe im IR-Spektrum die lokalen sterischen Randbedingungen des Benzols an den Sorptionszentren, wenn das Benzolmolekül nahe genug an den SiOHAl Gruppen lokalisiert ist. Der geringe, zusätzliche energetische Beitrag bei der Sorption in aciden MFI-Zeolithen führt zu einer bevorzugten Besetzung der Kreuzungen zwischen den Kanälen des Zeoliths. Die weitergehende

Untersuchung von Toluol und p-Xylol stützt diesen Befund und liefert sogar noch kompliziertere Wechselwirkungen. Wie auch im Falle der Sorption von Benzols konnten zwei Orientierungen bei der Sorption von Toluol identifiziert werden. Bei p-Xylol folgt einem anfänglich scharfen Anstieg eine schnelle Sättigung der der SiOHAl-Gruppen, wodurch das Langmuir Modell nicht zur Bescheribung des Sorptionprozesses angewendet werden kann. Ähnlich wie bei Toluol findet man bei geringer Bedeckung auch für p-Xylol zwei zufällig populierte Orientierungen, während bei höherem Bedeckungsgrad gefolgert werden kann, dass die Moleküle in der weniger sterisch gehinderten Orientierung adsorbieren werden. Die sterischen Effekte der zusätzlichen CH_3 - Gruppen führten zu einem zusätzlichen Verlust von Rotationsentropie und zu stärkerer Ordnung der Moleküle innerhalb der Poren. Die bevorzugte Adsorption an den Kanalkreuzungen führt zu räumlich gut getrennten und bezüglich der Position der SiOHAl-Gruppen zufällig orientierten Molekülen. In einem sogenannten Bellamy-Hallam-Williams (BHW) Diagramm können die zwei sterischen gehinderten Sorptionstrukturen anhand der Abweichung von der linearen Beziehung zwischen $\Delta\nu_{SiOH}$ (amorphous Silica) und $\Delta\nu_{SiOHAl}$ (acider zeolith) mit Hilfe einer Reihe von Molekülen (z.B. Alkane, N_2, CO) verdeutlicht werden. Die Steigung dieses Graphen ist ein direktes Maß für die Säurestärke des Zeoliths. Für größere Moleküle wie z.B. aromatische Moleküle deuten die Abweichungen vom linearen Verlauf hin zu kleineren Verschiebungen für νSiOHAl auf das Vorliegen geometrischer Behinderungen für das Molekül während der Sorption in den Poren hin.

Die Oberflächentransportwege des Benzols, Toluols und des p-Xylols in HZSM-5 wurden direkt mittels schneller zeitaufgelöster Rapid-Scan-IR-Spektroskopie verfolgt. Es kann daraus gefolgert werden, dass die postulierten mikrokinetischen Transportwege über einen schwach gebundenen physisorbierten Zustand (präadsorbierter Zustand) erfolgen, der eine zweidimensionale Beweglichkeit der Moleküle auf der Oberfläche zulässt, gefolgt von parallel verlaufenden Sorptionsprozessen an den SiOH-Gruppen an

der Oberfläche und den SiOHAl-Gruppen in den Poren. Aus diesen Experimenten konnte die sog. „sticking probability“ (Haftwahrscheinlichkeit) aromatischer Moleküle direkt berechnet werden. Dazu wurden die Sorptionsraten an den SiOH-Gruppen im Falle von Aerosil („amorphous silica“) und die Summe der Sorptionsraten an den SiOH und SiOHAl-Gruppen im Falle von HZSM-5 (poröses Material) herangezogen. Die Haftwahrscheinlichkeiten einer Serie von aromatischen Molekülen an HZSM-5 und Aerosil liegen im Größenordnungsbereich von 10^{-7} was das Vorliegen eines präadsorbierten Zustands bekräftigt. Ein Grund für die, verglichen mit n-Alkanen deutlich geringe Haftwahrscheinlichkeit aromatischer Moleküle sind die unterschiedliche Größe und Geometrie der Moleküle. Durch sterisch gehinderte Sorptionsgeometrien wird die Beweglichkeit der Moleküe verringert was zu einem größeren Verlust an molarer Entropie führt. Anhand statistisch thermodynamischer Überlegungen kann gezeigt werden, dass derart geringe Haftwahrscheinlichkeiten im präadsorbierten Zustand durch vollständigen Verlust der Rotationsfreiheitsgrade erzielt werden.

Zussammenfassend konnte die sterisch gehinderte Sorption aromatischer Moleküle auf MFI-Tap Zeoliten untersucht und hinsichtlich molekularer Wechselwirkungen, Orientierungen der Moleküle und des Einflusses von Oberflächentransportprozessen charakterisiert werden. Die nicht-spezifische Wechselwirkung der aromatischen Moleüle mit den Porenwänden stellt den energetischen Hauptbeitrag dar wohingegen die gerichtete Wechselwirkung mit den sauren, katalytisch aktiven Zentren nur geringfügig beiträgt. Dennoch reicht die geringfügige, gerichtete Wechselwirkung aus, um die Moleküle bei geringer Oberflächenbedeckung bevorzugt zu den Sorptionszentren in den Kanalkreuzungen zu lenken. Für die Sorption von Benzol können die beiden Banden der gestörten Hydroxylgruppen den beiden Orientierungen der Moleküle innerhalb den Poren zugeordnet werden die sich bei annähernd gleicher Adsorptionswärme in der Änderung der molaren Entropie unterscheiden. Zusätzlich wurde bei höheren

Bedeckungen eine dritte gestörte Hydroxylgruppenbande beobachtet, die der ungestörten Sorptionsgeometrie (z.B. in den Porenöffnungen) zugeordnet werden kann. Im Falle des Toluols und p-Xylols wurde bei hohen Bedeckungsgraden nur eine einzige gestörte Hydroxylbande gefunden was eine Bevorzugung der geometrisch weniger gehinderten Sorptionsgeometrie andeutet. Der Transport von aromatischen Molekülen an die Oberfläche des Zeolithen wurde über das Modell eines präadsorbierten Zustands beschrieben. Die Haftwahrscheinlichkeiten die für die aromatischen Moleküle auf amorphem und porösem Material hergeleitet wurden haben zu einem tieferen Verständnis der Oberflächensorptionsphänomene unter hochgradig sterisch anspruchsvollen Verhältnissen geführt. Der Entropieverlust (hauptsächlich aus der Hinderung von Rotationsbeiträgen) zusammen mit dem stetigen Anstieg der Adsorptionswärme von Benzol zu alkylsubstituierten aromatischen Molekülen trägt zum besseren Verständnis der energetischen und kinetischen Effekte bei formselektiven Reaktionen aromatischer Moleküle an MFI Zeolithen bei.

CURRICULUM VITAE

Rino R. Mukti was born in Jakarta, Indonesia, on April 25th 1977. After accomplishing high school in Jakarta in 1995, he directly started his Sarjana Sains in Chemistry at Institut Teknologi Bandung (ITB). He graduated in the millennium year 2000 along with additional advantage of being Indonesia representative for the 41st London International Youth Science Forum in 1999. His first thesis initiated the research on porous materials (i.e. natural zeolites) where it was subsequently extended to the level of Master of Science at the Department of Chemistry, Universiti Teknologi Malaysia (UTM), Johor, Malaysia under supervision of Prof. Dr. Halimaton Hamdan, FASc. He worked on synthetic mesoporous material and its application towards catalytic reaction. The chance of pursuing PhD thesis was taken in 2003 at Department of Chemistry, Technische Universität München under supervision of Prof. Dr. Johannes A. Lercher where the works mainly specialize on investigating the molecular adsorption and surface transport processes of aromatic over MFI zeolites using advanced IR spectroscopy.

LIST OF PUBLICATIONS

1. SURFACE TRANSPORT PROCESSES AND STICKING PROBABILITY OF AROMATIC IN HZSM-5
   R. R. Mukti, S. J. Reitmeier, A. Jentys, and J. A. Lercher
   The Journal of Physical Chemistry B, **2007**, to be submitted

2. ORIENTATION OF ALKYL-SUBSTITUTED AROMATIC MOLECULES DURING SORPTION IN THE PORES OF H/ZSM-5 ZEOLITES
   R. R. Mukti, A. Jentys, and J. A. Lercher
   The Journal of Physical Chemistry C, **2007**, 111, 3973-3980

3. ON THE STICKING PROBABILITYOF AROMATIC MOLECULES ON ZEOLITES. Comment on “Sticking Probability on Zeolites”
   A. Jentys, R. R. Mukti, and J. A. Lercher
   The Journal of Physical Chemistry B, **2006**, 110, 17691-17693

4. ENERGETIC AND ENTROPIC CONTRIBUTIONS CONTROLLING THE SORPTION OF BENZENE IN ZEOLITES
   Jentys, R. R. Mukti, H. Tanaka, and J. A. Lercher
   Microporous Mesoporous Materials, **2006**, 90, 284-292

LIST OF PRESENTATIONS

1. ORIENTATION OF ALKYL-SUBSTITUTED AROMATIC MOLECULES DURING SORPTION IN THE PORES OF HZSM-5
   Poster presented at 19. Deutsche Zeolith-Tagung, 7-9 March 2007, Leipzig, Germany

2. TRANSPORT AND STICKING PROBABILITY OF AROMATIC IN MEDIUM-PORE ZEOLITES
   Poster presented at 19. Deutsche Zeolith-Tagung, 7-9 March 2007, Leipzig, Germany

3. SORPTION AND ORIENTATION OF BENZENE IN MEDIUM-PORES ZEOLITES
   Oral presented at International Conference on Mathematics and Natural Sciences, 29-30 November 2006, Bandung, Indonesia

4. LOCALIZED INTERACTIONS OF AROMATIC SORPTION IN MEDIUM-PORE ZEOLITES
   Poster presented at XXXIX. Jahrestreffen Deutscher Katalytiker, 15-17 March 2006, Weimar, Germany

5. LOCALIZED INTERACTIONS OF AROMATIC MOLECULES DURING SORPTION IN ZSM-5
   Oral presented at 18. Deutsche Zeolith-Tagung, 1-3 March 2006, Hannover, Germany

6. ENERGETIC AND ENTROPIC CONTRIBUTIONS CONTROLLING THE SORPTION OF AROMATIC MOLECULES IN ZSM-5
   Oral presented at TC2 Ski Seminar, 14-17 February 2006, Obertauern, Austria

7. THERMODYNAMIC SORPTION OF BENZENE ON H/ZSM-5
   Oral presented at Lehrstuhl für Technische Chemie II, Technische Universität München, 3 May 2005, Garching, Germany